



저작자표시-비영리-변경금지 2.0 대한민국

이용자는 아래의 조건을 따르는 경우에 한하여 자유롭게

- 이 저작물을 복제, 배포, 전송, 전시, 공연 및 방송할 수 있습니다.

다음과 같은 조건을 따라야 합니다:



저작자표시. 귀하는 원저작자를 표시하여야 합니다.



비영리. 귀하는 이 저작물을 영리 목적으로 이용할 수 없습니다.



변경금지. 귀하는 이 저작물을 개작, 변형 또는 가공할 수 없습니다.

- 귀하는, 이 저작물의 재이용이나 배포의 경우, 이 저작물에 적용된 이용허락조건을 명확하게 나타내어야 합니다.
- 저작권자로부터 별도의 허가를 받으면 이러한 조건들은 적용되지 않습니다.

저작권법에 따른 이용자의 권리는 위의 내용에 의하여 영향을 받지 않습니다.

이것은 [이용허락규약\(Legal Code\)](#)을 이해하기 쉽게 요약한 것입니다.

[Disclaimer](#)

Studies of molecular mechanism of  
chemoresistance and epithelial to  
mesenchymal transition in tumor  
microenvironment

Yeseong Hwang

Department of Medical Science

The Graduate School, Yonsei University

Studies of molecular mechanism of  
chemoresistance and epithelial to  
mesenchymal transition in tumor  
microenvironment

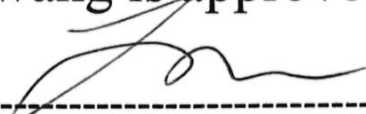
Directed by Professor Sungsoon Fang

The Doctoral Dissertation  
submitted to the Department of Medical Science,  
the Graduate School of Yonsei University  
in partial fulfillment of the requirements for the degree of  
Doctor of Philosophy in Medical Science

Yeseong Hwang

December 2023

This certifies that the Doctoral Dissertation of  
Yeseong Hwang is approved.



-----  
Thesis Supervisor : Sungsoon Fang



-----  
Thesis Committee Member#1 : Yong-ho Lee

구철룡

-----  
Thesis Committee Member#2 : Cheol Ryong Ku



-----  
Thesis Committee Member#3: Chang-Myung Oh

오창명

-----  
Thesis Committee Member#4: Se Kyu Oh

The Graduate School  
Yonsei University

December 2023

## ACKNOWLEDGEMENTS

I would like to sincerely thank God for his graces and powerful strength during Ph.D. course. I would like to express my gratitude to my supervisor Prof. Sungsoon Fang. He gave me the opportunity to experience bioinformatics analysis and carry out my Ph.D. research project. His support and continuous guidance helped me to establish logical reasoning for story outline and finish this research without incidence. I am also grateful to my Ph.D. dissertation committee professor Yong-ho Lee, Cheol Ryong Ku, Chang-Myung Oh, and doctor Se Kyu Oh for their meaningful comments and suggestions.

I also would like to appreciate my lab members. Doctor Hae-Kyung Lee, doctor Hyeonhui Kim, Minki Kim and Sugyeong Jo helped me to keep my research direction correctly with discussion. Jae Woong Jeong and Seyeon Joo helped me to perform bioinformatics analysis skillfully. Chae Min Lee and Ye-Chan Park gave me a valuable responsibility to lead research project.

I really want to thank my family. My mother, my father, my sister, my brother, sister-in-law for their infinite love and support.

Best regards,  
Yeseong Hwang

## <TABLE OF CONTENTS>

ABSTRACT.....	viii
PART1. Combined inhibition of glutaminolysis and one carbon metabolism enhances chemotherapeutic efficacy by accumulating ROS in anaplastic thyroid cancer .....	
1	1
I. INTRODUCTION .....	1
II. MATERIALS AND METHODS .....	4
1. Antibodies and Reagents .....	4
2. Cell culture and treatment.....	4
3. Sample preparation for LC-MS metabolomic analysis .....	5
4. Liquid Chromatography.....	5
5. Mass Spectrometry .....	6
6. Cell proliferation and viability assay .....	6
7. Colony formation assay.....	6
8. Analysis of nuclear fragmentation by Hoechst 33342 staining .....	7
9. LDH assay .....	7
10. Real-time RT-PCR.....	7
11. Immunoblot assay .....	7
12. Cell cycle assay.....	8
13. Measurement of ROS and GSH contents .....	8
14. RNA sequencing .....	9
15. ATAC sequencing .....	9
16. Acquisition of scRNA-seq data .....	9
17. Processing of the scRNA-seq data.....	10
18. Trajectory inference and pseudotime analysis based on TDS score .....	10

III. RESULTS	14
1. ATC displays enhanced serine and one carbon metabolism dependency compared to PTC	14
2. One carbon metabolism may seem to be intensified according to evolutionary path from PTC to ATC	18
3. Glutaminolysis was upregulated in patients with ATC	24
4. Inhibition of glutaminolysis compromises ATC cell proliferation	27
5. Glutaminolysis inhibition is not enough to trigger cell death in ATC	30
6. Glutamine deprivation enhances one carbon metabolism in ATC	33
7. Glutamine deprivation stress promotes ATF4-mediated one carbon metabolism in ATC	36
8. Co-inhibition of glutaminolysis and one carbon metabolism compromises redox balance by reducing GSH contents	39
9. Co-inhibition of glutaminolysis and one carbon metabolism reduces cell proliferation the most in ROS dependent manner	42
10. Glutaminolysis inhibition only enhances chemotherapy efficacy in ATC	45
11. Co-inhibition of glutaminolysis and one carbon metabolism synergistically increases chemotherapy efficacy in ATC	48
IV. DISCUSSION	51
V. CONCLUSION	54
PART2. One carbon metabolism promotes immunosuppressive molecular signatures of inflammatory cancer-associated fibroblasts to drive Epithelial-Mesenchymal transition in colorectal cancer	56
I. INTRODUCTION	56

II. MATERIALS AND METHODS .....	59
1. Acquisition of scRNA-seq data .....	59
2. Processing of the scRNA-seq data .....	59
3. Measuring DEGs between OHF and OLF .....	59
4. ssGSEA analysis .....	60
5. Cellchat analysis .....	60
6. Trajectory inference and pseudotime analysis .....	60
7. Visium spatial transcriptomics .....	60
8. Data sources of microarray and CCLE metabolomics .....	61
9. Overall survival analysis .....	61
10. Cell culture and treatment .....	61
11. Cell proliferation assay .....	62
III. RESULTS .....	64
1. One carbon metabolism is significantly upregulated in patients with CRC .....	64
2. Single cell analysis of patients with CRC .....	68
3. Fibroblast clusters divide into two subpopulations according to gene expression of one carbon metabolism .....	71
4. iCAFs preferentially reside in OHF .....	74
5. OHF might be pivotal role of EMT enhancement in iCAFs dependent manner ...	79
6. <i>CXCL12</i> secreted from iCAFs in OHF induces immunosuppression and subsequent EMT promotion in patients with CRC .....	86
IV. DISCUSSION .....	90
V. CONCLUSION .....	93
REFERENCES .....	95

ABSTRACT(IN KOREAN) .....	105
PUBLICATION LIST .....	108

## LIST OF FIGURES

### **PART1. Combined inhibition of glutaminolysis and one carbon metabolism enhances chemotherapeutic efficacy by accumulating ROS in anaplastic thyroid cancer.**

Figure 1. One carbon metabolism in ATC is more active than PTC	17
Figure 2. One carbon metabolism might be strengthened following evolution routes from PTC to ATC	23
Figure 3. ATC patients exhibit glutaminolysis enhancement	26
Figure 4. Inhibition of glutaminolysis impedes ATC cell proliferation	29
Figure 5. Glutaminolysis inhibition is not enough to trigger cell death in ATC	32
Figure 6. Glutamine deprivation enhances one carbon metabolism in ATC	34
Figure 7. Glutamine deprivation enhances ATF4-mediated one carbon metabolism in 8505C ATC cells	38
Figure 8. Co-inhibition of glutaminolysis and one carbon metabolism compromises redox balance by reducing GSH contents	40
Figure 9. Co-inhibition of glutaminolysis and one carbon metabolism reduces cell proliferation the most in ROS dependent manner	44
Figure 10. Glutaminolysis inhibition only enhances chemotherapy efficacy in ATC	47
Figure 11. Co-inhibition of glutaminolysis and one carbon metabolism synergistically increases chemotherapy efficacy in ATC	50

**PART2. One carbon metabolism promotes immunosuppressive molecular signatures of inflammatory cancer-associated fibroblasts to drive Epithelial-Mesenchymal transition in colorectal cancer.**

Figure 1. One carbon metabolism is significantly upregulated in patients with CRC.....	66
Figure 2. Single cell analysis of patients with CRC.....	70
Figure 3. Fibroblast divide into two subpopulations according to gene expression of one carbon metabolism .....	73
Figure 4. iCAFs preferentially reside in OHF.....	77
Figure 5. OHF might be pivotal role of EMT enhancement in iCAFs dependent manner .....	84
Figure 6. <i>CXCL12</i> secreted from iCAFs in OHF contributes to EMT in CRC patients.....	89

## LIST OF TABLES

Table 1. Sequences of primers used in real-time RT-PCR .....	12
Table 2. Quality control and percent of doublet for single cell analysis .....	13
Table 2. Clinical information of CRC patients in single cell analysis	63

## ABSTRACT

**Studies of molecular mechanism of chemoresistance and epithelial to mesenchymal transition in tumor microenvironment**

Yeseong Hwang

*Department of Medical Science  
The Graduate School, Yonsei University*

(Directed by Professor Sungsoon Fang)

Many types of cancers use serine-dependent one carbon metabolism to sustain tumorigenic environment. Serine is directly into tumor cells through serine uptake transporters or synthesized from glycolysis or gluconeogenesis-derived 3P, which are next involved in diverse physiological processes including ROS balance, purine, and DNA synthesis. Here, we observed the tumorigenic role of one carbon metabolism in two refractory anaplastic thyroid cancer (ATC) and colorectal cancer (CRC).

ATC is one of the most aggressive tumors with an extremely poor prognosis. Based on papillary thyroid cancer (PTC) exhibits enhanced level of one carbon metabolism protein and is dedifferentiated into ATC, we compared one carbon metabolism between ATC and PTC. Single cell RNA sequencing analysis revealed that one carbon metabolism was strengthened through evolutionary process from PTC to ATC. Also, we thought glutaminolysis inhibition induces cell death based on the several biological features related to glutamine metabolism upregulation such as HER-2 overexpression and frequent  $\beta$ -catenin nuclear localization in ATC. Nonetheless, ATC cells regulate ROS homeostasis via ATF4-mediated one carbon metabolism and subsequent inhibit cell proliferation arrest against glutamine metabolism inhibition. We next observed that co-inhibition of glutamine and one carbon metabolism could synergistically enhance the anticancer effect of drugs used in patients with ATC.

CRC is the third most common cancer type with the second poor prognosis. Patients with

CRC are commonly accompanied by epithelial-mesenchymal transition (EMT) leading to liver and lung metastasis. Here, our single cell analysis reported that fibroblast clusters were divided into two groups according to one carbon metabolism activation and inflammatory cancer-associated fibroblasts (iCAFs) associated with EMT dominantly resided in one carbon metabolism high fibroblast. Serine synthesis high groups in CRC patients with liver metastasis exhibited high level of iCAF and EMT genes. Serine synthesis and iCAFs genes high group especially showed inferior outcome in CRC patients with stage 3 and 4, indicating that one carbon metabolism has positive correlation with iCAFs and contributes to metastasis through EMT. Moreover, one carbon high fibroblast showed *CXCL12* outgoing signaling to *CXCR4* in immune cells such as T cell and macrophage, which might elicit infiltration of Treg and TAMs. *CXCL12* represented positive correlation with EMT genes including *SNAI2* and *VIM*. Collectively, our data demonstrate one carbon metabolism has a potential role of modulation of cell fate in metabolic stress or EMT promotion via tumor microenvironment components, iCAFs. Thus, one carbon metabolism can be therapeutic target for improving survival by enhancing antitumor effects in refractory cancer.

---

Key words : one carbon metabolism, refractory cancer, RNA sequencing

**PART1. Combined inhibition of glutaminolysis and one carbon metabolism enhances chemotherapeutic efficacy by accumulating ROS in anaplastic thyroid cancer.**

Yeseong Hwang

*Department of Medical Science  
The Graduate School, Yonsei University*

(Directed by Professor Sungsoon Fang)

**I. INTRODUCTION**

Anaplastic thyroid cancer (ATC) is an uncommon, but highly lethal type of dedifferentiated thyroid cancer. ATC patients with surgical resection are necessary chemotherapy to prolong survival. Conventional chemotherapy using doxorubicin or taxanes showed minimal survival benefit and therapies to target tyrosine kinase affecting oncogenic signaling pathway have been developed, including lenvatinib and sorafenib, multi-tyrosine kinase inhibitor. Nonetheless, combinational approach to overcome minimal effect of monotherapy is still needed in ATC (1-4).

Several studies showed important roles of glutamine metabolism on ATC tumor environment. It was reported that HER-2 overexpression and frequent  $\beta$ -catenin nuclear localization in ATC, which are associated with increased glutamine metabolism. Patients with ATC also showed the highest level of glutaminase 1 (GLS1) and glutamate dehydrogenase (GDH) compared to other thyroid cancer types (5-9). Glutamine is the most abundant amino acid and acts as a precursor of amino acids, proteins, lipids, and nucleotides in human. Exogenous glutamine is converted to glutamate by GLS, which is again synthesized into  $\alpha$ -ketoglutarate by GDH to participate in tricarboxylic acid cycle (10, 11). This ‘Glutaminolysis’ process is important for tumor growth as it sustains

mitochondrial function and reactive oxygen species (ROS) balance. Glutamate is also involved in glutathione (GSH) synthesis, which is a predominant antioxidant enzyme that protects cancer cells from various oxidative stresses such as chemotherapy and radiation (12-15). Based on essential roles of glutamine in cancer cell homeostasis, it has been reported that many cancer cells including lung adenocarcinoma; acute myeloid leukemia; breast; liver; and brain cancer are vulnerable to glutamine deprivation stress, suggesting the crucial role of glutamine in modulating cancer cell survival (16-19).

In contrast, many investigations were also reported that cancer cells exert alternative strategy to survive under glutamine metabolism inhibition. For example, some cancer cells promote glutamine synthesis through glutamine synthetase upregulation or autophagy-mediated glutamine recycling (20, 21). Another process is to activate one carbon metabolism pathway. During glutamine deprivation, some cancer cells particularly uptake serine, which is a major donor of one carbon metabolism. One carbon metabolism including folate and methionine cycle is important physiological process to overcome nutrition deficiency through diverse outputs such as amino acids, lipids and ROS imbalance through GSH synthesis (22-26).

Given that one carbon metabolism is crucial for maintaining tumorigenesis upon glutamine metabolism inhibition-induced nutrient reprogramming, we first investigated one carbon metabolism between ATC and PTC. Our bioinformatic data showed one carbon metabolism is more active in ATC and might be intensified following evolutionary route from PTC to ATC. Based on strong relationship between glutamine metabolism and biological features of ATC, we hypothesized ATC are vulnerable to glutaminolysis impairment. Unexpectedly, we found that ATC cells are resistant to cell death owing to the induction of one carbon metabolism by controlling redox balance during glutamine metabolism inhibition. We also confirmed that combined inhibition of glutamine and one carbon metabolism is sufficient to reduce cell proliferation more than treated alone and increase the efficacy of lenvatinib and sorafenib, a multitarget tyrosine kinase inhibitor for patients with ATC. Our data suggest possibility that ATC employs one carbon metabolism

to rapidly adapt to diverse stresses such as metabolic stress and chemotherapy and provide therapeutic target for ATC by inhibiting one carbon metabolism.

## II. MATERIALS AND METHODS

### 1. Antibodies and Reagents

The following antibodies and reagents were commercially acquired. BPTES (HY-12683, MedChemExpress, Monmouth, Oregon, USA), CBR-5884 (HY-100012, MedChemExpress, Monmouth, Oregon, USA), SHIN1 (HY-112066, MedChemExpress, Monmouth, Oregon, USA), DS18561882 (HY-130251, MedChemExpress, Monmouth, Oregon, USA), and sorafenib (HY-10201, MedChemExpress, Monmouth, Oregon, USA), Trolox (S3665, Selleckchem, Houston, Texas, USA), lenvatinib (S1164, Selleckchem, Houston, Texas, USA), Crystal violet (V5265, Thermo Fisher Scientific, Waltham, MA, USA), monobromobimane (mBBr) (M1378, Thermo Fisher Scientific, Waltham, MA, USA), H<sub>2</sub>DCFDA (D399, Thermo Fisher Scientific, Waltham, MA, USA), MitoSOX™ Red (M36008, Thermo Fisher Scientific, Waltham, MA, USA), RNase A (10109169001, Thermo Fisher Scientific, Waltham, MA, USA), Propidium Iodide (P3566, Thermo Fisher Scientific, Waltham, MA, USA), (3-(4,5-Dimethylthiazol-2-yl)-2,5-Diphenyltetrazolium Bromide) (MTT) (M6494, Thermo Fisher Scientific, Waltham, MA, USA), Hoechst 33342 (H3570, Thermo Fisher Scientific, Waltham, MA, USA), Lipofectamine™ RNAiMAX Transfection Reagent (13778150, Thermo Fisher Scientific, Waltham, MA, USA), DMSO (34943, Sigma-Aldrich, St. Louis, MO, USA), H<sub>2</sub>O<sub>2</sub> (216763, Sigma-Aldrich, St. Louis, MO, USA), Triton X-100 (0694, AMRESCO, Solon, Ohio, USA), PHGDH (sc-100317, Santa Cruz Biotechnology, Dallas, TX, USA), SHMT2 (sc-390641, Santa Cruz Biotechnology, Dallas, TX, USA), and β-actin (sc-47778, Santa Cruz Biotechnology, Dallas, TX, USA), MTHFD2 (98116S, Cell Signaling Technology, Danvers, MA, USA), mouse secondary antibody (7076S, Cell Signaling Technology, Danvers, MA, USA), rabbit secondary antibody (ab6721, Abcam, Cambridge, UK), small interfering RNA siCTRL (sc-37007, Santa Cruz Biotechnology, Dallas, TX, USA), siATF4 (sc-35112, Santa Cruz Biotechnology, Dallas, TX, USA).

### 2. Cell culture and treatment

8505C cells were purchased from European Collection of Authenticated Cell Cultures

(ECACC, Salisbury, UK). TPC-1 cells were purchased from Elabscience (TX, USA). The 8505C cells were grown in DMEM medium (10-013-CV, Corning, NY, USA)-1% penicillin-streptomycin (15140122, Gibco, Waltham, MA, USA) supplemented with 10% fetal bovine serum (35-015-CV, Corning, NY, USA). TPC-1 cells were grown in RPMI-1640 medium (10-041-CV, Corning, NY, USA)-1% penicillin-streptomycin (15140122, Gibco, Waltham, MA, USA) supplemented with 10% fetal bovine serum (35-015-CV, Corning, NY, USA). Two cells were tested for mycoplasma elimination using a Plasmocin solution (ant-mpt, Invivogen, San Diego, CA, USA). Following concentrations were employed for in vitro experiments: Glutamine-full medium consists of medium (8505C; LM-001-05, Welgene, Daegu, Korea, TPC-1; 10-041-CV, Corning, NY, USA)-1% penicillin-streptomycin (15140122, Gibco, Waltham, MA, USA) supplemented with 10% fetal bovine serum (35-015-CV, Corning, NY, USA); Glutamine-free medium consists of DMEM medium (LM-001-08, Welgene, Daegu, Korea)-1% penicillin-streptomycin (15140122, Gibco, Waltham, MA, USA) supplemented with 10% dialyzed fetal bovine serum (26400044, Gibco, Waltham, MA, USA); MTT, 0.2 mg/ml; Crystal violet solution, 0.1%; Hoechst 33342, 2 ug/ml; mBBr, 10 uM; H<sub>2</sub>DCFDA, 10 uM; MitoSOX™ Red, 5 uM; BPTES, 10 uM; CBR-5884, 60 uM; H<sub>2</sub>O<sub>2</sub>, 10uM; Trolox, 25 uM; lenvatinib, 50 uM; sorafenib, 10 uM.

### **3. Sample preparation for LC-MS metabolomic analysis**

8505C cells ( $8 \times 10^5$  cells/well) were seeded in 100 mm cell culture dish and treated with glutamine-free medium or BPTES for 72 h. After aspirating cell medium, cells were washed with 10 ml pre-cool PBS twice on ice. After removing pre-cool PBS, 1 ml pre-chilled 80% methanol was added immediately. After scraping cells with cell scraper on ice, mixture of cell lysate and methanol was transferred to 1.5 ml tubes and stored at -80°C deep freezer for overnight.

### **4. Liquid Chromatography**

UPLC separation was performed on a Thermo Scientific™ UltiMate 3000 RSLC system using Acquity UPLC BEH C18, 1.7 um, 2.1 × 100 mm. The flow rate and operating

temperature are 300  $\mu\text{l}/\text{min}$  and 50°C respectively. The LC solvent of phase A is 0.1% formic acid in distilled water and phase B is 0.1% formic acid in acetonitrile. Linear gradient was implemented from 5% B for 2 min, followed by increasing to 100% at 8 min, hold 100% B for 4 min, then decrease to 5% at 0.5 min, then equilibrate for another 2.5 min. The sample injection volume is 5  $\mu\text{l}$ .

### 5. Mass Spectrometry

The Thermo Scientific™ Q Exactive Orbitrap Plus™ mass spectrometer was operated under electrospray ionization (ESI) positive mode. Full scan type (80–1000  $m/z$ ) used resolution 70,000. Data-dependent MS/MS were acquired on a “Top5” data-dependent mode using the following parameters: resolution 17,500; 2 amu isolation window; normalized collision energy 30; dynamic exclusion 6 s. Source ionization parameters were: spray voltage, 3.5 kV; capillary temperature, 370°C; and S-Lens level, 55.

### 6. Cell proliferation and viability assay

For cell proliferation and viability assay, cells ( $5 \times 10^3$  and  $1 \times 10^4$  cells/well respectively) were treated with glutamine-free medium or reagents for the indicated times in 96-well plates. After incubating cells with 10  $\mu\text{l}$  MTT solution in 37°C incubator for 2 h, formazan was dissolved in 50  $\mu\text{l}$  DMSO. The absorbance was measured at 570 nm using a Multiskan GO spectrophotometer (51119300, Thermo Fisher Scientific, Waltham, MA, USA). Synergy effect of multiple-drugs treatment was calculated with the following equation provided at Synergy Finder ([https://synergyfinder.fimm.fi/synergy/synfin\\_docs/](https://synergyfinder.fimm.fi/synergy/synfin_docs/)).

$$1) S_{\text{HSA}} = E_{A, B, C} - \max(E_A, E_B, E_C)$$

$$2) S_{\text{Bliss}} = E_{A, B, C} - 100(1 - (1 - E_A/100)(1 - E_B/100)(1 - E_C/100))$$

$E_X$  means the percentage of viability inhibition by chemical X in indicated concentration.

### 7. Colony formation assay

8505C cells ( $5 \times 10^3$  cells/well) were seeded in 6-well plates and treated with glutamine-free medium, BPTES for 10 days. After washing with PBS twice, cells were fixed with

cold methanol at room temperature for 5 min and stained with crystal violet for 15 min. After crystal violet was slowly washed with distilled water 5 times, the plates were air-dried overnight. Then, each sample was added to 1 ml methanol and rotated for 20 min. The optical density of each well was measured at 570 nm using a Multiskan GO spectrophotometer (51119300, Thermo Fisher Scientific, Waltham, MA, USA).

#### **8. Analysis of nuclear fragmentation by Hoechst 33342 staining**

8505C cells ( $1 \times 10^5$  cells/well) grown on a chambered coverglass (154526, Thermo Fisher Scientific, Waltham, MA, USA) were treated with glutamine free medium, BPTES, and  $H_2O_2$  for 24 h. After staining with Hoechst 33342 solution for 10 min in a 37°C incubator, cells were washed with PBS and fixed with 4% paraformaldehyde at room temperature for 10 min. Fragmented cells were measured using fluorescence microscopy (BX53F, OLYMPUS, Tokyo, Japan).

#### **9. LDH assay**

8505C ( $5 \times 10^3$  cells/well) seeded in a 96-well plate were treated with glutamine-free medium or BPTES for the indicated times. Cell death was assessed based on the release of LDH into the extracellular medium, which was measured using a Cytotoxicity Detection Kit according to the manufacturer's protocol (C20301, Thermo Fisher Scientific, Waltham, MA, USA).

#### **10. Real-time RT-PCR**

RNA of 8505C cells was isolated using TRIzol reagent (15596018, Invitrogen, Waltham, MA, USA). cDNA was synthesized using 1 ug total RNA and ImProm-II™ Reverse Transcriptase (A3803, Promega, Madison, WI, USA). Real-time RT-PCR was performed using TOP Real™ qPCR 2X Pre-MIX (RT501S, Enzynomics, Daejeon, Korea) and specific primers in a CFX Connect Real-Time PCR instrument (1855201, Bio-Rad, Hercules, CA, USA). Gene expression was normalized to the *36B4* mRNA expression levels.

The primer sequences for real-time RT-PCR are represented in Table. 1.

#### **11. Immunoblot assays**

Protein lysates were lysed in mammalian lysis buffer (25 mM Tris-HCl, pH 7.8, 150 mM NaCl, 0.1% NP-40, 1 mM EDTA, 10% glycerol) supplemented with Xpert Protease Inhibitor Cocktail Solution (P3100-001, GenDEPOT, Katy, TX, USA). Protein concentrations were quantified using the Bio-Rad Protein Assay Kit (#5000006, Bio-Rad, Hercules, CA, USA). Samples were separated by SDS-PAGE (8-10%) and transferred onto nitrocellulose membrane (10600001, Amersham, Buckinghamshire, UK). Membranes were blocked with 5% skim milk-Tris-0.1% Tween 20 for 30 min and incubated diluted antibodies at 4°C overnight. After incubation with HRP-conjugated secondary antibodies for 1 h at room temperature, immunoblot signals were detected using Clarity Western ECL Substrate (BR1705061 and 1705062, Bio-Rad, Hercules, CA, USA). For gene silencing with siCTRL or siATF4, the cells were transfected for 48 h with Lipofectamine™ RNAiMAX Transfection Reagent according to the manufacturer's protocol.

### **12. Cell cycle assay**

8505C cells ( $1 \times 10^5$  cells/well) seeded in 12-well plates were treated with glutamine free medium and BPTES for 24 h. Then, the cells were harvested and fixed with 70% ethanol at 4°C for overnight. After washing with PBS, cells were incubated with PBS containing 0.1% Triton X-100, 20 ug/ml of Propidium Iodide, 0.2 mg/ml of RNase A for 15 min at 37°C incubator. Analysis of cell cycle progression was performed using flow cytometry (FACSVerse, BD Biosciences, Franklin Lakes, NJ, USA). Data analysis was conducted by FlowJo software (version 10.4.2).

### **13. Measurement of ROS and GSH contents**

To measure intracellular ROS, 8505C cells ( $2 \times 10^5$  cells/well) were seeded in a 12-well plate. After 24 h, the cells were treated with the indicated drugs; vehicle (DMSO), BPTES, CBR-5884, lenvatinib and sorafenib for the indicated times. Then, the cells were stained with H<sub>2</sub>DCFDA in 37°C incubator for 30 min. For mitochondrial ROS measurement, 8505C cells were stained with MitoSOX™ Red for 30 min at 37°C incubator. To determine the total GSH content, 8505C cells were stained with mBBr for 10 min in a 37°C incubator. Fluorescence intensity was quantified by flow cytometry (FACSVerse, BD Biosciences,

Franklin Lakes, NJ, USA) within 30 min, and the data were analyzed using FlowJo software (version 10.4.2).

#### **14. RNA sequencing**

Total RNA samples of 8505C cells were duplicated, and processing was performed by Macrogen Inc. (Seoul, Korea; www.macrogen.com). Library was constructed using the TruSeq Stranded mRNA LT Sample Prep Kit (Illumina, San Diego, CA, USA) according to the TruSeq Stranded mRNA Sample Preparation Guide (part #15031047 Rev. E). Next, sequencing was performed following the NovaSeq 6000 System User Guide (Document #1000000019358 v02). The sequence was qualified by FastQC (version 0.11.7), trimmed by Trimmomatic (0.38), and mapped using the HISAT2 (version 2.1.0) program. We assembled gene and transcript expression levels to read counts or fragments per kilobase of transcript per million mapped reads (FPKM) using StringTie (version 2.1.3b). Trimmed mean of M-value (TMM) normalization was performed to reduce systematic bias using read count by the edgeR package library. Finally, the DEGs were estimated using edgeR.

#### **15. ATAC sequencing**

Total RNA samples of 8505C cells were duplicated, and processing was performed by Macrogen Inc. (Seoul, Korea; www.macrogen.com). The sequence was qualified using FastQC (version 0.11.7), trimmed using Trim Galore (version 0.5.0), and aligned using the Bowtie2 (version 2.3.5.1) tool. Peak calling from alignment bam files was performed using MACS2 (version 2.1.1.20160309). Raw BAM files were normalized using the Galaxy tool based on the hg38.blacklist.bed file. The total peak signals from the raw bed files are depicted by ShinyCircos. Transcription start site or Functional elements peak signals were analyzed from computeMatrix in Galaxy tool. These two open sources were acquired from UCSC Genome Browser. The peak signals for each gene were visualized using GBiB tool.

#### **16. Acquisition of scRNA-seq data**

We obtained all the findings of single cell analysis from the GEO database. The scRNA-seq data consisting of thyrocytes from ATC (n=5) and PTC patients (n=7) were acquired from GSE148673 and GSE184362 datasets respectively. ‘Seurat (version 4.3.0)’ and

'DoubletFinder (version 2.0.3)' packages in R software (version 4.1.3) were used for scRNA-seq data preprocessing. First, scRNA-seq expression matrices were inserted into R using 'Read10X'. Quality control of each data was performed to filter out poor-quality cells based on numbers of genes per cell (nFeature), whole number of read counts (nCount) and the read counts percentage of mitochondrial genes per cell (percent\_MT). After eliminating doublets using 'doubletFinder\_v3', the scRNA-seq data were normalized by the 'LogNormalize', and the top 2000 highly variable genes were identified using 'FindVariableFeatures'. Integration of each data was performed using 'IntegrateData'. Information about quality control and percent of doublet are represented in Supplementary Table. 2 in more detail.

### **17. Processing of the scRNA-seq data**

Cell cycle score of each single cell was calculated using 'CellCycleScoring' and integrated data were regressed out to mitigate cell cycle heterogeneity on cell clustering. PCA was utilized with the top fifteen PCA values for dividing clusters using 'RunPCA'. Total seven major cell types were annotated to each cluster according to marker gene expression through 'FindAllMarkers'. Cluster visualization was performed using UMAP algorithm (resolution=0.15). 'DotPlot' was used to plot marker genes to identify each cell cluster identity. 'RunALRA' were performed to recover missing values in cluster of thyrocytes. 'FeaturePlot' was used to compare several genes related to cancer type-specific marker and one carbon metabolism between ATC and PTC.

### **18. Trajectory inference and pseudotime analysis based on TDS score**

To distinguish ATC and PTC in Thyrocyte Cluster, we first calculated TDS score using 'AddModuleScore' and further investigated expression level of several genes. Next, we assigned starting point of the pseudotime analysis based on TDS score using Monocle3

(version 1.3.1) package. Scatter plot of one carbon metabolism genes was created using 'FeatureScatter' along TDS score and pseudotime from PTC to ATC.

**Table1. Sequences of primers used in real-time RT-PCR**

Gene	Direction (5' to 3')	Sequences
<i>PHGDH</i>	F	CTG CGG AAA GTG CTC ATC AGT
	R	TGG CAG AGC GAA CAA TAA GGC
<i>SHMT2</i>	F	ATG TCT ATG CCC TAT AAG CTC AAC CC
	R	GCC GGA AAA GTC GAG CAG T
<i>MTHFD2</i>	F	AGG ACG AAT GTG TTT GGA TCA G
	R	GGA ATG CCA GTT CGC TTG ATT A
<i>MTHFD1L</i>	F	CTG CCT TCA AGC CGG TTC TT
	R	TTT CCT GCA TCA AGT TGT CGT
<i>PSAT1</i>	F	ACA GGA GCT TGG TCA GCT AAG
	R	CAT GCA CCG TCT CAT TTG CG
<i>SHMT1</i>	F	AGG AAA GGA GTG AAA AGT GTG GAT
	R	GAC ACC AGT GTC GCT CTG GAT CTG
<i>MTHFD1</i>	F	AGG ATG TGG ATG GAT TGA CTA GC
	R	CCC TTA GGC GTA CAA GGA ATG
<i>m36B4</i>	F	CGT CCT CGT TGG AGT GAC A
	R	CGG TGC GTC AGG GAT TG

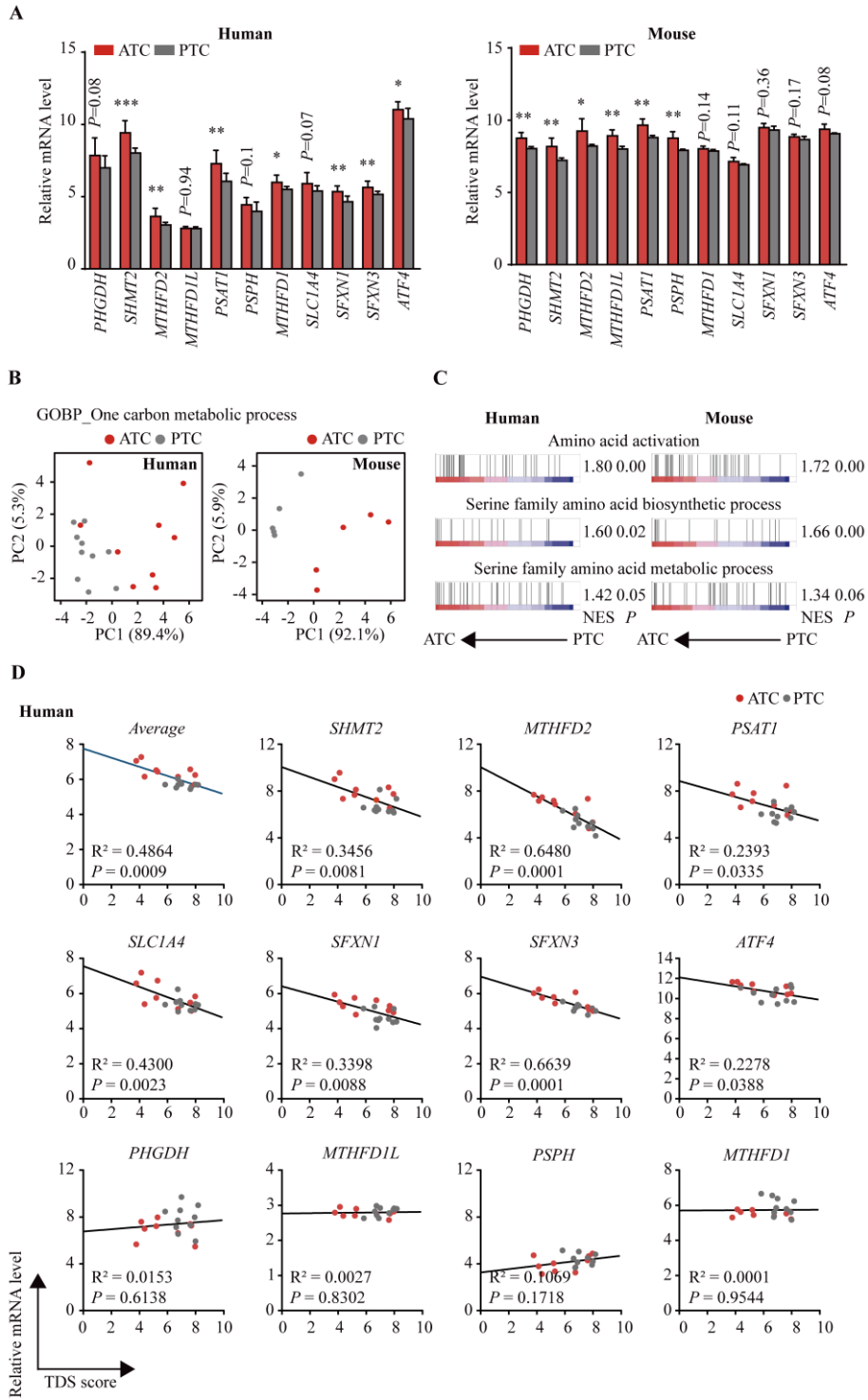
**Table2. Quality control and percent of doublet for single cell analysis**

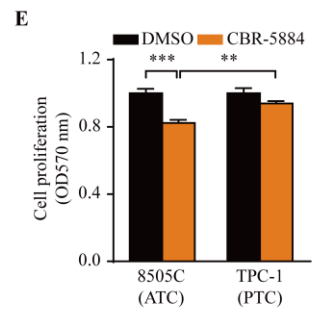
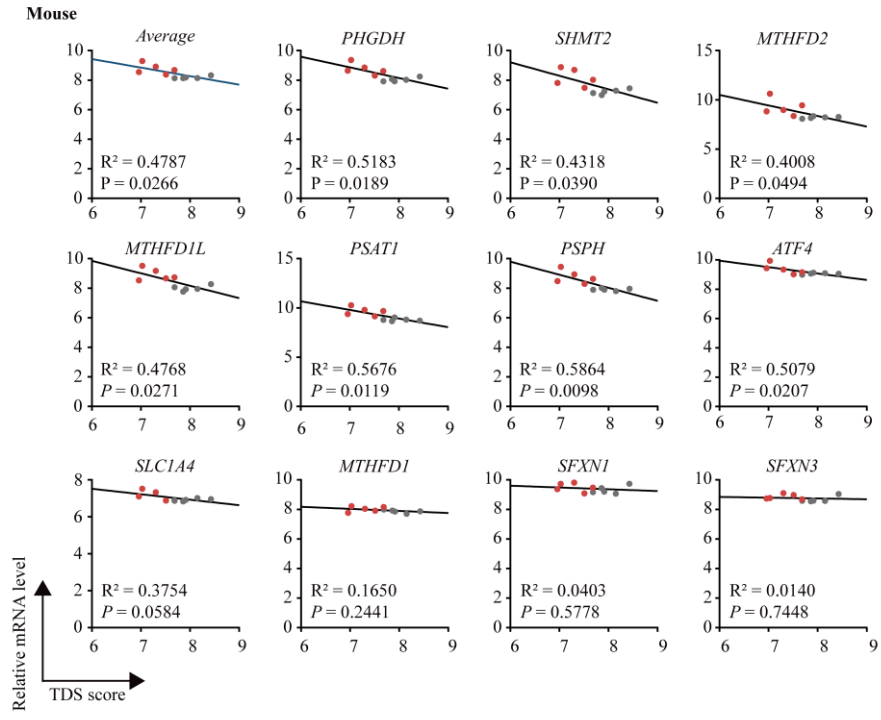
Sample	GSM	Percent		nFeature_RNA	nFeature_RNA	nCount_RNA	Doublet (%)
		MT (<)		(>)	(<)	(>)	
ATC1	4476491	10		500	6000	1000	1.0
ATC2	4476492	10		300	4500	1000	2.5
ATC3	4476493	15		300	6000	1000	1.3
ATC4	4476494	10		500	6000	1000	1.0
ATC5	4476495	10		500	6500	1000	2.5
PTC1	5585102	10		200	3500	1000	2.5
PTC2	5585104	10		200	1700	500	2.5
PTC3	5585107	10		200	2000	500	3.5
PTC4	5585112	10		200	3000	500	2.0
PTC5	5585117	10		200	4000	500	4.5
PTC6	5585119	10		500	4000	500	4.5
PTC_7	5585121	10		200	2000	500	8.0

### III. RESULTS

#### 1. ATC displays enhanced serine and one carbon metabolism dependency compared to PTC

It is well known that PTC histologically progresses to ATC by dedifferentiation (27, 28). To observe divergent characteristics associated with one carbon metabolism between ATC and PTC, we compared levels of total eleven one carbon metabolism genes in human and mouse datasets. mRNA levels of diverse one carbon metabolism-related genes such as *SHMT2*, *MTHFD2*, *PSATI* and *MTHFD1* in ATC were higher than those in patients with PTC. Tamoxifen-inducible TPO-creER;Braf<sup>V600E</sup>/p53<sup>-/-</sup> transgenic mice showing ATC features such as shortened survival and histologic morphology, also revealed high level of one carbon metabolism genes including *PHGDH*, *SHMT2*, *MTHFD2* compared to PTC mice despite different tendency with human (Fig. 1A). In two GEO datasets, we identified distinct pattern of one carbon metabolic process genes between ATC and PTC using principal component analysis (Fig. 1B). We also confirmed several pathways including amino acid activation, serine family amino acid biosynthetic and metabolic process of ATC were enriched compared with PTC in human and mouse, suggesting ATC might increase serine and one carbon metabolism dependency more than PTC (Fig. 1C). We next analyzed correlation between one carbon metabolism genes and the average of total sixteen thyroid differentiation score genes (hereafter TDS score), which represents thyroid function of PTC and significantly declines in ATC (29). We identified average of total eleven one carbon metabolism genes exhibited negative correlation with TDS score in human and mouse, again supporting strong correlation between ATC and one carbon metabolism (Fig. 1D). To further compare the vulnerability to serine synthesis reduction between ATC and PTC, we observed ATC and PTC cell proliferation in condition that the same cell number and concentration of CBR-5884 for 72 h. We confirmed that the ATC cell proliferation through CBR-5884 was more decreased than PTC cell (Fig. 1E). Our data represent ATC might intensify serine and one carbon metabolism availability during differentiation from PTC, which is likely to contribute to defense mechanism against antitumor stress.



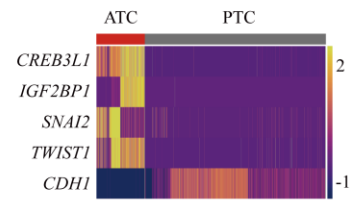
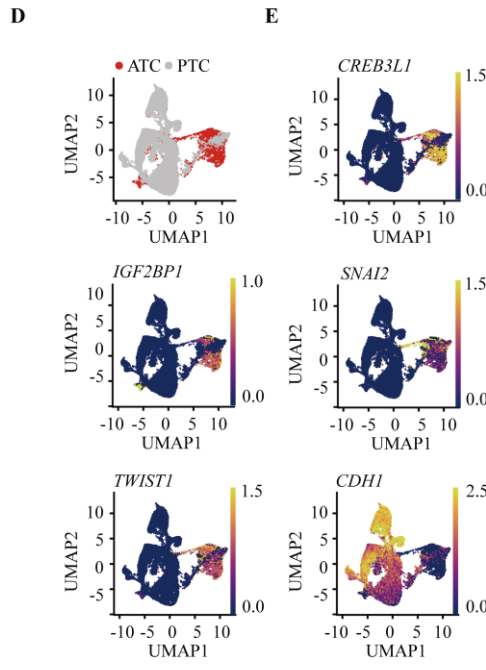
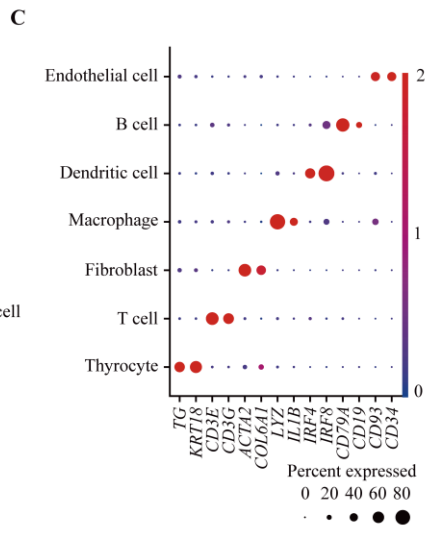
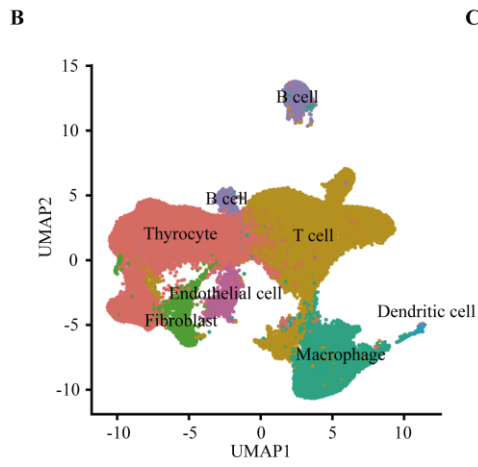
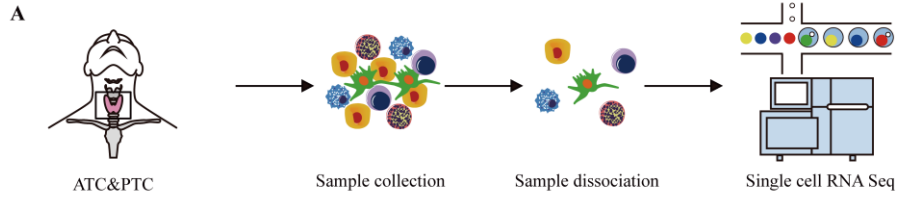


**Figure 1. One carbon metabolism in ATC is more active than PTC.** **A** Bar graphs show mRNA levels of one carbon metabolism-related genes in human and mouse GSE datasets (GSE29265; ATC patients (n=9)/PTC patients (n=10), GSE55933; TPO-creER;Braf<sup>V600E</sup>/p53<sup>-/-</sup> ATC mice (n=5)/TPO-creER;Braf<sup>V600E</sup> PTC mice (n=5)). **B** Principal component analysis represents separation of one carbon metabolic process genes between ATC and PTC. **C** GSEA plots show gene enrichment pattern of amino acid activation, serine family amino acid biosynthetic and metabolic process were increased in human and mouse ATC compared with PTC. **D** The average and several one carbon metabolism genes (*y*-axis) show negative correlation with TDS score (*x*-axis) in human and mouse ATC. The black lines indicate simple linear regression. **E** Two thyroid cancer cells were treated with CBR-5884 (60  $\mu$ M) for 72 h. Cell proliferation was measured by MTT. Data are expressed as the mean S.D. Statistical comparisons were performed using two-tailed Student's *t* test. (\* $P < 0.05$ ; \*\* $P < 0.01$ ; \*\*\* $P < 0.001$ )

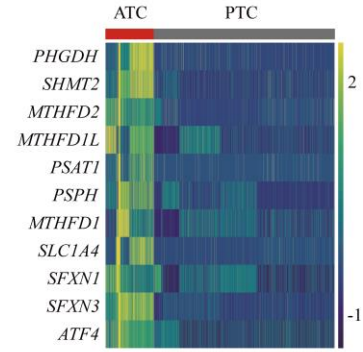
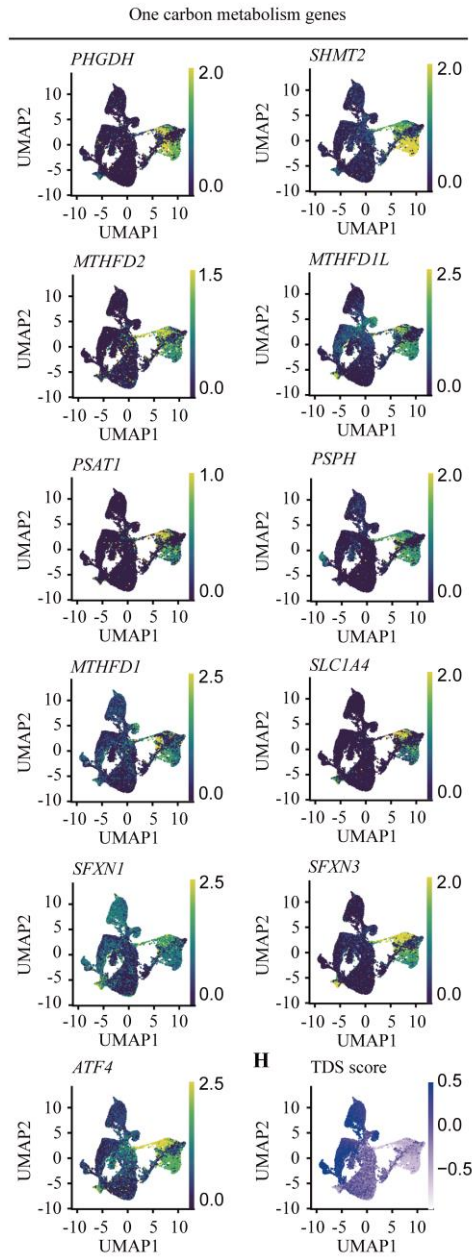
## 2. One carbon metabolism may seem to be intensified according to evolutionary path from PTC to ATC

To investigate possible transition of one carbon metabolism between ATC and PTC in detail, we conducted single cell RNA sequencing (scRNA-seq) analysis to compare expression level of one carbon metabolism genes in ATC and PTC patients GEO datasets. After integrating other datasets including ATC and PTC patients respectively, we first performed cluster annotation in total 75,356 cells including Thyrocyte with marker genes *TG*, *KRT18*; T cell with marker genes *CD3E*, *CD3G*; Fibroblast with marker genes *ACTA2*, *COL6A1*; Macrophage with marker genes *LYZ*, *IL1B*; Dendritic cell with marker genes *IRF4*, *IRF8*; B cell with marker genes *CD79A*, *CD19*; Endothelial cell with marker genes *CD93*, *CD34* (Fig. 2A-C). We next re-clustered total 24,728 thyrocyte cells and identified previously reported *CREB3L1*, *IGF2BP1*, EMT-related markers *SNAI2*, *TWIST1* upregulation and epithelial marker *CDHI* downregulation in ATC cluster (Fig. 2D, E) (27, 30). Interestingly, expression level of total 11 one carbon metabolism-related genes was significantly higher than those in PTC patients (Fig. 7F). These findings led us to investigate evolutionary transition of one carbon metabolism from PTC to ATC progression using trajectory inference and pseudotime analysis. Beforehand, we observed PTC-related genes *LGALS3*, *NPC2* and *S100A13* were expressed along ATC cluster, suggesting that origin of ATC may be partially derived from PTC (Fig. 2G) (27). We next performed trajectory inference and pseudotime analysis, appointing the top of ATC and PTC cluster area as root cells based on TDS score (Fig. 2H). Notably, our monocle3 analysis showed expression level of the average and several one carbon metabolism-related genes increased along pseudotime from PTC to ATC (Fig.2I-K). Based on intensified one carbon metabolism in ATC, we explored fate determination role of one carbon metabolism in ATC and PDTC patients with dedifferentiated and poorly differentiated aggressive thyroid cancer. We identified enrichment of poor prognosis-related genes in one carbon metabolism high groups (Fig. 2L). High group of one carbon metabolism genes exhibited inferior outcome in thirty-five ATC and PDTC patients (Fig. 2M), implying that one carbon

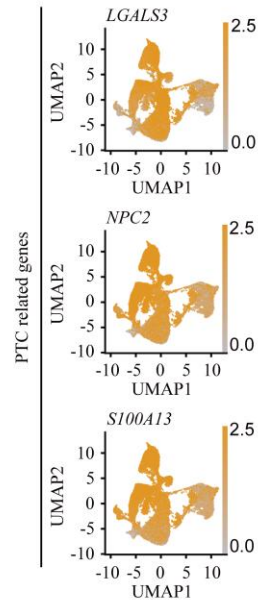
metabolism might be associated with poor prognosis in aggressive thyroid cancer. Collectively, our data suggest ATC might be evolved to employ one carbon metabolism from PTC and this process is plays a pivotal role for tumorigenicity in aggressive thyroid cancer.

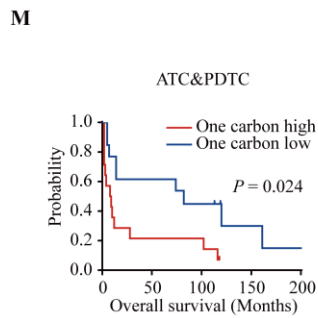
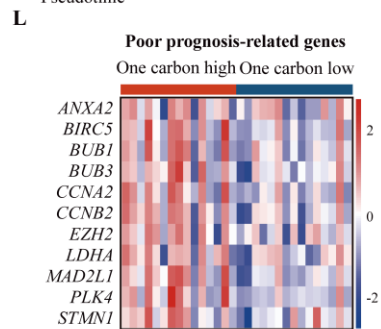
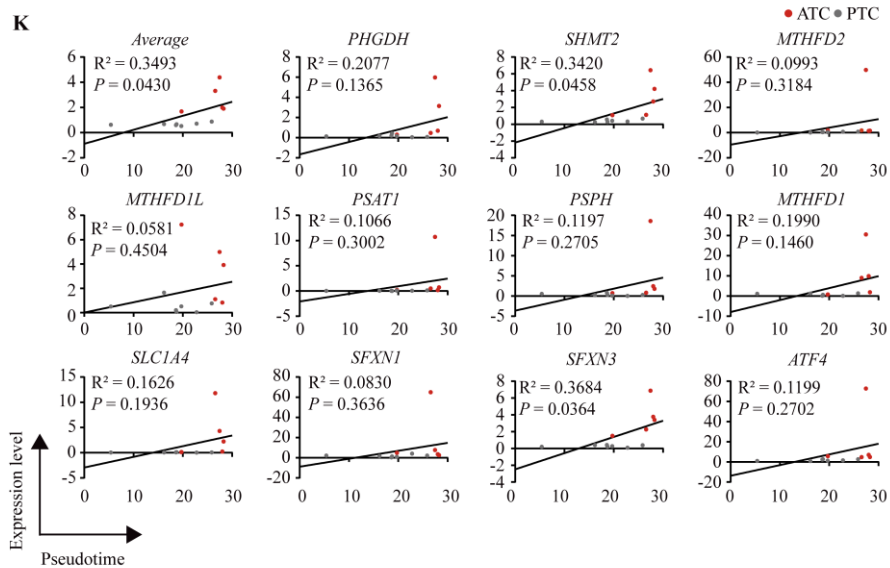
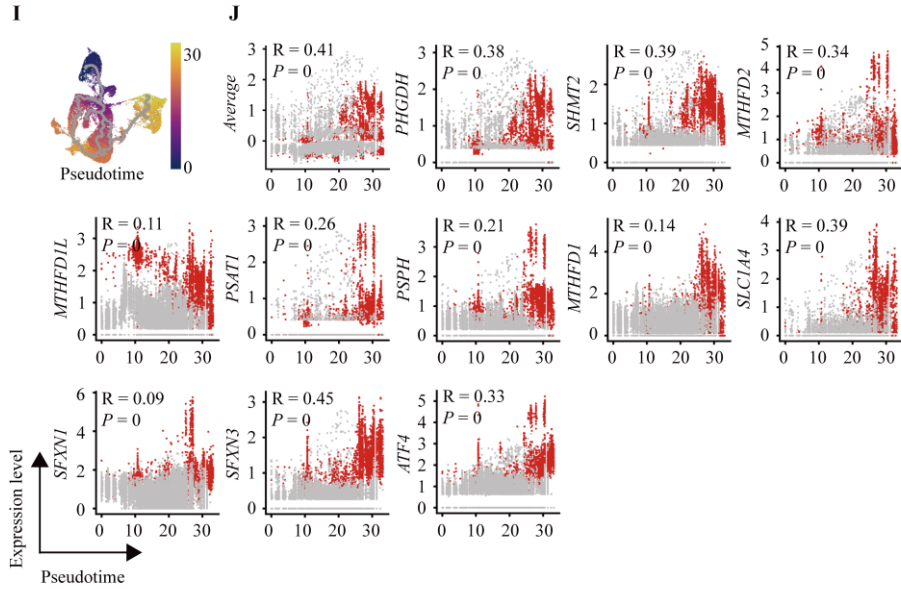


**F**



**G**

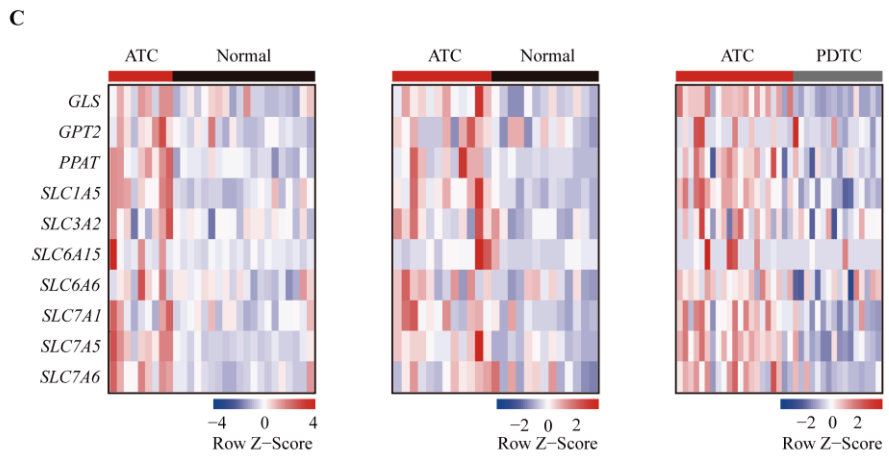
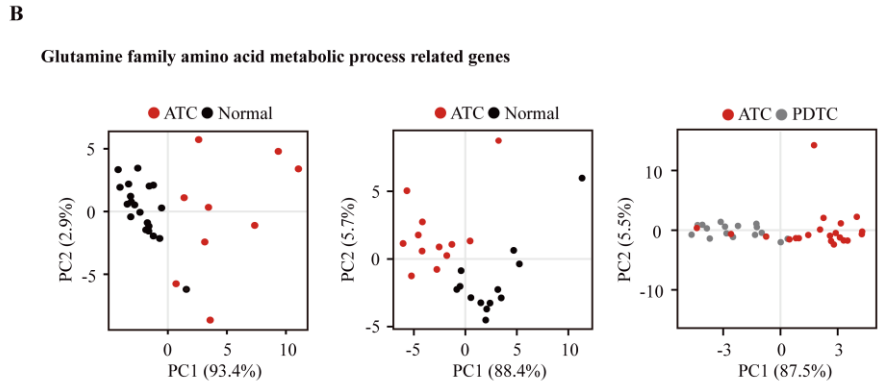
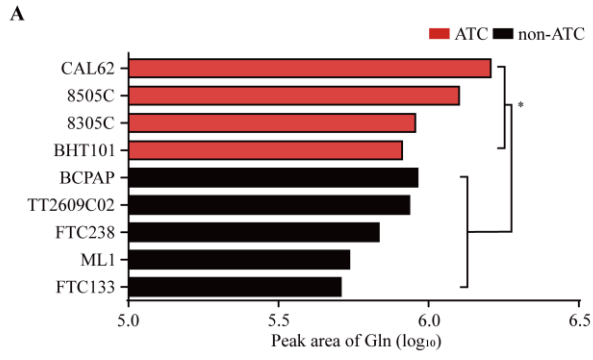




**Figure 2. One carbon metabolism might be strengthened following evolution routes from PTC to ATC.** **A** Workflow diagram shows integration of patients with ATC (n=5) and PTC (n=7) in sc-RNA seq analysis. **B** UMAP shows total clusters in integrated ATC and PTC patients. **C** Dot plot shows dot size meaning the marker expression percentage of cells and the color scale represents the average marker expression total clusters. **D** UMAP of integrated thyrocytes show division of ATC and PTC clusters. **E** UMAP of integrated thyrocytes represent markers for dividing ATC and PTC clusters (left). Heatmap shows the expression level of left panel 5 genes. Color scale means expression level of each gene (right). These five genes are statistically significant. ( $***P < 0.001$ ) **F** UMAP of integrated thyrocytes represent the comparison of total eleven one carbon metabolism-related genes between ATC and PTC clusters (left). Heatmap shows the expression level of left panel 11 genes. Color scale indicates expression level of each gene (right). These 11 genes are statistically significant. ( $***P < 0.001$ ) **G** UMAP show expression level of PTC-related genes. The orange color scale represents expression level of each gene. **H** UMAP of integrated thyrocytes shows decreased TDS score. Blue scale indicates expression level in TDS score genes. **I** Colored scale and gray line in UMAP of monocle3 analysis represent the pseudotime and inferred trajectory respectively from PTC to ATC differentiation. **J** Scatterplot of patients with ATC and PTC represents positive correlation between average expression level of total eleven one carbon metabolism genes ( $y$ -axis) and pseudotime ( $x$ -axis) in single cell level. **K** Average and several one carbon metabolism genes ( $y$ -axis) of ATC and PTC patients show positive correlation with pseudotime ( $x$ -axis) in each patient level. Black lines indicate simple linear regression. **L** Heatmap exhibits one carbon metabolism high groups had enrichment pattern of poor prognosis genes associated with thyroid cancer. Color scale represents expression level of each gene. **M** Kaplan-Meier survival curve shows the overall survival in aggressive thyroid cancer patients separated by one carbon metabolism-related genes high (n=15) and low (n=15) groups. The dataset of ATC and PTC patients is from GSE76039 (ATC (n=18)/PDTC patients (n=17)). Statistical comparisons were performed using ‘FindMarkers’ in R software (**E**, **F**).

### 3. Glutaminolysis was upregulated in patients with ATC

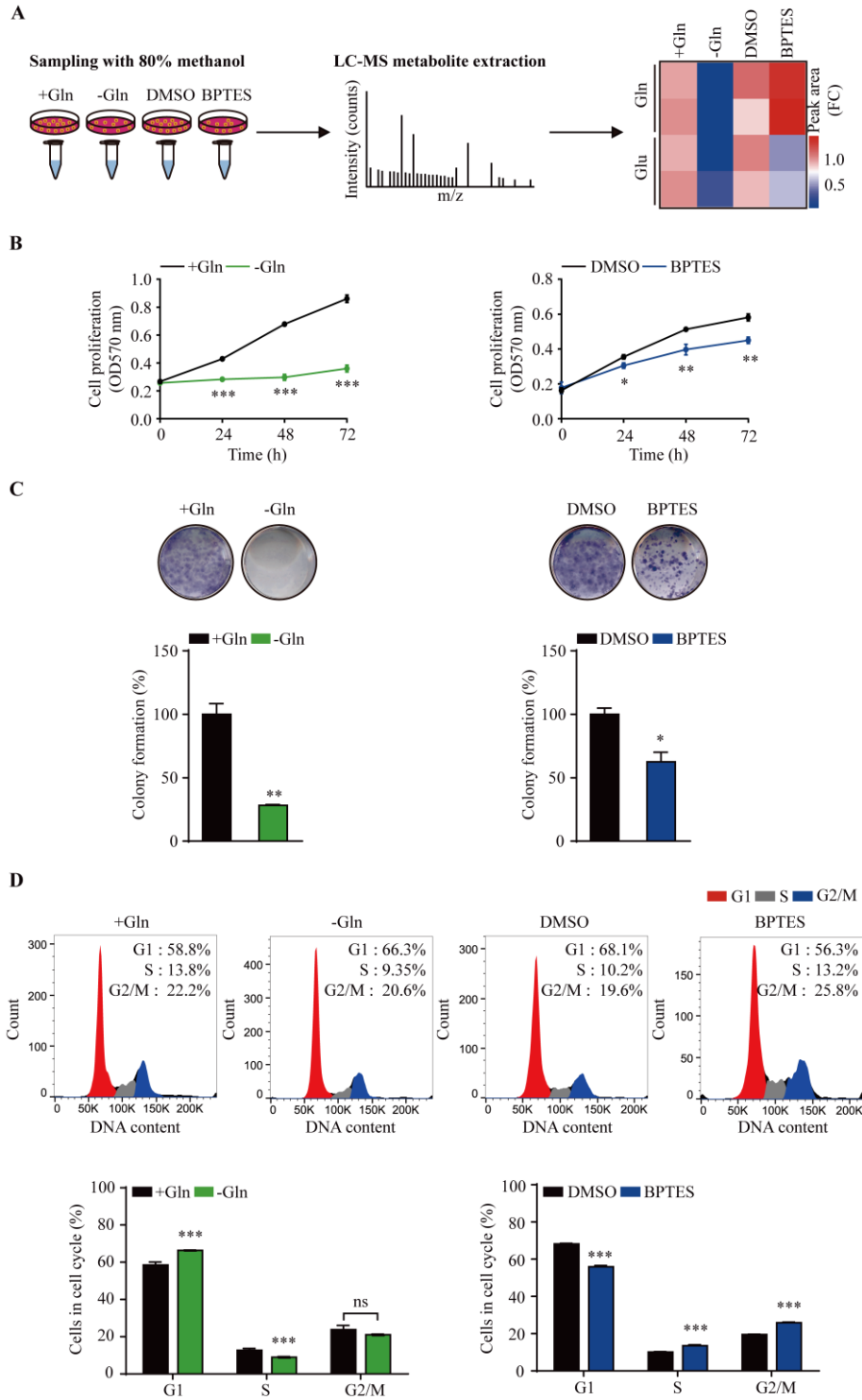
We identified glutamine concentration in total 9 thyroid cancer cell lines through Cancer Cell Line Encyclopedia (CCLE) (31). We observed glutamine level in ATC cell lines was higher than non-ATC groups, indicating that glutamine may be an important energy source for ATC cell metabolism (Fig. 1A) (32). Using Gene Expression Omnibus (GEO) data, we next compared gene expression levels associated with glutamine metabolism between patients with ATC and normal subjects or poorly differentiated thyroid cancer (PDTC) patients, who have an intermediate spectrum of differentiation leading to a longer survival compared to ATC patients (33). Principal component analysis exhibited that patients with ATC had distinct glutamine family amino acid metabolic process-related genes from normal or patients with PDTC (Fig. 1B). Additionally, the expression of glutaminolysis-related genes including *GLS*, *GPT2*, *SLCIA5* was highly upregulated in patients with ATC (Fig. 1C). Our data demonstrate patients with ATC have a high rate of glutaminolysis, which may indicate a high dependency of ATC on glutamine.



**Figure 3. ATC patients exhibit glutaminolysis enhancement.** **A** The bar graph shows comparison of glutamine concentration between ATC and non-ATC cell lines as revealed by CCLE metabolomic data. **B** Principal component analysis represents separation of glutamine family amino acid metabolic process genes in GSE datasets (left : GSE29265; ATC patients (n=9)/ normal subjects (n=20), middle : GSE65144; ATC patients (n=12)/ normal subjects (n=13), right : GSE76039; PDTC patients (n=16)/ATC patients (n=21)). **C** Heatmap shows comparison of glutaminolysis-related genes. The groups are indicated in **(B)**. Color scale means each gene expression level. Statistical comparisons were performed using two-tailed unpaired Student's *t* test. (\* $P < 0.05$ )

#### **4. Inhibition of glutaminolysis compromises ATC cell proliferation**

Based on positive correlation of ATC with glutaminolysis, we hypothesized aberrant glutamine metabolism through glutamine deprivation or GLS1 inhibition through BPTES could inhibit glutaminolysis in 8505C. When we first observed glutamine and glutamate level using LC-MS metabolite analysis, glutamine deprivation significantly decreased intracellular glutamine and BPTES had opposite effect. However, two approaches consistently reduced glutamate level (Fig. 4A), suggesting that glutamine deprivation and BPTES treatment are interchangeable in the case of glutaminolysis impairment (34, 35). Glutamine metabolism inhibition with glutamine deprivation or BPTES markedly reduced cell growth and the number of colonies stained with crystal violet (Fig. 4B, C). To determine why inhibition of glutaminolysis reduces cell proliferation, we investigated cell cycle progression (10, 36). While glutamine deprivation triggered cell cycle arrest by reducing S-phase and enhancing G1-phase fraction, BPTES arrested cell cycle by increasing S-phase and G2/M-phase fraction (Fig. 4D). Our data represents compromised glutaminolysis suppresses cell proliferation through cell cycle arrest in ATC.

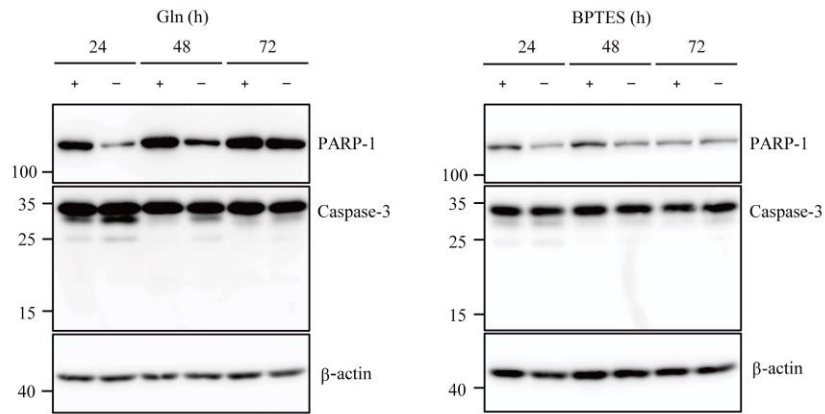


**Figure 4. Inhibition of glutaminolysis impedes ATC cell proliferation.** **A** Workflow depicts sample processing and LC-MS analysis treated with glutamine deprivation medium or BPTES (10  $\mu$ M) for 72 h in 8505C. Heatmap shows peak area of intracellular glutamate and glutamine in indicated groups. The scale means fold change of peak area of metabolite. The images of workflow are acquired from MOTIFOLIO site. **B** Cells were treated with glutamine deprivation or BPTES (10  $\mu$ M) for 72 h. Cell proliferation was measured by MTT. **C** Cells were treated with glutamine deprivation or BPTES (10  $\mu$ M) for 10 days. Colony formation was stained with crystal violet solution and dissolved in methanol for quantification. **D** Cells were treated with glutamine deprivation or BPTES (10  $\mu$ M) for 24 h. Cell cycle analysis was performed by Propidium Iodide staining in flow cytometry (top). Bar graph shows percentage of cells in each cell cycle fraction (bottom). Data are expressed as the mean S.D. of three independent experiments (n=3). Statistical comparisons were performed using two-tailed Student's *t* test. (\* $P$  < 0.05; \*\* $P$  < 0.01; \*\*\* $P$  < 0.001; ns, not significant)

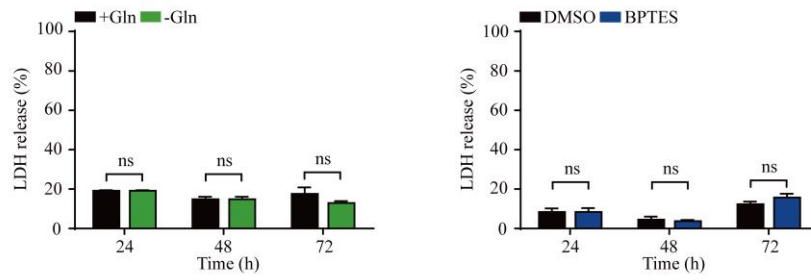
### **5. Glutaminolysis inhibition is not enough to trigger cell death in ATC**

Considering that aberrant glutaminolysis impedes cell proliferation, we next identified whether this cellular stress is accompanied by cell death. When we observed apoptosis marker PARP-1 and caspase-3, cleaved form was not detected. LDH release also did not show significant difference, suggesting that glutamine deprivation and BPTES do not elicit death features in ATC (Fig. 5A, B). When we finally observed DNA fragmentation stained with Hoechst 33342 under glutamine deprivation or BPTES treatment, cell nuclei were intact (Fig. 5C). Altogether, our data represent that inhibition of glutaminolysis fails to induce cell death and elicit significant DNA damage in ATC.

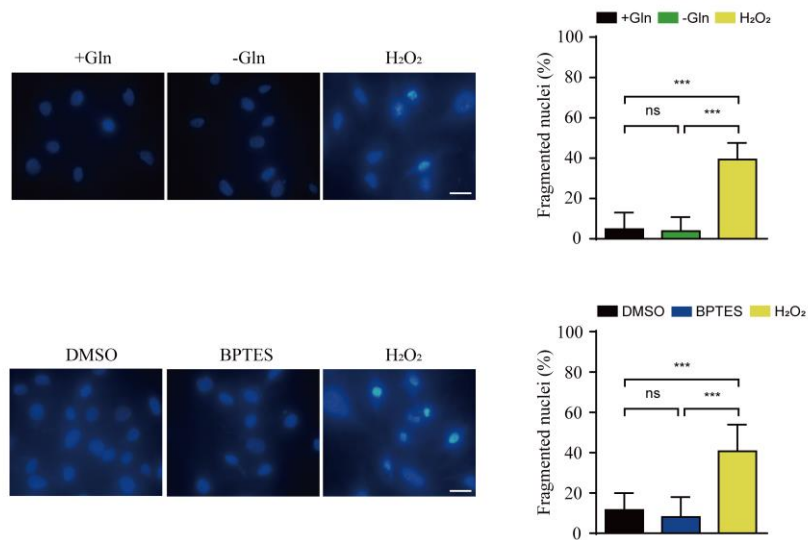
**A**



**B**



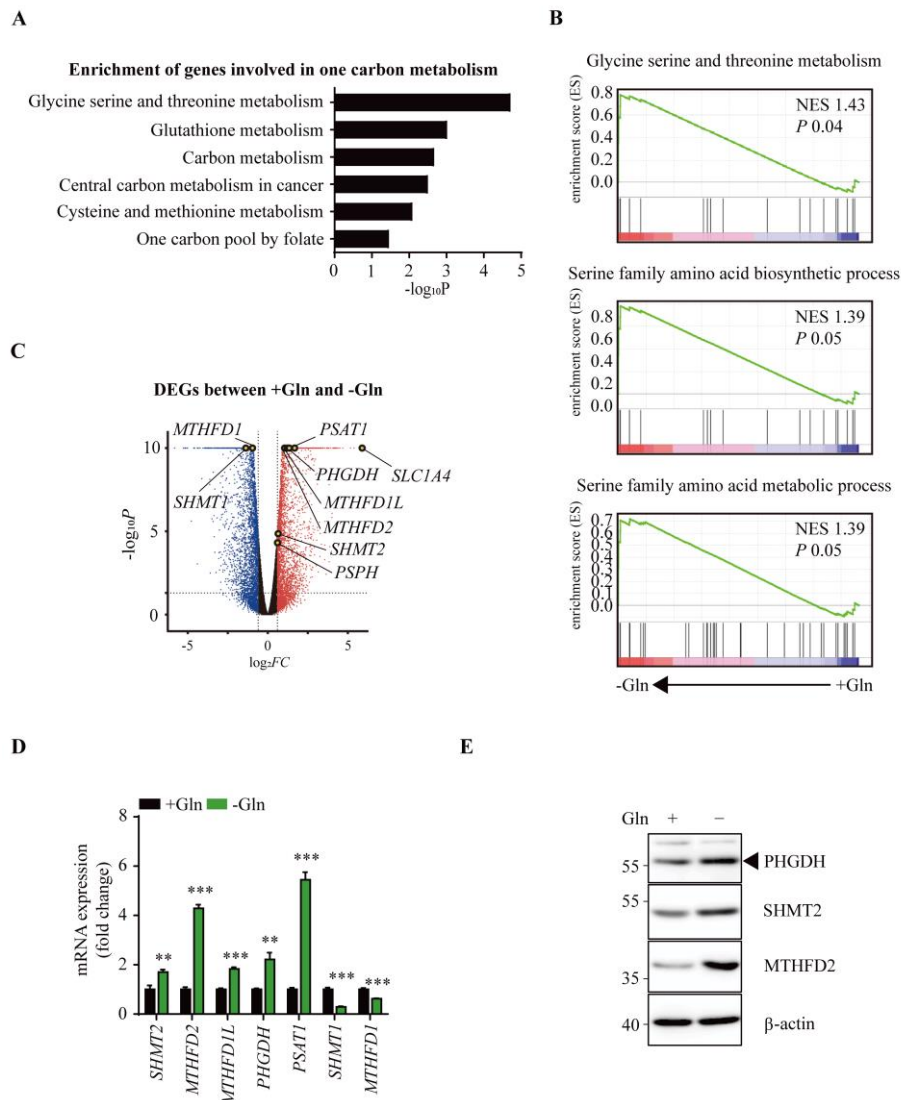
**C**



**Figure 5. Glutaminolysis inhibition is not enough to trigger cell death in ATC. A** Western blots show PARP-1, Caspase-3,  $\beta$ -actin treated with glutamine deprivation or BPTES for 72 h in 8505C. The number left to the immunoblot images indicates the protein size of the immunoband measured for this analysis. **B** Cells were treated with glutamine-free medium or BPTES (10  $\mu$ M) for 72 h. Cytotoxicity was measured by LDH assay. **C** Cells were treated with glutamine deprivation or BPTES (10  $\mu$ M) for 24 h respectively.  $H_2O_2$  (10  $\mu$ M) was used as a positive control. Randomly pictured numbers for quantifying percentage of fragmented nuclei are 10. Scale bar = 20  $\mu$ m. Data are expressed as the mean S.D. of three independent experiments ( $n=3$ ). Statistical comparisons were performed using two-tailed Student's t-test in B and ANOVA followed by Tukey's multiple comparison test in C. (\*\* $P < 0.001$ ; ns, not significant)

## 6. Glutamine deprivation enhances one carbon metabolism in ATC

To identify this signaling pathway, we used differentially expressed genes (DEGs) from cells cultured in glutamine-full and glutamine-free medium. We confirmed glutamine deprivation induced distinct differences in one carbon metabolism-related pathways contributing to tumorigenic effects in cancer cells (Fig. 6A) (24-26). Also, several pathways-related to serine metabolism were enriched in glutamine-deprived cells based on gene set enrichment analysis (GSEA) (Fig. 6B). To further identify gene expression level associated with one carbon metabolism, we performed DEGs analysis and real-time RT-PCR. Glutamine deprivation increased mitochondrial genes such as *SHMT2*, *MTHFD2*, *MTHFD1L* and de novo serine synthesis genes such as *PHGDH*, *PSAT1*, *PSPH* in cytosol. In contrast, cytosolic genes such as *SHMT1* and *MTHFD1* were downregulated (Fig. 6C). Our mRNA and protein level of one carbon metabolism were consistent with DEGs (Fig. 6D, E). In conclusion, 8505C ATC cells upregulate one carbon metabolism under glutamine deprivation-induced nutrient stress.

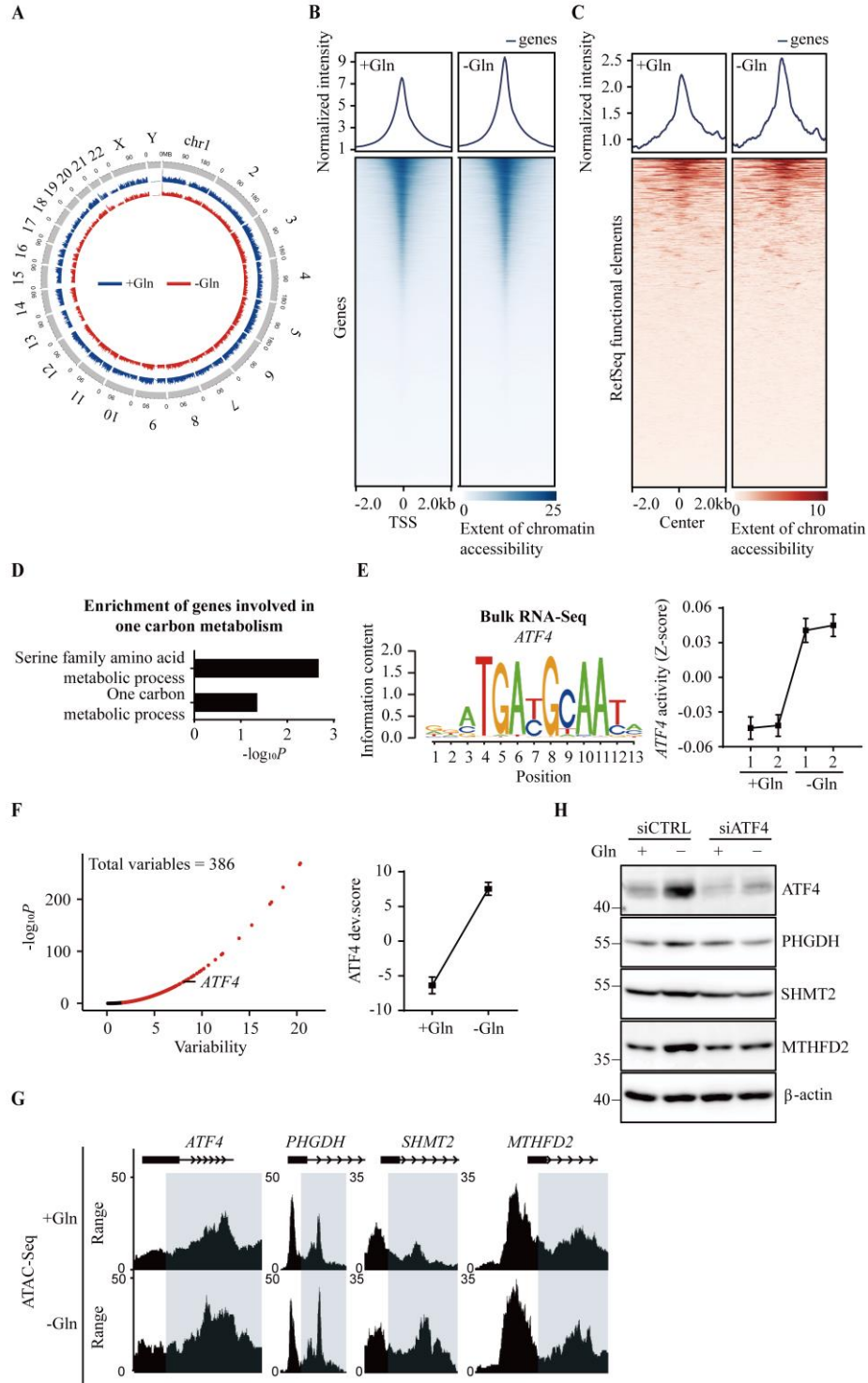


**Figure 6. Glutamine deprivation enhances one carbon metabolism in ATC.** **A** KEGG analysis of DEGs shows one carbon metabolism-related pathways were increased for 24 h glutamine deprivation. **B** GSEA plots show gene enrichment pattern of glycine serine and threonine metabolism, serine family amino acid biosynthetic and metabolic process were increased for 24 h glutamine deprivation. **C** Volcano plot represents up and down of one carbon metabolism-related genes for 24 h glutamine deprivation ( $|\log_2 FC| \geq 0.5$  \* $P < 0.05$ ).

**D** Cells were treated with glutamine deprivation for 24 h. *SHMT2*, *MTHFD2*, *MTHFD1L*, *PHGDH*, *PSAT1*, *SHMT1*, *MTHFD1* mRNA expressions were assessed by real-time RT-PCR. **E** Western blots show PHGDH, SHMT2, MTHFD2,  $\beta$ -actin expressions for 24 h glutamine deprivation. The number left to the immunoblot images indicates the protein size of the immunoband measured for this analysis. Data are expressed as the mean S.D. of three independent experiments (n=3). Statistical comparisons were performed using two-tailed Student's *t* test. (\*\* $P < 0.01$ ; \*\*\* $P < 0.001$ )

## 7. Glutamine deprivation stress promotes ATF4-mediated one carbon metabolism in ATC

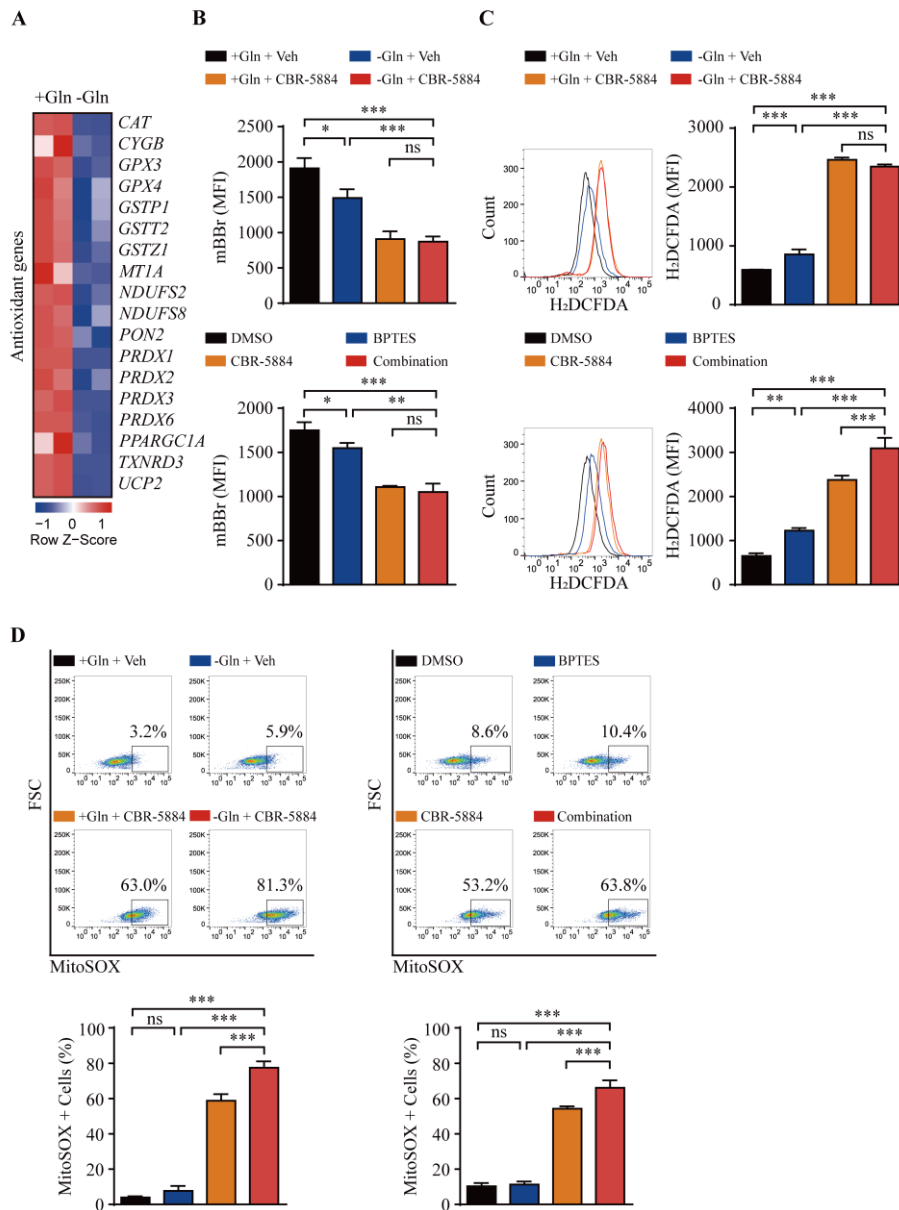
Next, we determined whether gene expression changes via glutamine deprivation are associated with chromatin accessibility, as chromatin modification is a rapid, reversible event that allows cells to adapt to environmental stress such as nutrient deprivation (37). Based on Assays for Transposase Accessible Chromatin with high-throughput sequencing (ATAC-Seq) data, we observed overall peak signals of chromosomes and confirmed no significant change in differential peaks (Fig. 7A). However, glutamine deprivation increased chromatin accessibility at the transcription start site and RefSeq functional elements (Figure. 7B, C). When we next identified regions with modified chromatin accessibility through gene ontology analysis, enrichment of biological processes associated with one carbon metabolism were increased under glutamine deprivation stress (Fig. 7D). ATF4 upregulates one carbon metabolism gene due to transcriptional dysregulation (38-40). As we predicted *ATF4* activity would increase in mRNA-seq analysis under glutamine deprivation (Fig. 7E), we confirmed *ATF4* activity under glutamine deprivation-induced metabolic reprogramming in ATAC-Seq data. Consistent with Integrated Motif Activity Response Analysis (ISMARA), *ATF4* was considered significant in 386 variables, and the developmental score was increased in glutamine deprivation (Fig. 7F). We also observed ATAC-Seq peaks for *ATF4* and downstream factors such as *PHGDH*, *SHMT2*, and *MTHFD2* were high in the absence of glutamine through Genome Browser in a Box (GBiB) (Fig. 7G). Our in vitro experiment directly showed that enhanced one carbon metabolism-related protein through glutamine deprivation was abrogated by genetic inhibition of ATF4 (Fig. 7H), indicating that ATF4 is a critical transcriptional regulator of one carbon metabolism under glutamine deprivation in ATC cells. Our data demonstrate glutamine deprivation upregulates one carbon metabolism pathway, which could be alternative strategy to endure glutamine deprivation-induced metabolic changes in ATC cells.



**Figure 7. Glutamine deprivation enhances ATF4-mediated one carbon metabolism in 8505C ATC cells.** **A** ShinyCircos graph depicts the genome-wide chromatin accessibility on chromosomes in glutamine-full and glutamine-free medium cultured cells for 24 h. **B** The Heatmap shows ATAC-Seq peaks on transcription start site aligned to their centre  $\pm 2$  kb. Color intensity shows extent of chromatin accessibility. **C** Heatmap of ATAC-Seq peaks based on RefSeq functional elements aligned to their centre  $\pm 2$  kb. Cells were treated with glutamine deprivation for 24 h. **D** Gene ontology analysis shows enrichment of biological processes related to one carbon metabolism in glutamine deprivation cells.  $p$ -value is based on the binomial test ( $*P < 0.05$ ). **E** ISMARA motif analysis shows significant activity change of *ATF4* under glutamine-free medium cultured cells for 24 h.  $Z$ -score means motif activity of *ATF4*. **F** *ATF4* motif activity during glutamine deprivation for 24 h was significantly upregulated as revealed by chromVAR. **G** GBiB shows comparison of ATAC-Seq peak signals from indicated genes in glutamine-full and glutamine-free medium cultured cells for 24 h. **H** Immunoblot assay of ATF4, PHGDH, SHMT2, MTHFD2,  $\beta$ -actin in siCTRL and siATF4-transfected cells under glutamine deprivation for 24 h. The number left to the immunoblot images indicates the protein size of the immunoband measured for this analysis.

## **8. Co-inhibition of glutaminolysis and one carbon metabolism compromises redox balance by reducing GSH contents**

Given that one carbon metabolism controls redox balance, which protects cancer cells from growth arrest during diverse stresses (23, 41-43), we next studied one carbon metabolism and its causal relationship with resistance to glutamine metabolism inhibition. We first identified decreased levels of antioxidant-related DEGs such as *CAT*, *TXNRD3*, and *GPX4* (Fig. 8A). Total GSH levels stained with monobromobimane (mBBr) were reduced in the inhibition of glutaminolysis, indicating that glutamine metabolism inhibition only triggers oxidative stress (Fig. 8A, B). We next treated with PHGDH inhibitor CBR-5884 to initiate one carbon metabolism and identified whether inhibition of one carbon metabolism exerts additive effects on GSH decrease (44). CBR-5884 promoted total GSH reduction with inhibition of glutamine metabolism (Fig. 8B). As reduced GSH level triggers cellular ROS increase (45, 46), we compared intracellular ROS levels as revealed by H<sub>2</sub>DCFDA staining. Inhibition of glutamine metabolism increased cellular ROS, which was strongly accumulated by CBR-5884, suggesting the critical role of one carbon metabolism in the regulation of redox balance (Fig. 8C). Since mitochondrial one carbon metabolism including *SHMT2*, *MTHFD2* and *MTHFD1L* were increased during glutamine deprivation, we also observed mitochondrial ROS level (Fig. 6C, D). While inhibition of glutaminolysis did not increase mitochondrial ROS, one carbon metabolism inhibition increased mitochondrial ROS, which was aggravated upon glutamine and one carbon metabolism inhibition (Fig. 8D). Altogether, our data demonstrate that combined inhibition of glutaminolysis and one carbon metabolism induces ROS overload by decreasing antioxidant level and GSH contents in ATC.



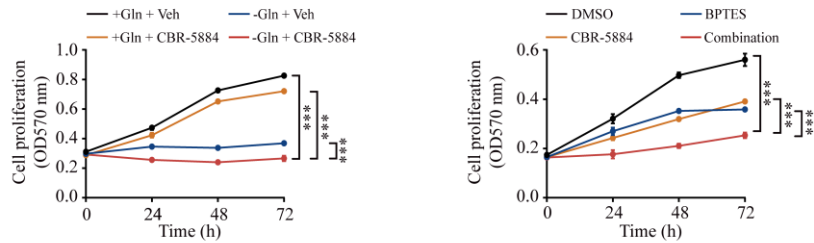
**Figure 8. Co-inhibition of glutaminolysis and one carbon metabolism compromises redox balance by reducing GSH contents.** **A** Heatmap shows decreased level of antioxidant related genes during glutamine deprivation for 24 h in 8505C ATC cells ( $|FC| \geq 1.4$ ,  $*P < 0.05$ ). Row Z-score represents transformed FPKM values. **B** Cells were

treated with indicated groups (glutamine-free medium, BPTES, 10  $\mu$ M; CBR-5884, 60  $\mu$ M) for 24 h. The bar graph shows detection of total GSH levels in indicated groups by mBBr staining (10  $\mu$ M) in flow cytometry. **C** Cells were treated with indicated groups (glutamine-free medium; BPTES, 10  $\mu$ M; CBR-5884, 60  $\mu$ M) for 24 h. Bar graph shows intracellular ROS level in indicated groups by H<sub>2</sub>DCFDA staining (10  $\mu$ M) in flow cytometry. Representative histograms are shown (left panel). **D** Cells were treated with indicated groups (glutamine-free medium; BPTES, 10  $\mu$ M; CBR-5884, 60  $\mu$ M) for 24 h. Bar graph shows mitochondrial ROS accumulation in indicated groups by MitoSOX<sup>TM</sup> Red staining (5  $\mu$ M) in flow cytometry. Representative plots are shown (upper panel).

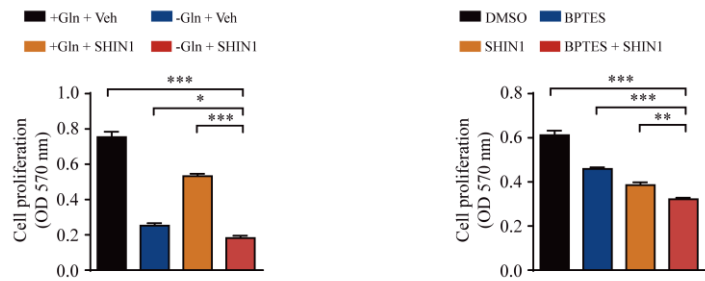
### **9. Co-inhibition of glutaminolysis and one carbon metabolism reduces cell proliferation the most in ROS dependent manner**

We identified co-inhibition of glutaminolysis and one carbon metabolism accumulates ROS the most in ATC. To observe the relationship between ROS accumulation and cell proliferation, we first conducted cell proliferation assay. Co-inhibition of glutamine and one carbon metabolism blocked cell growth more than treated alone (Fig. 9A). This implies that ATC cells employ one carbon metabolism pathway to endure metabolic stress from glutamine metabolism inhibition. This compromised cell proliferation was consistently represented in the one carbon metabolism inhibitors SHMT1/2 and MTHFD2 (Fig. 9B, C). To confirm possible impairment of proliferation due to ROS overload, we treated cells with antioxidant Trolox (47, 48). When Trolox reduced ROS levels, cell proliferation was rescued in combination (BPTES + CBR-5884) treatment (Fig. 9D, E). Our data demonstrate one carbon metabolism is a compensatory pathway to avoid glutamine metabolism inhibition, and excessive ROS via glutamine and one carbon metabolism inhibition is a key factor for blocking tumorigenesis.

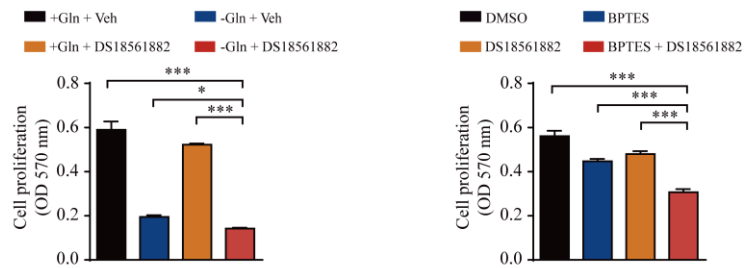
**A**



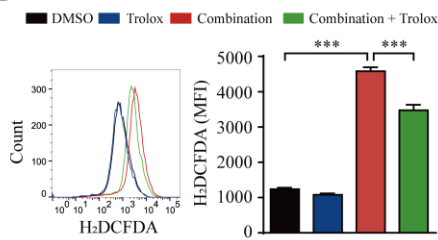
**B**



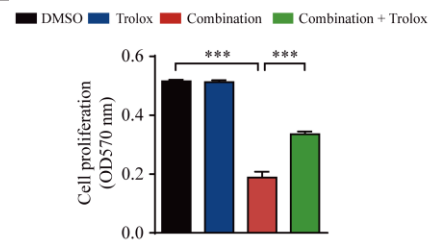
**C**



**D**



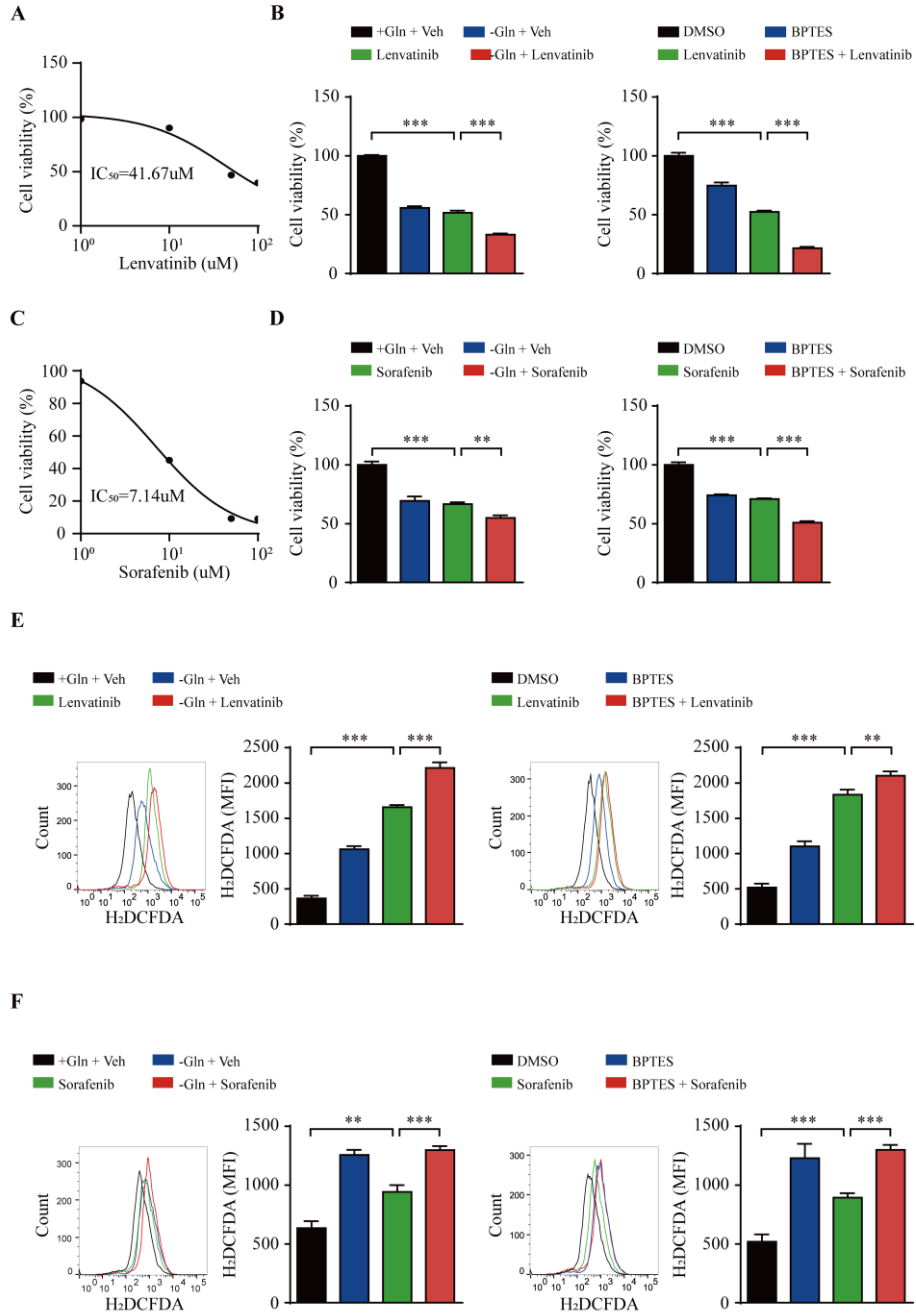
**E**



**Figure 9. Co-inhibition of glutaminolysis and one carbon metabolism reduces cell proliferation the most in ROS dependent manner.** **A** Cells were treated with indicated groups (glutamine-free medium; BPTES, 10  $\mu$ M; CBR-5884, 60  $\mu$ M) for 72 h. Cell proliferation was measured by MTT. **B** Cells were treated with SHIN1 (20  $\mu$ M) under glutamine metabolism inhibition for 72 h. Cell proliferation was measured by MTT. **C** Cells were treated with DS18561882 (60  $\mu$ M) under glutamine metabolism inhibition for 72 h. Cell proliferation was measured by MTT. **D** Cells were treated with indicated groups for 24 h (BPTES, 10  $\mu$ M; CBR-5884, 60  $\mu$ M; Trolox, 25  $\mu$ M). The bar graph shows intracellular ROS level in indicated groups by H<sub>2</sub>DCFDA staining (10  $\mu$ M) in flow cytometry. Representative histograms are shown (left panel). **E** Cells were treated with indicated groups for 72 h (BPTES, 10  $\mu$ M; CBR-5884, 60  $\mu$ M; Trolox, 25  $\mu$ M). Cell proliferation was measured by MTT. Data are expressed as the mean S.D. of three independent experiments (n=3). Statistical comparisons were performed using ANOVA followed by Tukey's multiple comparison test. (\* $P$  < 0.05; \*\* $P$  < 0.01; \*\*\* $P$  < 0.001; ns, not significant)

## **10. Glutaminolysis inhibition only enhances chemotherapy efficacy in ATC**

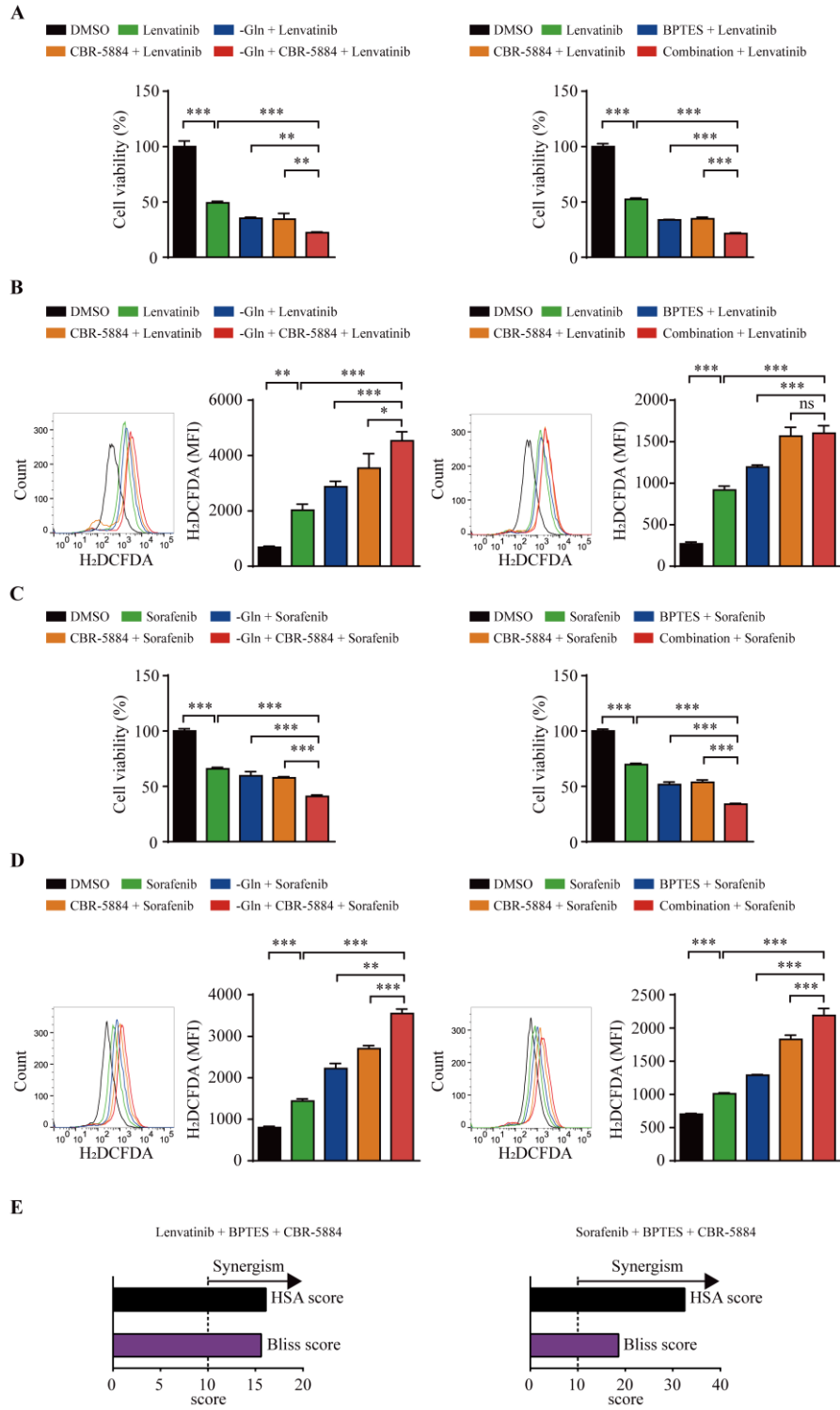
Based on our results that ROS overload disrupts cell tumorigenicity, we studied clinical synergy of co-inhibitory pathways with lenvatinib and sorafenib, which block multi-tyrosine kinases such as Vascular Endothelial Growth Factor Receptor (VEGFR) and Platelet Derived Growth Factor Receptor (PDGFR) in patients with ATC (2, 3). First,  $IC_{50}$  values of two drugs were calculated (Fig. 10A, C) and confirmed the inhibition of glutaminolysis only increases drug efficacy (Fig. 10B, D). Additionally, glutamine metabolism inhibition contributed to additive effect of drug-induced ROS accumulation (Fig. 10E, F). Our data show that glutaminolysis impairment only enhances drug efficacy in terms of cell viability inhibition and ROS overburden.



**Figure 10. Glutaminolysis inhibition only enhances chemotherapy efficacy in ATC.** **A,** **C** Cells were treated with lenvatinib or sorafenib in a dose-range 1-100  $\mu$ M for 48 h.  $IC_{50}$  value of lenvatinib was calculated using GraphPad Prism 9 software. **B** Cells were treated with indicated groups (glutamine-free medium; lenvatinib, 50  $\mu$ M; sorafenib, 10  $\mu$ M; BPTES, 10  $\mu$ M) for 48 h. Cell viability was measured by MTT. **D** Cells were treated with indicated groups (glutamine-free medium; sorafenib, 10  $\mu$ M; BPTES, 10  $\mu$ M) for 48 h. Cell viability was measured by MTT. **E** Cells were treated with indicated groups (glutamine-free medium; lenvatinib, 50  $\mu$ M; BPTES, 10  $\mu$ M) for 9 h. Bar graph shows intracellular ROS level in indicated groups by  $H_2DCFDA$  staining (10  $\mu$ M) in flow cytometry. Representative histograms are shown (left panel). **F** Cells were treated with indicated groups (glutamine-free medium; sorafenib, 10  $\mu$ M, BPTES; 10  $\mu$ M) for 9 h. Bar graph shows intracellular ROS level in indicated groups by  $H_2DCFDA$  staining (10  $\mu$ M) in flow cytometry. Representative histograms are represented (left panel). Data are expressed as the mean S.D. of three independent experiments ( $n=3$ ). Statistical comparisons were performed using ANOVA followed by Tukey's multiple comparison test. (\*\* $P < 0.01$ ; \*\*\* $P < 0.001$ )

### **11. Co-inhibition of glutaminolysis and one carbon metabolism synergistically increases chemotherapy efficacy in ATC**

To identify whether co-inhibition of glutaminolysis and one carbon metabolism enhances chemotherapy efficacy more than glutaminolysis inhibition only, we treated with combination with lenvatinib and sorafenib in 8505C ATC cells. We observed co-inhibition of glutamine and one carbon metabolism most strongly suppressed cell viability and enhanced ROS levels after treatment with chemotherapeutic agents (Fig. 11A-D). To demonstrate that this concept of triple inhibition indeed exerts synergistic effect on cell death, we employed Highest single agent (HSA) and Bliss reference model. We showed that multi-drug combinations elicited synergy effect in lenvatinib and sorafenib-treated ATC cells (Fig. 11E). In conclusion, our data imply combined targeting of glutaminolysis and one carbon metabolism could be efficient in enhancing chemotherapy efficacy by accumulating ROS for ATC.



**Figure 11. Co-inhibition of glutaminolysis and one carbon metabolism synergistically increases chemotherapy efficacy in ATC.** **A** Cells were treated with indicated groups (glutamine-free medium; Lenvatinib, 50 uM; BPTES, 10 uM; CBR-5884, 60 uM) for 48 h. Cell viability was measured by MTT. **B** Cells were treated with indicated groups (glutamine-free medium, Lenvatinib, 50 uM; BPTES, 10 uM; CBR-5884, 60 uM) for 9 h. Bar graph shows intracellular ROS level in indicated groups by H<sub>2</sub>DCFDA staining (10 uM) in flow cytometry. Representative histograms are shown (left panel). **C** Cells were treated with indicated groups (glutamine-free medium; sorafenib, 10 uM; BPTES, 10 uM; CBR-5884, 60 uM) for 48 h. Cell viability was measured by MTT. **D** Cells were treated with indicated groups (glutamine-free medium; sorafenib, 10 uM; BPTES, 10 uM; CBR-5884, 60 uM) for 9 h. Bar graph shows intracellular ROS level in indicated groups by H<sub>2</sub>DCFDA staining (10 uM) in flow cytometry. Representative histograms are shown (left panel). **E** Cells were treated with indicated single drug (lenvatinib, 50 uM; sorafenib; 10 uM; BPTES, 10 uM; CBR-5884, 60 uM) for 48 h. The synergistic effects of multiple drugs were confirmed using HSA and Bliss model. Data are expressed as the mean S.D. of three independent experiments (n=3). Statistical comparisons were performed using ANOVA followed by Tukey's multiple comparison test. (\* $P < 0.05$ ; \*\* $P < 0.01$ ; \*\*\* $P < 0.001$ ; ns, not significant)

#### IV. DISCUSSION

Despite many candidate drugs continuously show chemotherapeutic possibilities, establishing proper targeted therapy remain unclarified on account of molecular drivers for tumorigenesis and high rate of metastasis in ATC patients (2, 49, 50). Immunotherapy has recently arisen in the treatment of ATC such as spartalizumab and pembrolizumab targeting PD-1 and PD-L1 interaction. Nonetheless, limitations to immunotherapy showing discouraging results with chemotherapy and expensive cost lead to other strategy for overcoming ATC pathogenesis (51-53). Therefore, scrutinizing molecular details to improve in prognosis of ATC patients is indispensable.

It was reported that PTC patients had a high expression of glycine and serine metabolism-related proteins such as PHGDH, PSAT1, PSPH and SHMT1 (54, 55). In our analysis to study one carbon metabolism process between ATC and PTC, we observed one carbon metabolism-related genes and serine family amino acid process in ATC were higher compared with PTC, which led us to hypothesize that evolutionary transition might provoke enhancement of one carbon metabolism in ATC. Indeed, single cell analysis showed expression level of one carbon metabolism-related genes in ATC cluster was higher more than PTC. Furthermore, pseudotime inference analysis based on TDS score exhibited the increase of average and several one carbon metabolism genes along the pseudotime from PTC to ATC. In ATC and PDTC groups with inferior prognosis compared with well-differentiated PTC, we confirmed one carbon metabolism contributes to poor outcome in aggressive thyroid cancer patients.

ATC shows higher metabolic activity compared with other thyroid cancers. Additionally, level of GLS1 and GDH is the highest in ATC among patients with thyroid cancer, we thought glutaminolysis impairment might trigger significant damage, leading to cell death (7, 56). In publicly available CCLE and GEO datasets, we identified level of glutamine was significantly high among other cancer types and ATC was especially higher compared to non-ATC thyroid cell types (31). Patients with ATC also had a higher expression of glutaminolysis-related genes than normal subjects or patients with PDTC.

However, we observed one carbon metabolism serves as an endurable strategy to compensate for rapid turnover of 8505C under glutamine metabolism inhibition. There are several mechanisms by which cancer cells synthesize serine, a major donor of one carbon metabolism under diverse environmental stresses. They tend to acquire serine via uptake through transporters, glycolysis, autophagy activation, and others (23, 26, 57, 58). Therefore, it is necessary to investigate the main pathway driving serine synthesis under our experimental conditions. We also observed decrease in the mRNA levels of *SHMT1* and *MTHFD1*, similar with previous papers. These proteins consume formate to entail several tumorigenic pathways in the cytosol. Therefore, direct role of formate, a byproduct of one carbon metabolism, on cell fate needs to be studied (57, 59, 60).

Since cancer cells undergo metabolic reprogramming to adapt to nutrient changes, many investigations targeting cancer cell metabolism have been reported (16, 61, 62). Metabolic adaptation is usually achieved through changes in gene expression. This event occurs through epigenetic modification, which represents a rapid and reversible response and involves diverse enzymes including histone (de)methylases, (de)acetylases, and DNA. Indeed, genes on- and off-systems are rapidly controlled by dynamically changing chromatin architecture in response to nutrient stress (63, 64). Our bioinformatic data analysis showed glutamine deprivation increased the transcription start site and RefSeq functional element peak, which suggests an elevation of transcription factor activity via chromatin opening. We confirmed ATF4 levels were notably increased, and one carbon metabolism was positively controlled through ATF4 in the genetic inhibition experiment.

GSH is a predominant enzyme protecting cancer cells from oxidative stress (45, 46). We observed inhibition of glutamine metabolism decreased total GSH contents. Many signaling pathways involving NADPH production such as pentose phosphate pathway (PPP), and one carbon metabolism synthesize GSH in cancer cells (43, 65). Previous studies showed effect of glutamine deprivation on PPP deactivation in cancer and ROS increase during PPP inhibition in thyroid cancer (10, 66, 67). We accordingly consider the

possibility that PPP is deactivated and thereby GSH contents are decreased upon glutamine deprivation despite our observation that one carbon metabolism is responsible for GSH loss. Based on predominant antioxidant function of GSH, we hypothesized GSH content loss is responsible for significant ROS accumulation in glutamine and one carbon metabolism. We also demonstrated ROS is directly involved in cell proliferation following Trolox treatment. Our results were consistent with those of previously reported other cancer types such as glioblastoma or leukemia (22, 23).

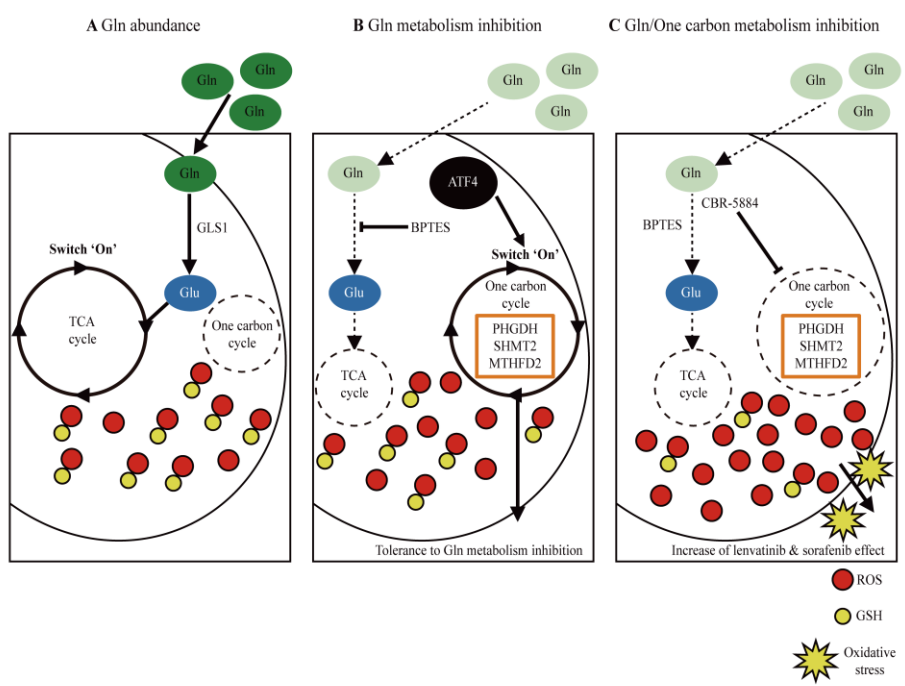
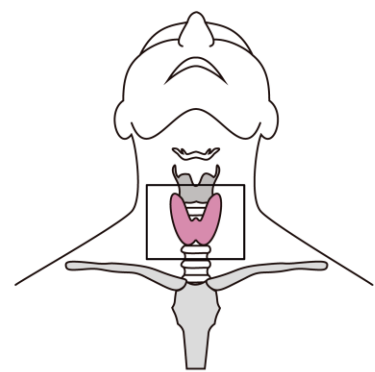
Lenvatinib and sorafenib are chemotherapeutic reagents targeting multi-tyrosine kinases for ATC. Several clinical studies have reported monotherapy with a multi-tyrosine kinase inhibitor is not recommended for mild effects in patients with ATC (68, 69). Recently, many investigations have shown combination treatment with these drugs is more effective than drug monotherapy for ATC (70-73). We also showed co-inhibition of glutamine and one carbon metabolism increased the efficacy of lenvatinib and sorafenib. In addition, combinational inhibition of glutamine and one carbon metabolism synergistically induced ROS accumulation, which might contribute to tumor suppression with chemotherapy reagents. Despite the lack of reported cases in patients with ATC, glutamine levels in most cancers gradually decrease with increasing distance from a blood vessel, indicating possible occurrence of one carbon metabolism activation in the central tumor microenvironment (23, 74). Thus, our concept of co-inhibition of glutamine and one carbon metabolism may contribute to the development of a therapeutic strategy for ATC.

It was reported that PTC patients had a high expression of glycine and serine metabolism-related proteins such as PHGDH, PSAT1, PSPH and SHMT1. In conclusion, our study represent ATC might increase availability of one carbon metabolism leading to escape from diverse stresses such as metabolic stress and anticancer drug.

## V. CONCLUSION

In this study, data show that one carbon metabolism was gradually more active during progression from PTC to ATC and acts as alternative strategy against glutamine deprivation stress. **A** In glutamine rich status, cells use glutamine as a metabolite for cell growth. glutamine is recruited to tricarboxylic acid cycle, which controls antioxidant genes including GSH and supply diverse nutrients to cells. **B** In glutamine metabolism inhibition via glutamine deprivation or BPTES treatment, antioxidant-related genes including GSH decrease leading to redox imbalance. Nonetheless, ATF4-dependent one carbon metabolism makes redox imbalance mild and acts as an alternative strategy to tolerate to glutamine metabolism inhibition stress. **C** In co-inhibition of two pathways, excessive ROS aggravates the severity of anti-proliferation. it can increase lenvatinib and sorafenib-induced cell death through oxidative stress in 8505 ATC cells. The image of thyroid gland is acquired from MOTIFOLIO site.

**PTC**  **ATC**  
**One carbon metabolism**



**PART2. One carbon metabolism promotes immunosuppressive molecular signatures of inflammatory cancer-associated fibroblasts to drive epithelial-mesenchymal transition in colorectal cancer.**

Yeseong Hwang

*Department of Medical Science  
The Graduate School, Yonsei University*

(Directed by Professor Sungsoo Fang)

## **I. INTRODUCTION**

Colorectal cancer (CRC) is the third most common cancer type with second leading causes of cancer-associated inferior prognosis worldwide. Although numerous treatments including surgical resection, chemotherapy, radiation strategies are currently applied to CRC patients, new treatment options are still needed to enhance efficiency of therapy and safety (75, 76). Patients with CRC commonly develop liver or lung metastasis accompanied by epithelial-mesenchymal transition (EMT). EMT plays an important role in tumor development during which epithelial cells are switched into mesenchymal cells leading to migration and invasion. During EMT, diverse types of cells around the tumor including fibroblast, endothelial cells, and immune cells secrete several growth factors and cytokines, so that they contribute to tumor metastasis (77-80). Therefore, scrutinizing the mutual communication in tumor microenvironment (TME) components is very important for metastasis suppression in CRC patients.

Cancer-associated fibroblasts (CAFs) is the most abundant component in TME. They usually form extracellular matrix (ECM) and grow rapidly than normal fibroblasts. They are involved in oncogenic signaling such as immunosuppression, metabolic reprogramming, and promotion of metastatic cascades (81-83). CAFs are principally

divided into two types: inflammatory CAFs (iCAFs) and myofibroblastic CAFs (myCAFs). iCAFs are histologically distal to TGF- $\beta$  producing tumor and mainly activated by IL-1 $\alpha$  (81). They have high expression of cytokines and growth factors such as IL-6, CXCLs, VEGFs, and FGFs and secrete them around the TME components. These cytokines trigger diverse signals including immune cell recruitment, EMT, and IL-6/JAK/STAT signaling (81, 84-86). MyCAFs exhibit direct contact with tumor and are mainly activated by TGF- $\beta$ /SMAD2/SMAD3. They upregulate myogenesis, collagen formation, ECM organization, and focal adhesion (81, 84, 87). All two types of CAFs elicit tumor-promoting and suppressing effects respectively depending on cancer types and cellular conditions. While iCAFs expressing high level of osteoglycin reduces EMT and subsequent favorable outcome in pancreatic adenocarcinoma, iCAFs enhances cytokines secretion such as CXCL1, 2 leading to radiotherapy resistance (88-91). In the case of myCAFs, type 1 collagen expressing myCAFs restrain tumor progression by mechanically suppressing tumor spread in pancreatic ductal adenocarcinoma and CRC. However, myCAFs expressing ACTA2 accelerate aggressive phenotype of tumors by reducing chemotherapy response in pancreatic ductal adenocarcinoma (86, 92). Thus, investigating CAFs pathophysiology in accordance with TME is very important for improving therapy response and survival rate in cancer.

Recently, single cell analysis technique reveal that CAFs are dramatically heterogeneous and have plastic systems. For example, many types of CAFs such as antigen presenting CAFs, adipogenic CAFs, tumor-associated macrophage CAFs, and endothelial CAFs were annotated by specific gene markers. Pseudotime trajectory inference also showed CAFs origin can be diverse TME components and switched each other depending on cancer types and cellular contexts: iCAFs to myCAFs or vice versa. Likewise, single cell analysis provided clues to understand CAFs heterogeneity including their origin and biological features (93-96).

One carbon metabolism is important physiological process for tumorigenicity in many types of cancers. Serine, a major donor of one carbon metabolism, is directly into tumor

cells by serine uptake transporters or synthesized from glycolysis or gluconeogenesis-derived 3P (26). Serine is involved in GSH synthesis to reduce oxidative stress through SHMT2, MTHFD2, and MTHFD1L in mitochondria. It also contributes to purine and DNA synthesis through MTHFD1, TYMS etc in cytosol, which provide energies for tumor progression (24, 25). CRC patients with one carbon metabolism high genes such as *PHGDH*, *ATIC* and *SUCLG2* also exhibit inferior prognosis (97, 98). In addition, dietary methionine restriction for one carbon metabolism inhibition, which compromise nucleotide synthesis and redox balance, also sensitizes CRC to 5-fluorouracil chemotherapy in PDX mouse models (99). Nonetheless, the role of one carbon metabolism in TME is sparsely deciphered compared to many studies about modulation of one carbon metabolism in tumor cells. Here, we found that iCAFs phenotype is predominant in one carbon metabolism high fibroblast (OHF) compared to one carbon metabolism low fibroblast (OLF) cluster, which mainly secrete *CXCL12* leading to EMT promotion in patients with CRC. Also, *CXCL12/CXCR4* signaling was strongly appeared in T cell and macrophage, which might induce immunosuppressive effects leading to enhanced EMT process. Our findings demonstrate inhibiting one carbon metabolic process by targeting iCAFs could exert anti-tumorigenic potential in patients with CRC.

## **II. MATERIALS AND METHODS**

### **1. Acquisition of scRNA-seq data**

We acquired all the single cell RNA-seq data of CRC patients from the Gene Expression Omnibus (GEO) database. The GEO accession number is GSE144735. ‘Seurat (version 4.3.0)’ package in R software (version 4.1.3) was used for scRNA-seq data preprocessing. First, we imported ‘preprocessed scRNA-seq expression matrix tsv file’ into R. The scRNA-seq data were normalized by the ‘NormalizeData’, and the top 2000 highly variable genes were confirmed using ‘FindVariableFeatures’. Integration of each data was conducted using ‘IntegrateData’.

### **2. Processing of the scRNA-seq data**

Principal Component Assay was performed for discriminating clusters for using ‘RunPCA’. Next, annotation was conducted based on marker gene expression through ‘FindAllMarkers’ in total 14 major cell types. The annotated clusters were visualized using UMAP algorithm (resolution=0.4). Expression of marker genes in each cell cluster identity was represented in ‘DotPlot’. ‘FeaturePlot’ was used to compare several genes associated with one carbon metabolism in fibroblast clusters.

### **3. Measuring DEGs between OHF and OLF group**

We performed subclustering analysis after dividing fibroblast clusters into OHF and OLF using ‘RenameIds’. ‘FindMarkers’ were used to extract DEGs with logFC value higher than 0.25. We used EnrichR web-based tool to confirm top ten transcription factor associated with upregulated DEGs in OHF group. To perform protein-protein interaction network analysis using upregulated DEGs in OHF group, we used STRING web-based tool and Cytoscape. After adjusting the cutoff value for combined score being 0.9 in STRING,

image was edited in Cytoscape. We employed ‘DoROtheEA (version 1.6.0)’ to compare the activity of TF-related to EMT.

#### **4. ssGSEA analysis**

R package ‘escape (version 1.4.0)’ analysis was employed to compare pathway enrichment between OHF and OLF group according to the developer’s vignette. The molecular signature database of hallmark, keg, and gobp was from ‘MSigDB’. ‘stat\_compare\_means’ was used to identify p-values and significance level.

#### **5. CellChat analysis**

R package CellChat (version 1.6.1) was used to explore cell-cell communication between fibroblast and other cell types according to the developer’s vignette. Incoming and outgoing signal of CXCL were visualized in Chord diagram using ‘netVisual\_chord\_cell’. Inferring the outgoing signal of CXCL from fibroblast to other cells were confirmed using “netVisual\_bubble”.

#### **6. Trajectory inference and pseudotime analysis**

Based on *CREB3LI* expression, we assigned ‘C9’ as starting point and further investigated correlation between pseudotime and expression level of iCAF/myCAF-related genes through ‘FeatureScatter’ in Monocle3 (version 1.3.1). The iCAFs signature and EMT score values were calculated using ‘AddModuleScore’.

#### **7. Visium spatial transcriptomics**

We used publicly available gene-spot matrices of 3 CRC patients which were processed ST data from ST and Visium samples. The GEO accession number is GSE226997. The data

were analyzed with the ‘Seurat (version 4.3.0)’ package in R. First, we imported ‘tissue image png file’ into R using ‘Read10X\_Image’. We also imported ‘preprocessed ST data matrix h5 file’ into R using ‘Load10X\_Spatial’. The ST data were normalized by the ‘NormalizeData’, and the top 2000 highly variable genes were identified using ‘FindVariableFeatures’. Next, PCA was performed for dividing clusters for using ‘RunPCA’ and made nearest neighbors for graph clustering using ‘FindNeighbors’. We acquired cell subtypes using ‘FindClusters’ (resolution = 0.5) and confirmed expression matrix using ‘RunUMAP’. Signature scoring of iCAFs signature, EMT score was acquired with the ‘AddModuleScore’. Spatial feature expression plots were acquired using ‘SpatialFeaturePlot’. Based on *SPARC* expression level, we identified fibroblast cluster and confirmed correlation between iCAFs signature and EMT score using ‘FeatureScatter’.

#### **8. Data sources of expression data and CCLE metabolomics**

Total two gene expression datasets for comparing one carbon metabolic process between tumor and normal subjects were retrieved from GSE20916 and GSE81558. The dataset for observing expression level of iCAFs and EMT genes in patients with liver metastasis was acquired from GSE41258. CPTAC protein database was acquired from [https://linkedomics.org/data\\_download/CPTAC-COAD/](https://linkedomics.org/data_download/CPTAC-COAD/). CCLE metabolomics data for identifying serine concentrations in diverse cancer types were obtained from <https://sites.broadinstitute.org/ccle>.

#### **9. Overall survival analysis**

All the survival data represented here except for CRC patients with stage 3 and 4 were acquired from cSurvival platform. After selecting TCGA-COAD, we used ‘mode of analysis’ function to identify survival rate according to average expression of multiple genes. Also, we performed survival analysis through REACTOME or GOBP pathway using ‘select database’ function. Survival data of CRC patients with stage 3 and 4 were retrieved from Kaplan-Meier Plotter. All the survival graphs were edited from Prism9.

#### **10. Cell culture and treatment**

DLD1, HCT-15, HCT-116, HT29, LOVO, and SW480 were obtained from KLCB (Korean

Cell Line Bank, Seoul, Korea). The cells were grown in RPMI-1640 medium (10-013-CV, Corning, NY, USA)-1% penicillin-streptomycin (15140122, Gibco, Waltham, MA, USA) supplemented with 10% fetal bovine serum (35-015-CV, Corning, NY, USA). Cells were tested for mycoplasma elimination using a Plasmocin solution (ant-mpt, Invivogen, San Diego, CA, USA). For in vitro treatment, following concentration was employed: CBR-5884 (HY-100012, MedChemExpress, Monmouth, Oregon, USA), 60  $\mu$ M.

#### **11. Cell proliferation assay**

All the cells ( $3 \times 10^3$  cells/well) were seeded in 96-well plates for proliferation. Cells were treated with DMSO or CBR-5884 for 72 h. Cells were incubated for 1 h in a 37°C incubator after addition of 10  $\mu$ l of CCK-8 solution (Dojindo Laboratories, Kumamoto, Japan) and the absorbance was measured at 450 nm using a Multiskan GO spectrophotometer (51119300, Thermo Fisher Scientific, Waltham, MA, USA).

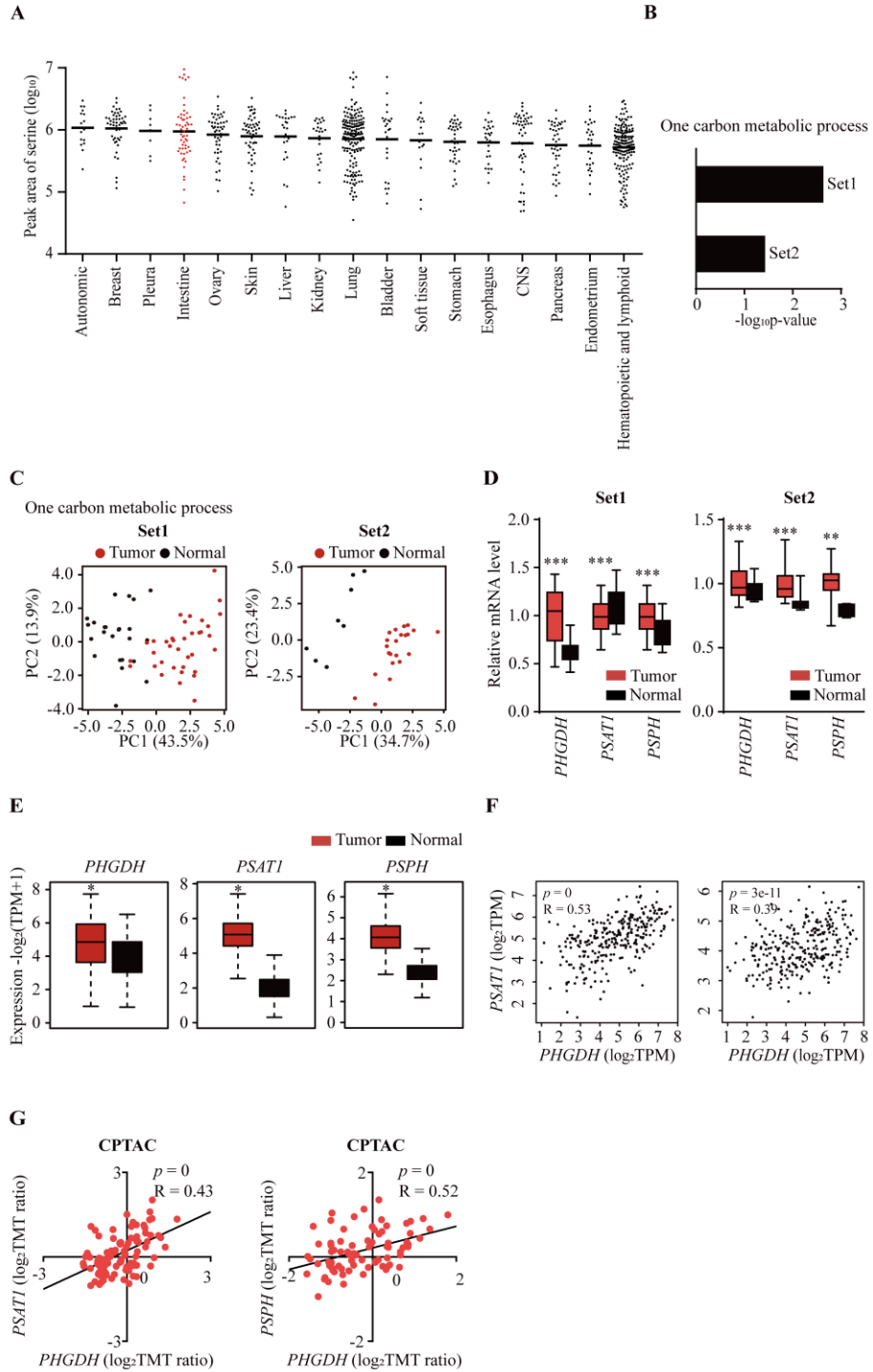
**Table1. Clinical information of CRC patients in single cell analysis**

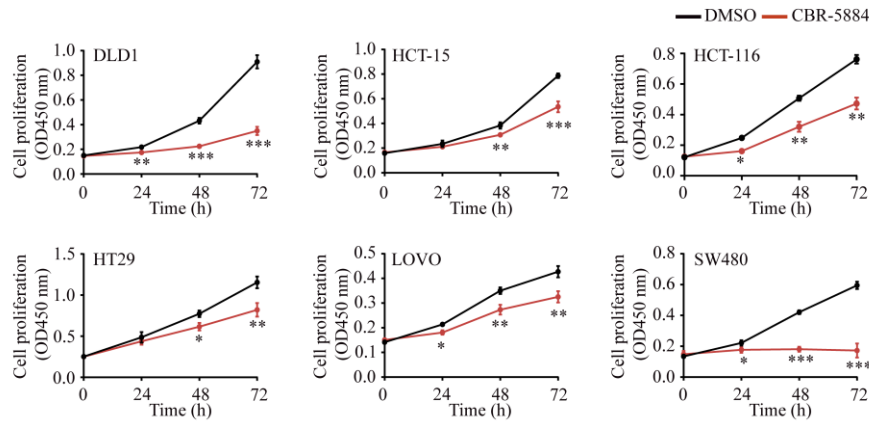
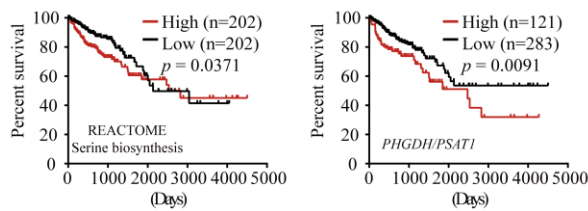
Sample	GSM	Stage	Region	Pathologic
CRC1	4476491	IIB	Caecum	Global moderately differentiated adenocarcinoma
CRC2	4476492	IIIB	Rectosigmoid	Moderately differentiated adenocarcinoma non-neoplastic adjacent tissues
CRC3	4476493	IVA	Sigmoid	Moderately differentiated adenocarcinoma
CRC4	4476494	IIA	Sigmoid	Moderately differentiated adenocarcinoma
CRC5	4476495	IIA	Ascending	Moderately differentiated adenocarcinoma

### III. RESULTS

#### 1. One carbon metabolism is significantly upregulated in patients with CRC

We first confirmed serine concentration, a major donor of one carbon metabolism, in diverse cancer types using the Cancer Cell Line Encyclopedia (CCLE). Intestinal cell lines showed high level of intracellular serine (Fig. 1A). In two Gene Expression Omnibus (GEO) datasets, CRC patients and normal subjects exhibited distinct difference of one carbon metabolic process (Fig. 1B). Principal component analysis also showed separated pattern of one carbon metabolic genes (Fig. 1C). Patients with CRC also had high level of serine *de novo* biosynthesis genes including *PHGDH*, *PSAT1*, *PSPH* (Fig. 1D, E), indicating the possibility that patients with CRC might have activation of one carbon metabolism compared to normal subjects. *PHGDH* had positive correlation with *PSAT1* and *PSPH* in the gene and protein level (Fig. 1F, G). Considering that CRC might be dependent on one carbon metabolism for tumor progression, we confirmed that one carbon metabolism inhibition indeed suppresses proliferation in CRC cell lines. When we treated with CBR-5884 to inhibit *PHGDH*, the initiating enzyme for one carbon metabolism, cell proliferation was significantly reduced in diverse CRC cell lines (Fig. 1H). cSurvival also showed serine biosynthesis and *PHGDH/PSAT1* high group patients exhibit poor prognosis in CRC (Fig. 1I). Altogether, our data demonstrate that possible involvement of one carbon metabolism in patients with CRC tumorigenesis.



**H**

**I**


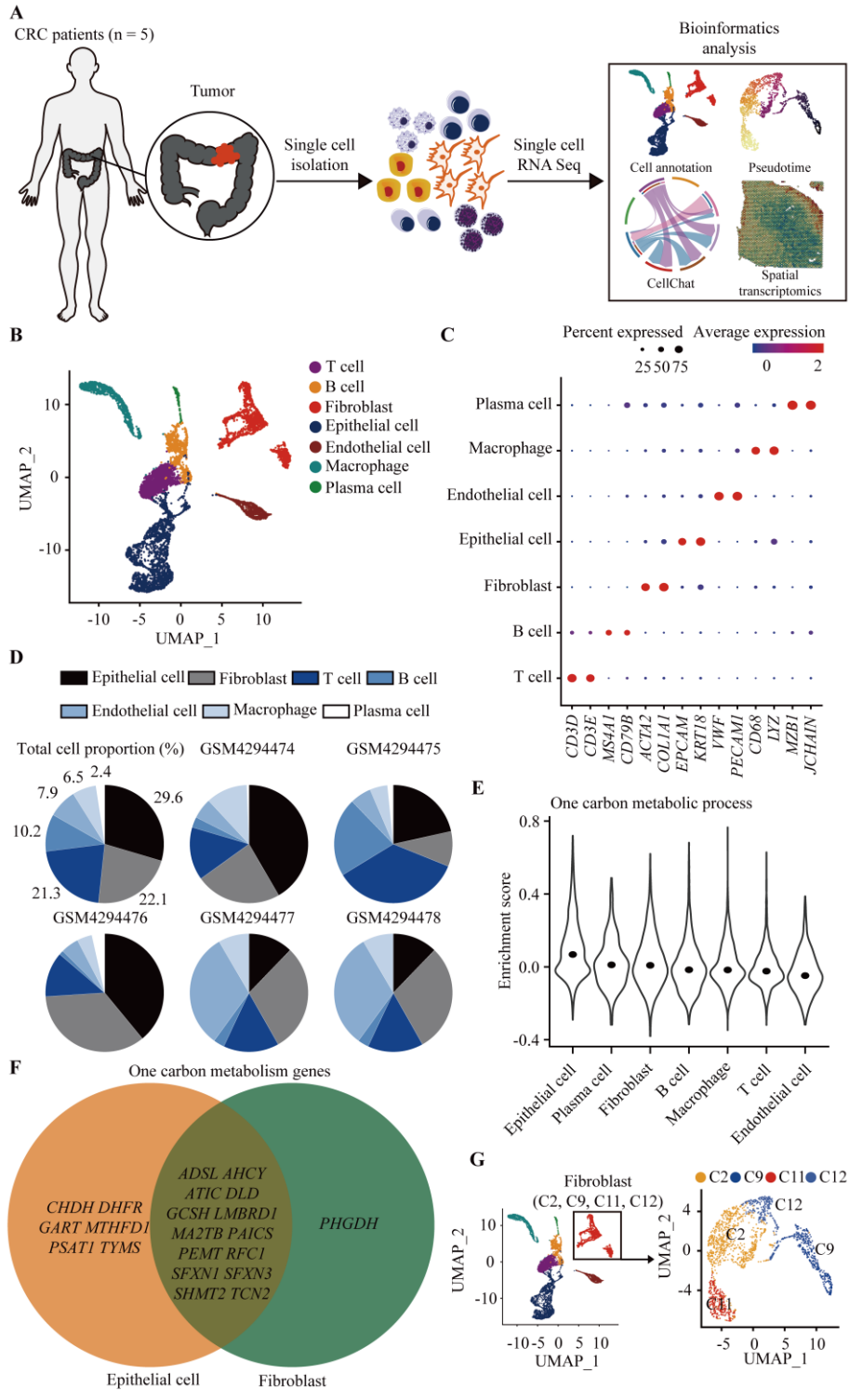
**Figure. 1 One carbon metabolism is significantly upregulated in patients with CRC.**

**A** Dot graph shows serine concentration of diverse cancer types using CCLE metabolomic data. **B** The bar graph shows significant difference of one carbon metabolic process between patients with CRC and normal subjects in two GSE datasets (GSE20916; normal subjects (n=24)/CRC patients (n=36), GSE81558; normal subjects (n=9)/CRC patients (n=23)). Set1 and 2 are GSE 20916 and 81558 respectively. GSEA analysis was performed with DAVID. **C** Principal component analysis shows separation of one carbon metabolic process genes in GSE datasets. **D** Bar graphs show mRNA levels of serine de novo biosynthesis genes including *PHGDH*, *PSAT1*, and *PSPH* in GSE datasets. **E** Gene expression analysis associated with serine de novo biosynthesis genes was performed with GEPIA2 in CRC (n=275) and normal subjects tissues (n=349) from TCGA and GTEx. ( $|\log_2 FC| \geq 0.5$   $P < 0.05$ ). **F** Expression correlation analysis of serine de novo biosynthesis genes was performed with GEPIA2 in CRC tissues from TCGA. Pearson correlation

coefficient was used. **G** Correlation analysis showed positive correlation of PSAT1/PSPH protein level with that of PHGDH in TCGA-COAD using CPTAC database. The number of patients in PHGDH/PSAT1 and PHGDH/PSPH are 97 and 82 respectively. **H** CRC cells were treated with CBR5884 (60 uM) for PHGDH inhibition for 72 h. Cell proliferation was measured by CCK-8. **I** Kaplan-Meier survival curves of the serine biosynthesis and *PHGDH/PSAT1* high group showed inferior outcomes compared to low group in TCGA-COAD from cSurvival platform. Data are expressed as the mean S.D. of three independent experiments (n=3). Statistical comparisons were performed using two-tailed Student's *t* test. (\* $P < 0.05$ ; \*\* $P < 0.01$ ; \*\*\* $P < 0.001$ )

## 2. Single cell analysis of patients with CRC

To observe the role of one carbon metabolic process in the level of tumor microenvironment, we performed single cell RNA sequencing (scRNA-seq) analysis of patients with CRC using GEO datasets (Fig. 2A). During analysis total of 8,179 cells, we identified total of 7 cell types including T cell (21.3%) with marker genes *CD3D*, *CD3E*; B cell (10.2%) with marker genes *MS4A1*, *CD79B*; Fibroblast (22.1%) with marker genes *ACTA2*, *COL1A1*; Epithelial cell (29.6%) with marker genes *EPCAM*, *KRT18*; Endothelial cell (7.9%) with marker genes *VWF*, *PECAMI*; Macrophage (6.5%) with marker genes *CD68*, *LYZ*; Plasma cell (2.4%) with marker genes *MZB1*, *JCHAIN* (Fig. 2B-D). Patients with CRC also showed different percentage of cell types respectively, indicating that cell heterogeneity is dominant feature of patients with CRC (Fig. 2D). We next identified the enrichment score of one carbon metabolic process in total cluster using single sample gene set enrichment analysis (ssGSEA). Enrichment score of one carbon metabolic process in fibroblast was third among all clusters (Fig. 2E). Additionally, we observed total 20 one carbon metabolism-related genes were mainly expressed in epithelial cell and fibroblast clusters as represented in Venn diagram (Fig. 2F). Based on cancer-associated fibroblasts (CAFs) are the most abundant in TME components and important player for tumorigenicity in CRC (100-102), we next extracted subsets of fibroblast and observed gene expression pattern of total 15 one carbon metabolism in fibroblast cluster more detail (Fig. 2G).

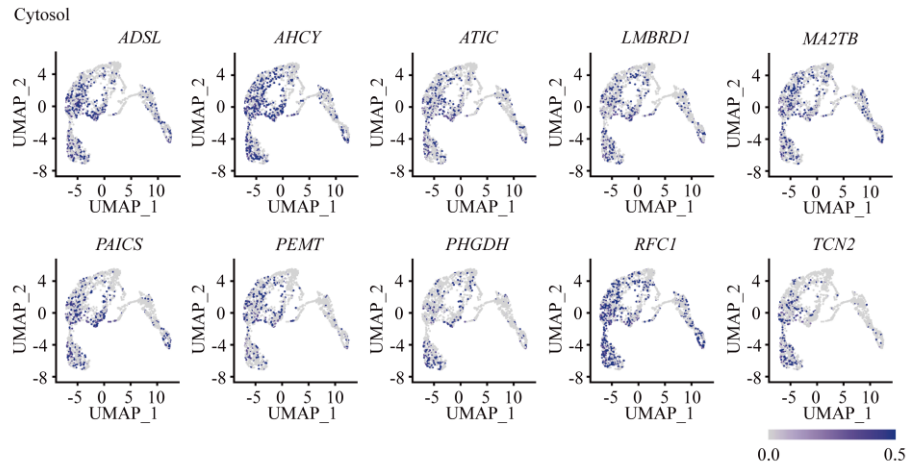


**Figure 2. Single cell analysis of patients with CRC.** **A** Workflow diagram shows single cell RNA sequencing of 5 CRC and subsequent analytical methods. **B** The dimensional reduction is conducted with UMAP. Each dot means a cell and colored by major cell types. **C** Dot plot represents canonical marker genes (rows) across major cell types (columns). **D** Pie graph shows the proportion of major cell types in total 5 CRC patients and the heterogeneity of cell distribution in each patient. **E** Venn diagram shows the enrichment of diverse one carbon metabolism genes in epithelial cell and fibroblast clusters. **F** The dimensional reduction is performed with UMAP of fibroblast. Each dot represents a cell and colored by total 4 fibroblast clusters.

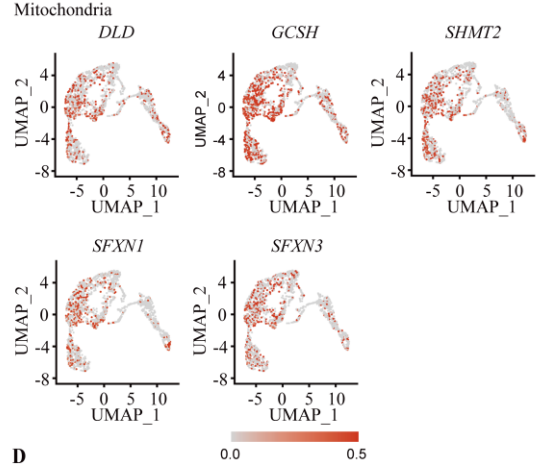
### **3. Fibroblast clusters divide into two subpopulations according to gene expression of one carbon metabolism**

Interestingly, most of cytosolic and mitochondrial one carbon metabolism gene expression levels were upregulated in cluster ‘C2, C11’ and downregulated in ‘C9, C12’ (Fig. 3A, B). So, we considered cluster ‘C2, C11’ one carbon high fibroblast (OHF) and cluster ‘C9, C12’ one carbon low fibroblast (OLF) (Fig. 3C). Single sample gene set enrichment analysis (ssGSEA) indeed showed OHF group was enriched in one carbon metabolism-related pathway such as ‘One carbon metabolic process’, ‘Serine family amino acid metabolic process’, ‘Glutathione metabolism’, and ‘Purine metabolism’, meaning that our standard of dividing into OHF and OLF was well established (Fig. 3D). Collectively, our findings showed that discretization of fibroblast cluster according to one carbon metabolism in patients with CRC.

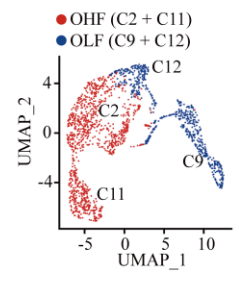
**A**



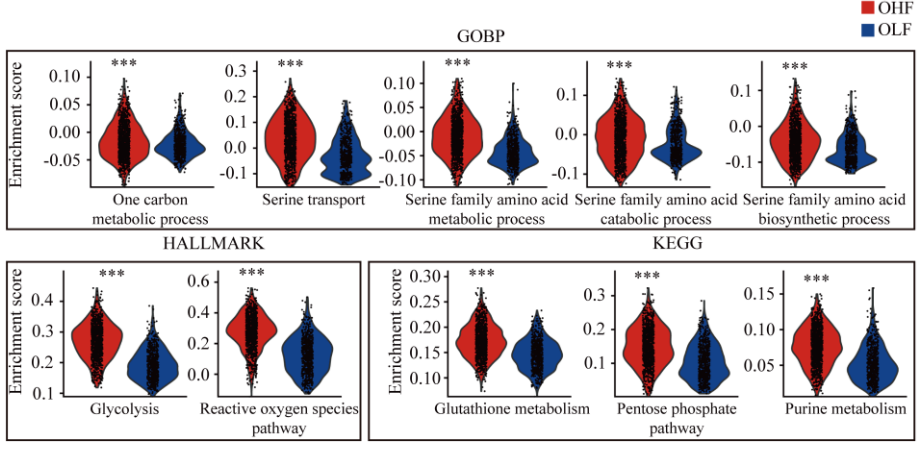
**B**



**C**



**D**

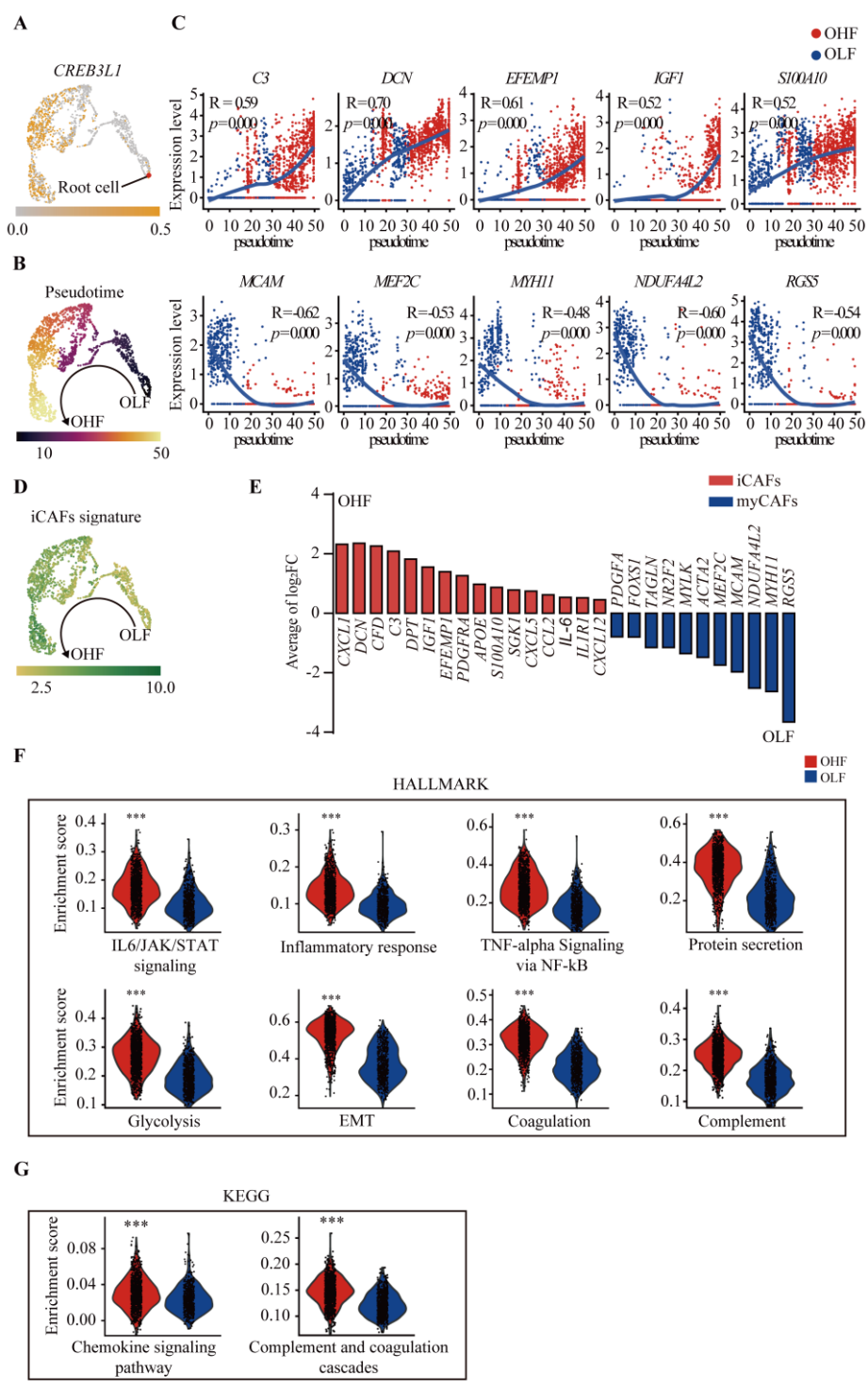


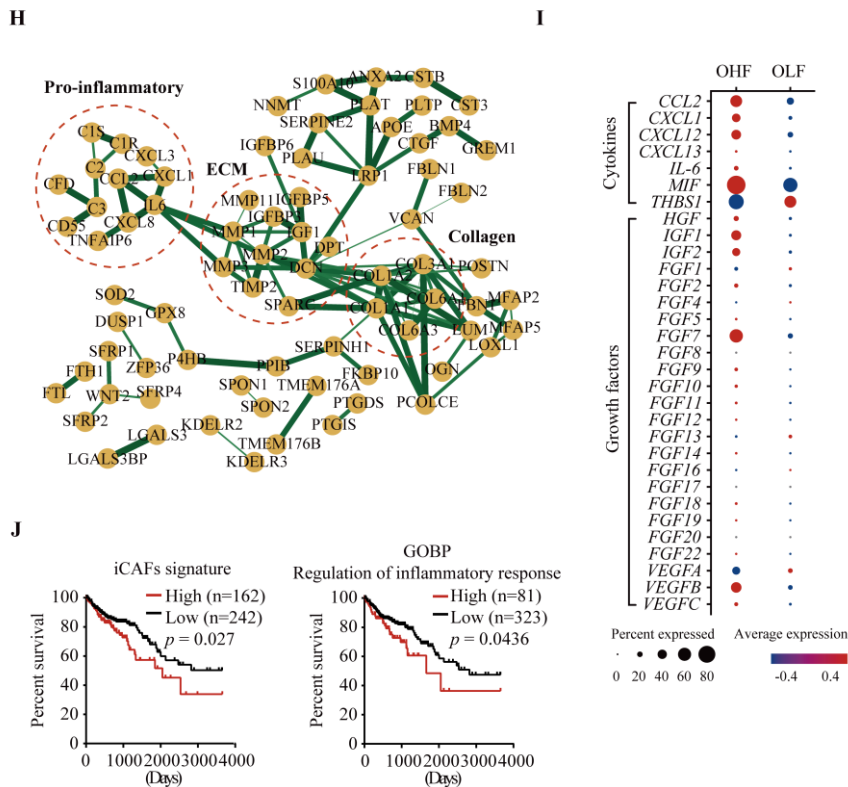
**Figure 3. Fibroblast divide into two subpopulations according to gene expression of one carbon metabolism.** **A, B** UMAP plots shows normalized expression levels of genes associated with one carbon metabolism in cytosol and mitochondrial respectively. **C** UMAP plots exhibits fibroblast clusters are named as one carbon metabolism high and low fibroblast. **D** Violin plots indicate enrichment score of diverse pathways related to one carbon metabolism is higher in ‘C2 + C11’ group compared to ‘C9 + C12’ using ssGSEA.

#### 4. iCAFs preferentially reside in OHF

Given that CAFs are heterogenous population and abundant in patients with CRC (103, 104), we confirmed whether dominant CAFs subtypes exist according to one carbon metabolism activation. We first investigated the evolutionary transition using trajectory inference and pseudotime analysis to confirm whether CAFs switching occurs from myofibroblastic CAFs (myCAFs) to inflammatory CAFs (iCAFs) or vice versa. To point out root cells, we observed high level of de-differentiated related gene *CREB3L1*. Expression level of *CREB3L1* was higher in OHF to low group, which is consistent with our previous studies in anaplastic thyroid cancer (Fig. 4A). Intriguingly, our monocle3 tool analysis showed expression level of several iCAFs-related genes such as *C3*, *DCN*, *IGF1* was increased along pseudotime from OLF to OHF. In contrast, expression level of myCAFs-related genes such as *MCAM*, *MEF2C*, *RGS5* was decreased along pseudotime from OLF to OHF, suggesting that myCAFs have a possibility to change into iCAFs according to evolutionary path in CRC (Fig. 4B, C). When we scored iCAFs signature with total 31 iCAFs-related genes (105), the score was higher in OHF (Fig. 4D). We next analyzed differential expressed genes (DEGs) between OHF and OLF. DEGs analysis showed myCAFs genes such as *TAGLN*, *MYLK*, *ACTA2*, *RGS5* were upregulated in OLF, iCAFs genes including *CXCL1*, *C3*, *IL-6*, *PDGFRA* were upregulated in OHF (Fig. 4E). We also confirmed diverse iCAFs-related pathways such as IL-6/JAK/STAT signaling, protein secretion, and inflammatory response, and complement and coagulation cascades were enriched in OHF compared to low group using ssGSEA (Fig. 4F, G). In our protein-protein interaction network analysis, several upregulated DEGs in OHF showed spreading patterns involved in iCAFs-related pathways including pro-inflammatory, ECM, and collagen signaling, suggesting that OHF exhibits iCAFs features dominantly (Fig. 4H). It is well established that iCAFs secrete many pro-inflammatory cytokines and growth factors to other types of cells leading to diverse biological events including EMT, immunosuppression, extracellular matrix organization, and metastasis (84, 106, 107). So, we next compared expression level of various cytokines and growth factors secreted from

iCAFs and observed that many cytokines and growth factors were dramatically higher in OHF such as *CXCL1*, *CXCL12*, *IL-6*, *HGF* and *IGF1* (Fig. 4I). cSurvival also showed inferior outcome in iCAF high-related groups such as iCAFs signature, inflammatory response (Fig. 4J). Altogether, our data show that iCAFs are mainly reside in OHF and have a possible contribution to poor prognosis in patients with CRC.





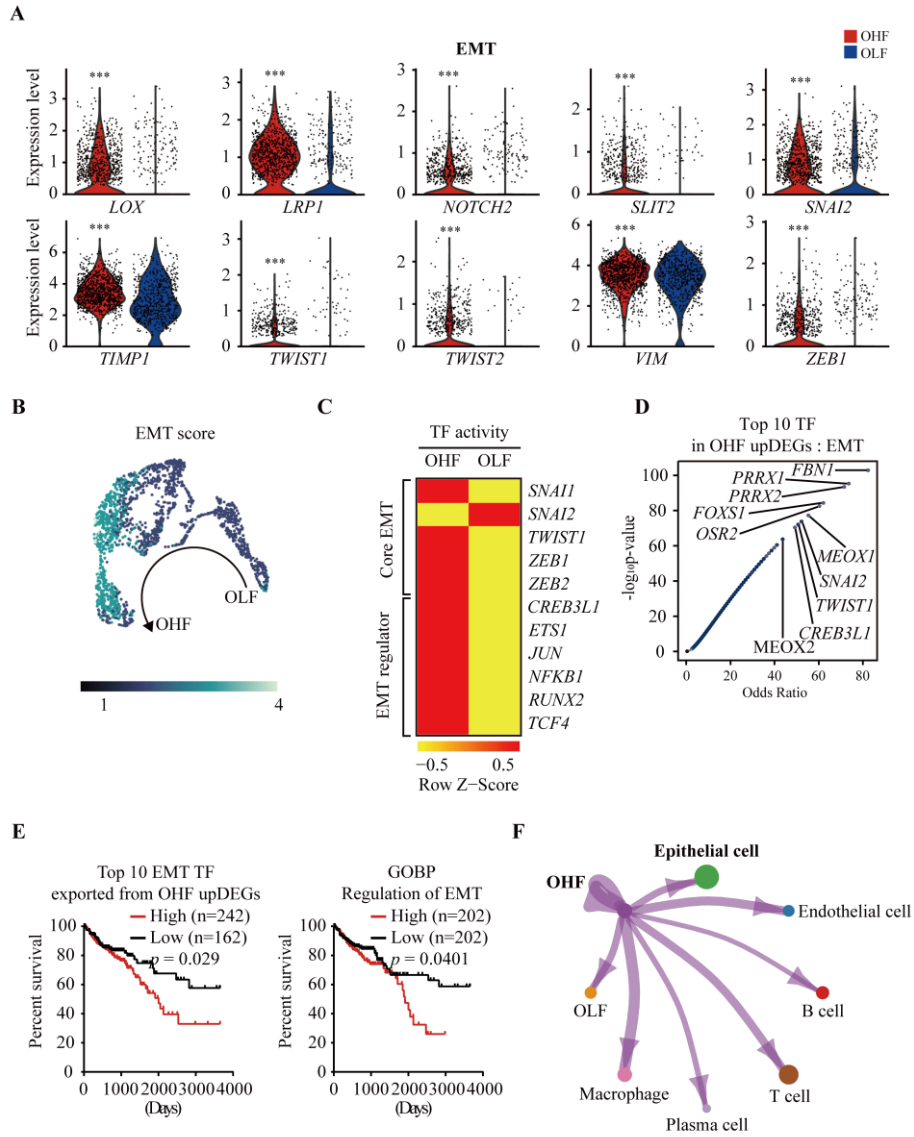
**Figure 4. iCAFs preferentially reside in OHF.** **A** UMAP of integrated fibroblasts shows root cell position based on *CREB3L1*. Color scale represents *CREB3L1* expression level. **B** UMAP of integrated fibroblasts exhibits pseudotime analysis one carbon metabolism low to high group. Color scale represents pseudotime in Monocle3. **C** Dot plots represent the correlation between pseudotime and iCAFs/myCAFs gene expression level. **D** iCAFs signature are enriched along evolutionary trajectory of one carbon metabolism low to high. **E** Bar graph represents upregulated DEGs associated with iCAFs and myCAFs in one carbon metabolism high and low groups respectively. ( $|\log_2 FC| \geq 0.5$   $P < 0.05$ ) **F, G** Violin plots of HALLMARK and KEGG show enrichment score of diverse pathways related to iCAFs are higher in one carbon metabolism high group compared to low using ssGSEA. **H** Protein-protein interaction network analysis illustrates largest connected component of iCAF-related complex. **I** Dot plot represents the expression level of cytokines and growth

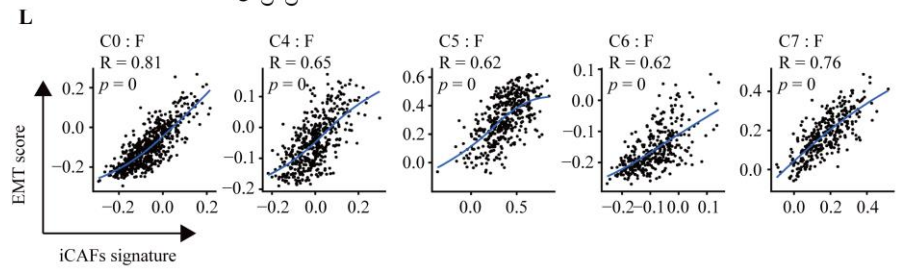
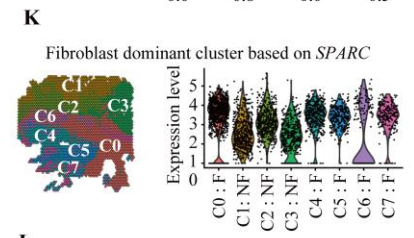
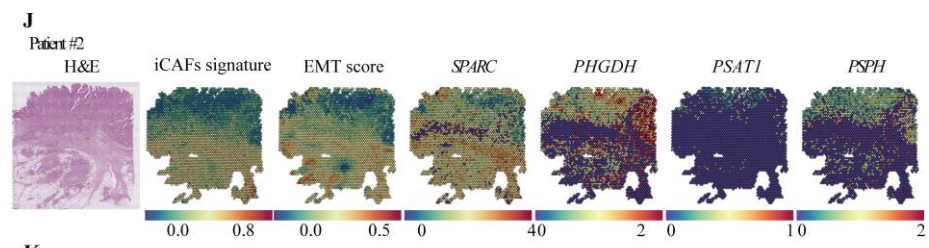
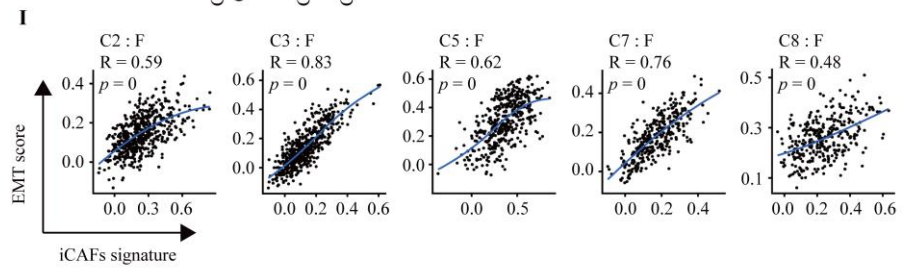
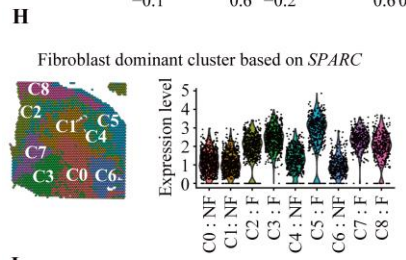
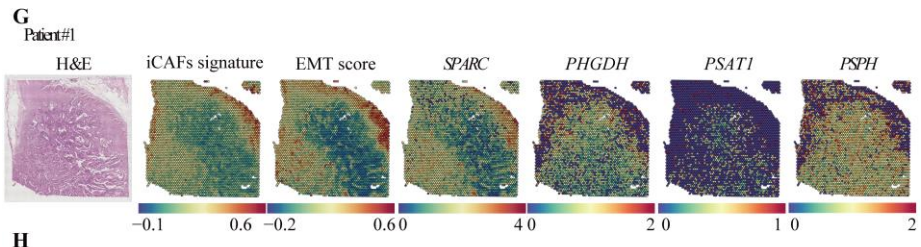
factors between one carbon metabolism high and low fibroblast. **J** Kaplan-Meier survival curves of iCAFs signature and regulation of inflammatory response high group exhibits poor prognosis compared to low group in TCGA-COAD from cSurvival platform.

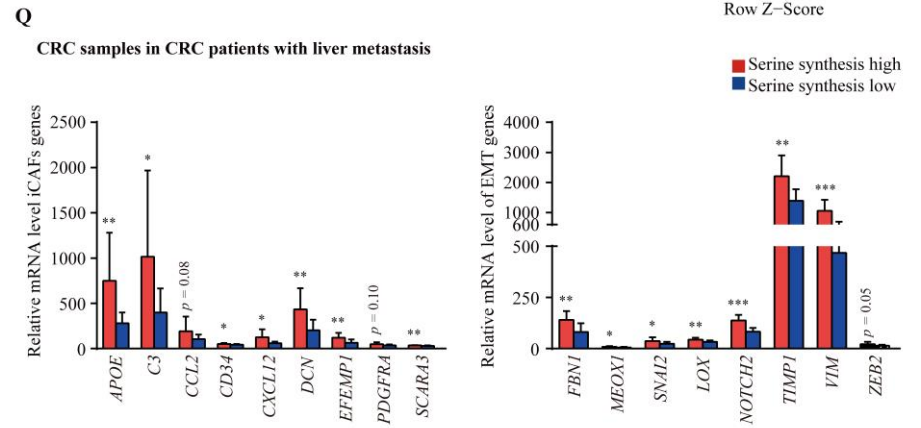
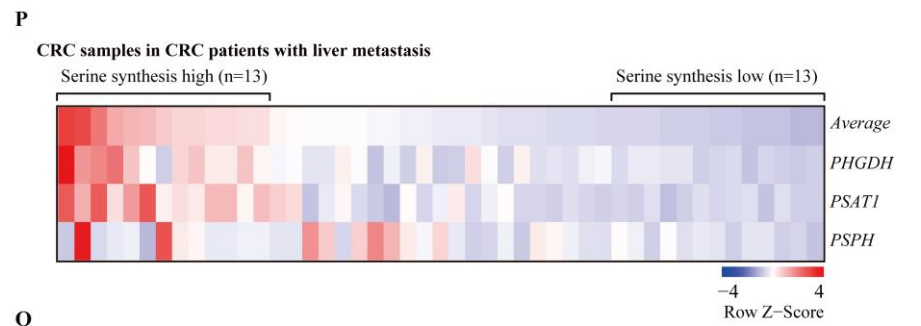
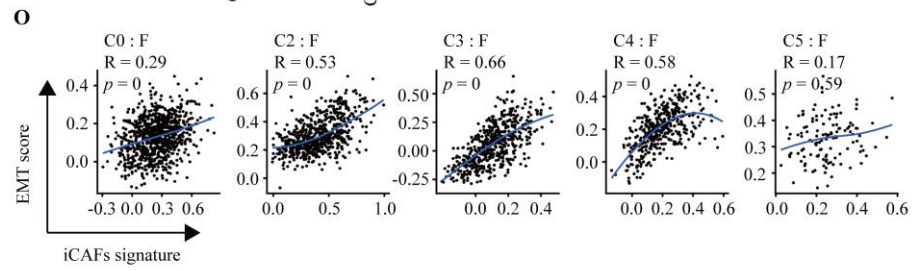
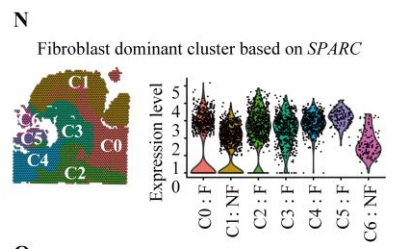
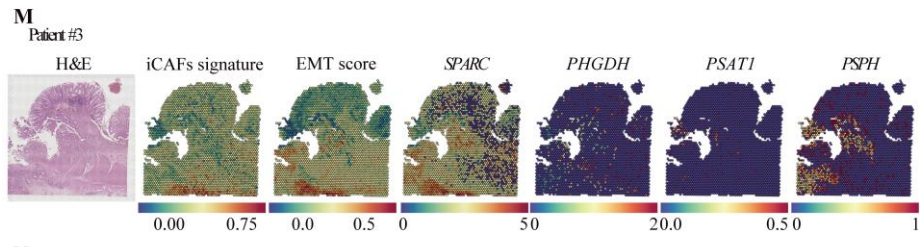
## 5. OHF might be pivotal role of EMT enhancement in iCAFs-dependent manner

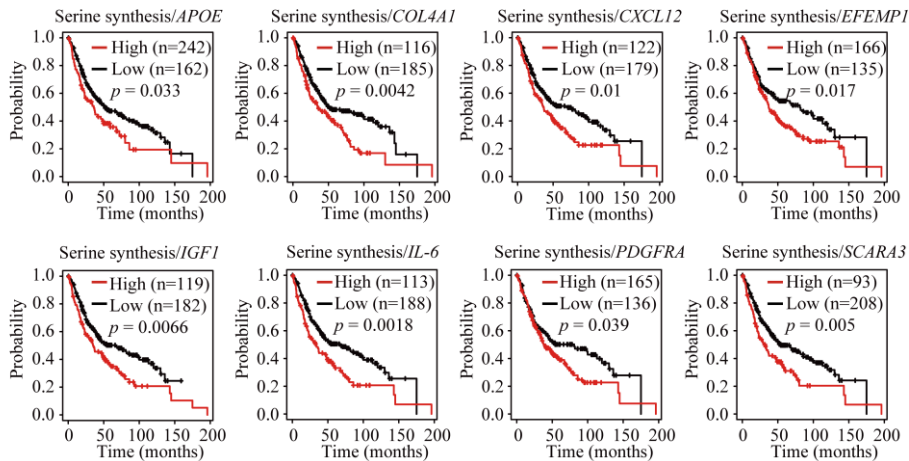
Given that EMT-related genes were enriched in iCAFs cluster (93), we identified causal relationship between iCAFs and promotion of EMT. We confirmed enrichment score and expression level associated with EMT were higher in OHF (Fig. 4F, 5A). When we observed EMT score with total 200 EMT genes (93), the score was higher in OHF (Fig. 5B). We next identified transcription factor (TF) activity associated with EMT using DoRothEA tool between OHF and OLF group. OHF exhibited higher EMT TF activity such as *CREB3L1*, *TWIST1*, and *ZEB2* (Fig. 5C). The top 10 TFs modulating upregulated DEGs in OHF group were also associated with EMT including *FBNI*, *TWIST1*, and *CREB3L1* (Fig. 5D), suggesting that iCAFs in OHF showed the possibility to enhance EMT signaling. cSurvival showed poor prognosis in top 10 TFs associated with EMT and regulation of EMT high groups in CRC patients (Fig. 5E). Also, we identified the most largest epithelial cell cluster receives cell signaling from OHF, which might imply that OHF-driven EMT signal is transmitted to epithelial cell (Fig. 5F). We next analyzed spatial transcriptomic profile and observed status of iCAFs and EMT around the fibroblast from three CRC patient tissues. Our findings showed that expression level of iCAFs signature and EMT score were mainly expressed in fibroblast abundant parts of the tissue with marker gene *SPARC* in 3 CRC patients. Also, we observed *de novo* serine synthesis including *PHGDH*, *PSATI*, and *PSPH* were partially upregulated in fibroblast clusters despite different tendency respectively (Fig. 5G, J, M). To further investigate correlation between iCAFs signature and EMT score in this part, we discriminated each cluster into fibroblast dominant and non-dominant cluster (F and NF respectively) based on *SPARC* (Fig. 5H, K, N). iCAFs signature achieved positive correlation with EMT score in most of F cluster (Fig. 5I, L, O), suggesting that the iCAFs are enough to execute EMT promotion in patients with CRC. It was reported the most common metastatic site in patients with CRC is liver (108). So, we observed the expression level of iCAFs and EMT genes between *de novo* serine synthesis gene (*PHGDH/PSATI/PSPH*) high and low group in patients with this group. Diverse iCAFs and EMT genes were higher in *de novo* serine synthesis high

group (Fig. 5P, Q). In survival plot in CRC patients with stage 3 and 4, high level of *de novo* serine synthesis and iCAFs genes have inferior outcome (Fig. 5R). Altogether, our data demonstrate iCAFs in OHF show positive relation with EMT-related signature and metastasis, which might lead to poor outcome in patients with CRC.







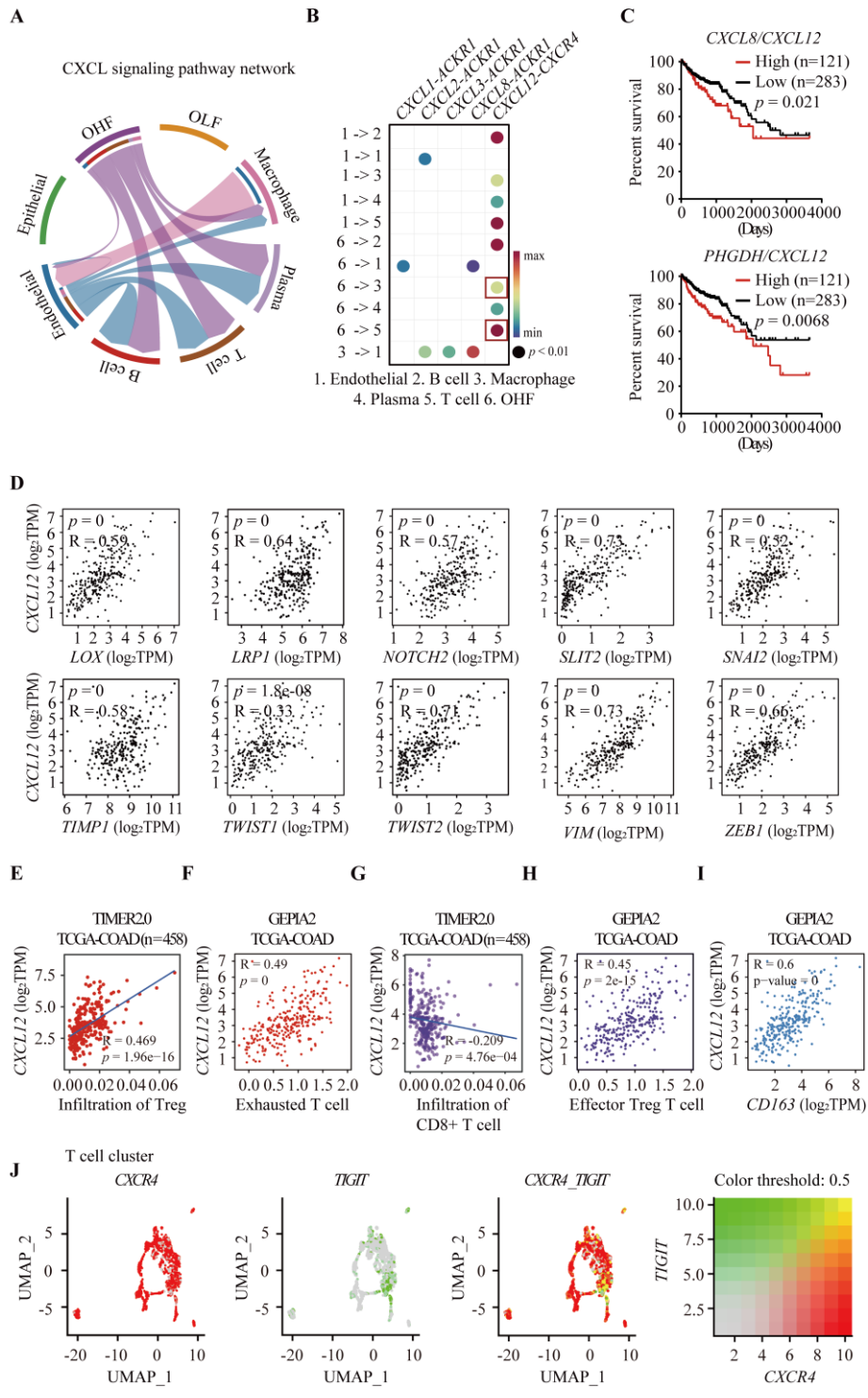
**R**
**CRC patients with stage 3 and 4**


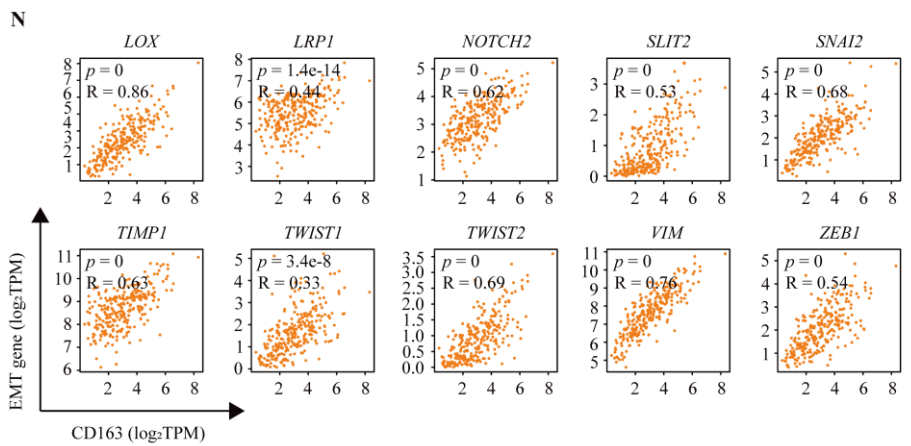
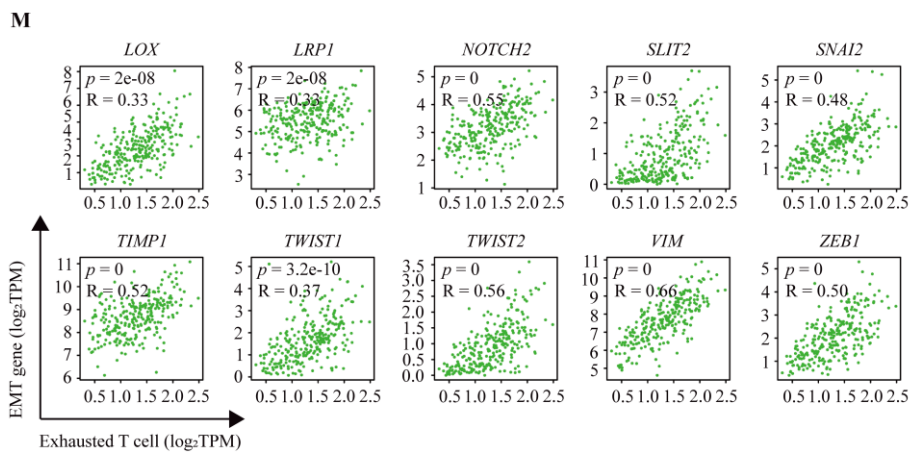
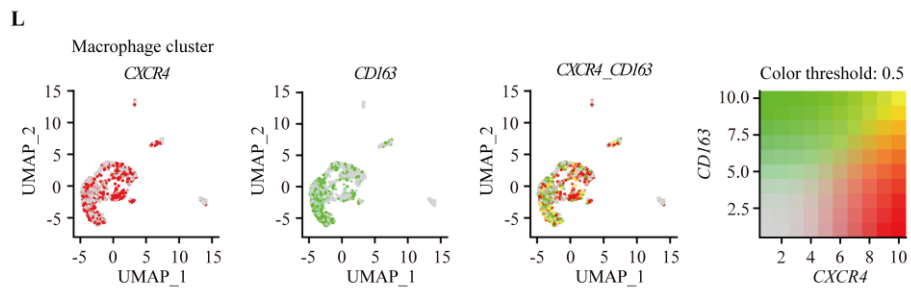
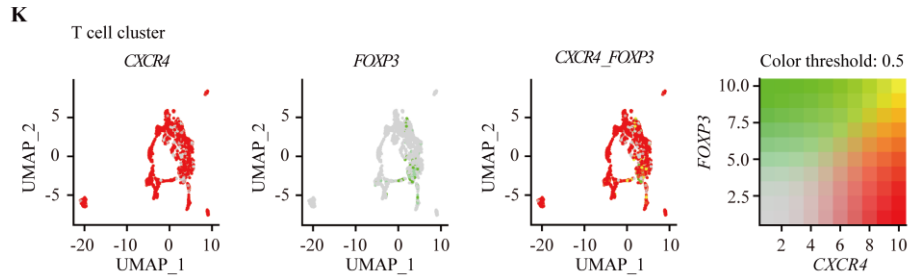
**Figure 5. OHF plays an important role of EMT enhancement in iCAFs-dependent manner.** **A** Violin plots represent enhancement of expression level associated with EMT genes in one carbon metabolism high group compared to low group. **B** UMAP of integrated fibroblasts indicate that EMT score is enriched in OHF group compared to OLF. **C** Heatmap shows TF activity of EMT between OHF and OLF using DoROtheEA. UMAP of fibroblast exhibits EMT signature are higher along the one carbon metabolism low to high group. **D** Volcano plot represents the top 10 transcription factor modulating upregulated DEGs in one carbon metabolism high fibroblast from Enrichr platform. ( $|\log_2 FC| \geq 0.5$   $P < 0.05$ ) **E** Kaplan-Meier survival curves of top 10 TFs associated with EMT and regulation of EMT high group shows inferior outcome compared to low group in patients with CRC TCGA-COAD from cSurvival platform. **F** Circle plot displays communication of OHF with other cell types. Circle size and edge width indicate the number of cells in each cell cluster and communication score between OHF and other cell clusters respectively. **G, J, M** Spatial transcriptomic spot of CRC patient tissues illustrates enrichment of iCAFs signature, EMT score and serine *de novo* biosynthesis genes in fibroblast dominant part of the tissue. **H, K, N** DimPlot shows the position number of each cluster in tissue (left). Violin plot represents F and NF cluster based on expression level of *SPARC*. **I, L, O** Dot plots represent the

correlation between iCAFs signature and EMT score in each F cluster in CRC patients. **P** Heatmap shows grouping of CRC patients with liver metastasis according to average of *de novo* serine synthesis high and low. The dataset is GSE41258. **Q** Bar graphs represent the relative mRNA level of iCAFs and EMT genes between indicated groups in **P**. **R** Kaplan-Meier survival curves of CRC patients with stage 3 and 4 show serine synthesis and iCAFs gene high group shows poor prognosis compared to low group in TCGA-COAD from Kaplan-Meier Plotter.

## 6. *CXCL12* secreted from iCAFs in OHF induces immunosuppression and subsequent EMT promotion in patients with CRC

iCAFs secrete CXCL cytokine leading to EMT and immunosuppressive effect in TME (109). So, we used CellChat to observe communication network of CXCL signaling between fibroblasts and other TME components. While OLF has no signal to other cell, OHF showed outgoing signal to diverse cell types (Fig. 6A). OHF especially showed strong *CXCL12/CXCR4* axis with T cell and macrophage and high expression level of *CXCL12* compared to low group (Fig. 4I, 6B). Survival plot of high level of *CXCL8/CXCL12* and *PHGDH/CXCL12* had inferior outcome in patients with CRC (Fig. 6C). We next identified association between *CXCL12* and EMT-related genes previously mentioned. To further identify *CXCL12* secretion from iCAFs and causal relationship with EMT progression, we observed whether positive correlation appears between *CXCL12* and diverse EMT-related genes in patients with CRC. As expected, *CXCL12* showed positive correlation with EMT genes including *SLIT2*, *SNAI2*, and *TWIST1* in GEPIA2 (Fig. 6D). We next confirmed whether *CXCL12* is involved in immunosuppression in patients with CRC (85). Infiltration of Treg and exhausted T cell signature were positive correlation with *CXCL12* in TCGA-COAD (Fig. 6E, F). We also identified *CXCL12* had negative correlation with CD8<sup>+</sup> T cell and positive correlation with Effector Treg T cell signature (Fig. 6G, H). *CXCR4* showed high co-expression Combined feature plot showed high co-expression of *CXCR4* with *TIGIT* and *FOXP3* in T cell cluster, suggesting that *CXCL12* secreted from OHF might have a possibility to provoke immunosurveillance escape in T cell. Furthermore, we thought tumor-associated macrophage (TAM) accumulation based on *CXCL12/CXCR4* axis was observed in macrophage cluster (Fig. 6B) (84). We confirmed TAM marker *CD163* was co-expressed with *CXCL12* in macrophage cluster and positive correlation with *CXCL12* (Fig. 6I, L). Finally, exhausted T cell signature and *CD163* showed positive correlation with diverse EMT genes (Fig. 6M, N). Consequently, our data demonstrate that iCAFs in OHF might trigger immunosuppressive effect through *CXCL12* secretion leading to EMT progression in patients with CRC.





**Figure 6. CXCL12 secreted from iCAFs in OHF contributes to EMT in CRC patients.**

**A** Chord diagram shows network of *CXCL* signaling pathways between cell clusters. **B** Dot plot represents relative significance of diverse *CXCL* cytokines and receptors in each cell type. **C** Kaplan-Meier survival curves represent high level of *CXCL8/CXCL12* and *PHGDH/CXCL12* groups showed poor prognosis compared to low group in patients with CRC TCGA-COAD from cSurvival platform. **D** Expression correlation analysis between *CXCL12* and EMT-related genes was conducted with GEPIA2 in CRC tissues from TCGA. Pearson correlation coefficient was used. **E** Correlation analysis represents *CXCL12* has positive correlation with infiltration of Treg from TIMER2.0. **F** Expression correlation analysis between *CXCL12* and exhausted T cell signature was conducted with GEPIA2 in CRC tissues from TCGA. Pearson correlation coefficient was used. **G** Correlation analysis represents *CXCL12* has negative correlation with infiltration of CD8<sup>+</sup> T cell from TIMER2.0. **H** Expression correlation analysis between *CXCL12* and effector Treg T cell signature was conducted with GEPIA2 in CRC tissues from TCGA. Pearson correlation coefficient was used. **I** Expression correlation analysis between *CXCL12* and TAM marker gene *CD163* with GEPIA2 in CRC tissues from TCGA. Pearson correlation coefficient was used. **J** Combined feature plot shows high co-expression of *CXCR4* and exhausted T cell marker gene *TIGIT* in T cell cluster. **K** Combined feature plot represents high co-expression of *CXCR4* and Treg marker gene *FOXP3* in T cell cluster. **L** Combined feature plot exhibits high co-expression of *CXCR4* and TAM marker gene *CD163* in macrophage cluster. **M** Expression correlation analysis between exhausted T cell signature and EMT-related genes was conducted with GEPIA2 in CRC tissues from TCGA. Pearson correlation coefficient was employed. **N** Expression correlation analysis between *CD163* and EMT-related genes was conducted with GEPIA2 in CRC tissues from TCGA. Pearson correlation coefficient was used.

#### IV. DISCUSSION

Diverse TME components surrounding the CRC tumor lead to oncogenic signaling such as high rate of metastasis and immune dysfunction including T cell inhibition and tumor-associated macrophage infiltration (110, 111). FDA approval of immunotherapy for metastatic CRC has been achieved such as nivolumab and pembrolizumab antagonizing PD-L1 receptor. However, heterogeneity in the TME components and their tumorigenic communication network induce immunotherapy resistance leading to positive effect in a limited number of patients (112, 113). Therefore, investigating molecular details of TME components to enhance curative effects in patients with CRC is essential.

One carbon metabolism plays an essential role in CRC tumorigenesis. PHGDH is highly upregulated in CRC tumor tissues compared to normal intestinal mucosa. High level of PHGDH contributes poor outcome in patients with CRC (114, 115). Also, 5-Fluorouracil resistant CRC cells, which is a primary drug for metastatic and advanced CRC patients, exhibit enhanced state of serine metabolism leading to maintenance of 5-Fluorouracil resistance (57). In publicly available CCLE and GEO datasets, we identified that the concentration of serine in CRC was significantly high among other types of cancer cells and mRNA level of one carbon metabolism-related genes was higher compared to normal subjects. Our single cell analysis in 5 patients with CRC to compare expression of one carbon metabolism-related genes showed that total 21 one carbon metabolism genes were mainly expressed in epithelial cell and fibroblast clusters. Based on CAFs are common inhabitant of TME and function as potential initiator for tumor progression (100, 116), we further investigated one carbon metabolism focusing on fibroblast clusters. Intriguingly, fibroblast clusters divided into two parts according to one carbon metabolism activation and iCAFs mainly were found in OHF cluster.

However, how iCAFs exhibit high level of one carbon metabolism needs to be studied. We assumed why iCAFs cluster represents active one carbon metabolism. First, we found iCAFs cluster has high level of glycolysis pathway, which is consistent with previous. Glycolysis is the most readily available metabolic process in diverse types of cancer.

During glycolysis, glucose is converted into intermediate 3-phosphoglycerate (26, 117). Considering that 3-phosphoglycerate is catalyzed into serine by serine *de novo* biosynthesis genes *PHGDH*, *PSAT1*, and *PSPH*, we thought iCAFs might increase the possibility to employ one carbon metabolism. Second, previous study in pancreatic cancer showed that hypoxia induces iCAFs feature in TME (118). Hypoxia also triggers mitochondrial ROS accumulation leading to activation of HIF transcription factor families and their tumorigenic target genes. Nonetheless, cancer cells adjust steady state of ROS level to avoid excessive ROS-induced cell death or senescence (119-121). Given that one carbon metabolism has a crucial role in mitochondrial redox maintenance, iCAFs have a possible occurrence of increased one carbon metabolism in patients with CRC.

Recent investigations showed that characteristics of EMT were prominently observed in iCAFs cluster compared to myCAFs (88, 93). Our single cell analysis data showed that iCAFs in OHF represented enrichment of EMT-associated genes such as *SNAI2*, *TWIST1*, and *VIM*. EMT score and TF activity associated with EMT were also higher than OLF group. Additionally, spatially resolved transcriptomics data of CRC patient tissues revealed positive correlation between EMT score and iCAFs signature in fibroblast dominant area, indicating that iCAFs/EMT axis might contribute to metastasis in patients with CRC.

We suggested that promotion of EMT is likely due to *CXCL12*, which is mainly known to be secreted from iCAFs (84). Our CellChat analysis represented that iCAFs in OHF imposed *CXCL12* outgoing patterns to immune cells including T cell, B cell, and macrophage. Although downstream effectors of *CXCL12/CXCR4* axis are different according to cell type or conditions, it was reported that *CXCL12/CXCR4* axis triggers EMT in diverse cancer types including gastric cancer, glioblastoma, hepatocellular carcinoma, and sacral chondrosarcoma (122, 123).

*CXCL12/CXCR4* interaction led to immunosuppression with T cell exhaustion, activation of regulatory T cells or macrophage, and impairment of B cell proliferation. (85, 124, 125). Based on enhancement of EMT through T cell dysfunction or TAM activation (126, 127), we considered *CXCL12*-induced EMT is likely due to compromised immune

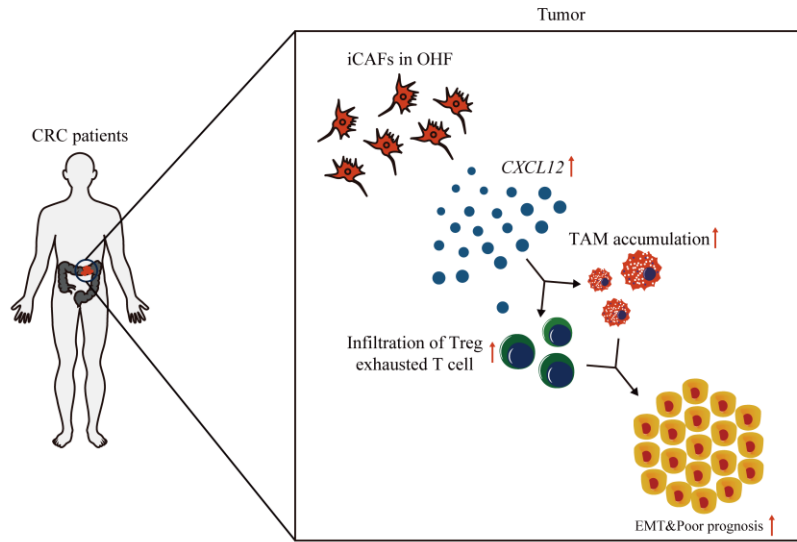
system. Our data in TCGA-COAD also showed *CXCL12* has positive correlation with exhausted T cell and infiltration of regulatory T cell (Treg) signature. Additionally, TAM accumulation marker gene *CD163* was strongly expressed in macrophage cluster and positive correlation with *CXCL12* in TCGA-COAD. Finally, diverse EMT-related genes represented positive correlation with T cell exhaustion signature and *CD163*, suggesting that possible occurrence of EMT due to immunosuppression in *CXCL12* dependent manner.

Although our data focus on immunosuppression through *CXCL12* secreted from iCAFs with activation of one carbon metabolism, myCAFs also contribute to immunosuppression in diverse cancers. In pancreatic ductal adenocarcinoma, TGF- $\beta$  driven LRRC15+ myCAFs suppressed the response to anti-PDL1. TGF- $\beta$  neutralization diminished myCAFs leading to enhancement of CD8+ T-cell infiltration and anti-PD1 response in subcutaneous 4T1 implantation model of breast cancer. In nonresponder groups during immunotherapy trial for non-small cell lung cancer and melanoma, myCAFs are enriched but not iCAFs signatures, implicating myCAFs-mediated immune evasion (94, 128, 129). Therefore, the influence of myCAFs on immune evasion also needs to be studied in our analysis.

Conclusively, our studies reported close relationship between one carbon metabolism and iCAFs in patients with CRC TME. Activation of one carbon metabolism fibroblasts exhibit iCAFs features rather than myCAFs. One carbon metabolism high iCAFs secrete diverse cytokines and growth factors and especially *CXCL12* cytokine exerts EMT promotion with immune cells in CRC patients. Our findings provide that iCAFs with active one carbon metabolism might be used as a powerful prognostic biomarker for estimating EMT and potential targets for improvement of survival by inhibiting iCAFs-induced *CXCL12* and subsequent immune evasion in CRC patients.

## V. CONCLUSION

One carbon metabolism was increased in patients with CRC compared to normal subjects. Our single cell analysis showed that enrichment score of one carbon metabolic process in fibroblast cluster was higher more than other TME components including immune cells and endothelial cells. Fibroblast clusters were also discretized into two types according to one carbon metabolism activation and iCAFs associated with EMT were preferentially reside in OHF. iCAFs in OHF mainly secreted *CXCL12* cytokine to immune cells such as T cell and macrophage, which induced immunosuppressive effects including infiltration of Treg, T cell exhaustion, and TAM accumulation. These signatures also represented positive correlation with diverse EMT-related genes such as *SNAI2*, *TWIST1*, and *VIM*. Altogether, our data suggest that activated one carbon metabolism of iCAFs has crucial role in enhancing EMT through immune escape and can be therapeutic target for improving survival by inhibiting metastasis and immune exhaustion in patients with CRC.



## REFERENCE

1. Are C, Shaha AR. Anaplastic thyroid carcinoma: biology, pathogenesis, prognostic factors, and treatment approaches. *Annals of surgical oncology*. 2006;13:453-64.
2. De Leo S, Trevisan M, Fugazzola L. Recent advances in the management of anaplastic thyroid cancer. *Thyroid research*. 2020;13(1):1-14.
3. Maniakas A, Zafereo M, Cabanillas ME. Anaplastic thyroid cancer: New horizons and challenges. *Endocrinology and Metabolism Clinics*. 2022;51(2):391-401.
4. Lim SM, Shin S-J, Chung WY, Park CS, Nam K-H, Kang S-W, et al. Treatment outcome of patients with anaplastic thyroid cancer: a single center experience. *Yonsei medical journal*. 2012;53(2):352-7.
5. Wei W, Jiang D, Rosenkrans ZT, Barnhart TE, Engle JW, Luo Q, et al. HER2-targeted multimodal imaging of anaplastic thyroid cancer. *American journal of cancer research*. 2019;9(11):2413.
6. Garcia-Rostan G, Tallini G, Herrero A, D'Aquila TG, Carcangiu ML, Rimm DL. Frequent mutation and nuclear localization of  $\beta$ -catenin in anaplastic thyroid carcinoma. *Cancer research*. 1999;59(8):1811-5.
7. Kim HM, Lee YK, Koo JS. Expression of glutamine metabolism-related proteins in thyroid cancer. *Oncotarget*. 2016;7(33):53628.
8. Youngblood VM, Kim LC, Edwards DN, Hwang Y, Santapuram PR, Stirdivant SM, et al. The ephrin-A1/EPHA2 signaling axis regulates glutamine metabolism in HER2-positive breast cancer. *Cancer research*. 2016;76(7):1825-36.
9. Cadoret A, Ovejero C, Terris B, Souil E, Levy L, Lamers WH, et al. New targets of  $\beta$ -catenin signaling in the liver are involved in the glutamine metabolism. *Oncogene*. 2002;21(54):8293-301.
10. Yoo HC, Yu YC, Sung Y, Han JM. Glutamine reliance in cell metabolism. *Experimental & molecular medicine*. 2020;52(9):1496-516.
11. Zhang J, Pavlova NN, Thompson CB. Cancer cell metabolism: the essential role of the nonessential amino acid, glutamine. *The EMBO journal*. 2017;36(10):1302-15.
12. DeBerardinis RJ, Mancuso A, Daikhin E, Nissim I, Yudkoff M, Wehrli S, et al. Beyond aerobic glycolysis: transformed cells can engage in glutamine metabolism that exceeds the requirement for protein and nucleotide synthesis. *Proceedings of the National Academy of Sciences*. 2007;104(49):19345-50.
13. Welbourne T. Ammonia production and glutamine incorporation into glutathione in the functioning rat kidney. *Canadian journal of biochemistry*. 1979;57(3):233-7.
14. Xiong Y, Xiao C, Li Z, Yang X. Engineering nanomedicine for glutathione depletion-augmented cancer therapy. *Chemical Society Reviews*. 2021;50(10):6013-41.

15. Yang L, Venneti S, Nagrath D. Glutaminolysis: a hallmark of cancer metabolism. *Annual review of biomedical engineering*. 2017;19:163–94.
16. Jin H, Wang S, Zaal EA, Wang C, Wu H, Bosma A, et al. A powerful drug combination strategy targeting glutamine addiction for the treatment of human liver cancer. *Elife*. 2020;9:e56749.
17. Kung H-N, Marks JR, Chi J-T. Glutamine synthetase is a genetic determinant of cell type-specific glutamine independence in breast epithelia. *PLoS genetics*. 2011;7(8):e1002229.
18. Jacque N, Ronchetti AM, Larrue C, Meunier G, Birsen R, Willems L, et al. Targeting glutaminolysis has antileukemic activity in acute myeloid leukemia and synergizes with BCL-2 inhibition. *Blood, The Journal of the American Society of Hematology*. 2015;126(11):1346–56.
19. Hu J, Chen Q, Ding X, Zheng X, Tang X, Li S, et al. Glutamine metabolism in the proliferation of GS-expression pituitary tumor cells. *Endocrine connections*. 2020;9(3):223–33.
20. Pavlova NN, Hui S, Ghergurovich JM, Fan J, Intlekofer AM, White RM, et al. As extracellular glutamine levels decline, asparagine becomes an essential amino acid. *Cell metabolism*. 2018;27(2):428–38. e5.
21. Mukha A, Kahya U, Linge A, Chen O, Löck S, Lukiyanchuk V, et al. GLS-driven glutamine catabolism contributes to prostate cancer radiosensitivity by regulating the redox state, stemness and ATG5-mediated autophagy. *Theranostics*. 2021;11(16):7844.
22. Polet F, Corbet C, Pinto A, Rubio LI, Martherus R, Bol V, et al. Reducing the serine availability complements the inhibition of the glutamine metabolism to block leukemia cell growth. *Oncotarget*. 2016;7(2):1765.
23. Tanaka K, Sasayama T, Nagashima H, Irino Y, Takahashi M, Izumi Y, et al. Glioma cells require one-carbon metabolism to survive glutamine starvation. *Acta neuropathologica communications*. 2021;9(1):1–14.
24. Newman AC, Maddocks OD. One-carbon metabolism in cancer. *British journal of cancer*. 2017;116(12):1499–504.
25. Locasale JW. Serine, glycine and one-carbon units: cancer metabolism in full circle. *Nature Reviews Cancer*. 2013;13(8):572–83.
26. Yang M, Vousden KH. Serine and one-carbon metabolism in cancer. *Nature Reviews Cancer*. 2016;16(10):650–62.
27. Luo H, Xia X, Kim GD, Liu Y, Xue Z, Zhang L, et al. Characterizing dedifferentiation of thyroid cancer by integrated analysis. *Science Advances*. 2021;7(31):eabf3657.
28. Molinaro E, Romei C, Biagini A, Sabini E, Agate L, Mazzeo S, et al. Anaplastic thyroid carcinoma: from clinicopathology to genetics and advanced therapies. *Nature Reviews Endocrinology*. 2017;13(11):644–60.
29. Landa I, Ibrahimasic T, Boucai L, Sinha R, Knauf JA, Shah RH, et al.

Genomic and transcriptomic hallmarks of poorly differentiated and anaplastic thyroid cancers. *The Journal of clinical investigation*. 2016;126(3):1052–66.

30. Haase J, Misiak D, Bauer M, Pazaitis N, Braun J, Pötschke R, et al. IGF2BP1 is the first positive marker for anaplastic thyroid carcinoma diagnosis. *Modern Pathology*. 2021;34(1):32–41.

31. Li H, Ning S, Ghandi M, Kryukov GV, Gopal S, Deik A, et al. The landscape of cancer cell line metabolism. *Nature medicine*. 2019;25(5):850–60.

32. Pilli T, Prasad KV, Jayarama S, Pacini F, Prabhakar BS. Potential utility and limitations of thyroid cancer cell lines as models for studying thyroid cancer. *Thyroid*. 2009;19(12):1333–42.

33. Romei C, Tacito A, Molinaro E, Piaggi P, Cappagli V, Pieruzzi L, et al. Clinical, pathological and genetic features of anaplastic and poorly differentiated thyroid cancer: A single institute experience. *Oncology letters*. 2018;15(6):9174–82.

34. Kim M, Gwak J, Hwang S, Yang S, Jeong SM. Mitochondrial GPT2 plays a pivotal role in metabolic adaptation to the perturbation of mitochondrial glutamine metabolism. *Oncogene*. 2019;38(24):4729–38.

35. Yoon BK, Kim H, Oh TG, Oh SK, Jo S, Kim M, et al. PHGDH preserves one-carbon cycle to confer metabolic plasticity in chemoresistant gastric cancer during nutrient stress. *Proceedings of the National Academy of Sciences*. 2023;120(21):e2217826120.

36. Lee J-S, Kang JH, Lee S-H, Hong D, Son J, Hong KM, et al. Dual targeting of glutaminase 1 and thymidylate synthase elicits death synergistically in NSCLC. *Cell death & disease*. 2016;7(12):e2511–e.

37. Morrison AJ. Chromatin-remodeling links metabolic signaling to gene expression. *Molecular metabolism*. 2020;38:100973.

38. Ye J, Mancuso A, Tong X, Ward PS, Fan J, Rabinowitz JD, et al. Pyruvate kinase M2 promotes de novo serine synthesis to sustain mTORC1 activity and cell proliferation. *Proceedings of the National Academy of Sciences*. 2012;109(18):6904–9.

39. Selvarajah B, Azuelos I, Platé M, Guillotin D, Forty EJ, Contento G, et al. mTORC1 amplifies the ATF4-dependent de novo serine-glycine pathway to supply glycine during TGF- $\beta$ 1-induced collagen biosynthesis. *Science signaling*. 2019;12(582):eaav3048.

40. Ducker GS, Rabinowitz JD. One-carbon metabolism in health and disease. *Cell metabolism*. 2017;25(1):27–42.

41. Li G, Wu J, Li L, Jiang P. p53 deficiency induces MTHFD2 transcription to promote cell proliferation and restrain DNA damage. *Proceedings of the National Academy of Sciences*. 2021;118(28):e2019822118.

42. May JL, Kouri FM, Hurley LA, Liu J, Tommasini-Ghelfi S, Ji Y, et al. IDH3 $\alpha$  regulates one-carbon metabolism in glioblastoma. *Science advances*.

2019;5(1):eaat0456.

43. Konno M, Asai A, Kawamoto K, Nishida N, Satoh T, Doki Y, et al. The one-carbon metabolism pathway highlights therapeutic targets for gastrointestinal cancer. *International journal of oncology*. 2017;50(4):1057-63.
44. D'Avola A, Legrave N, Tajan M, Chakravarty P, Shearer RL, King HW, et al. PHGDH is required for germinal center formation and is a therapeutic target in MYC-driven lymphoma. *The Journal of clinical investigation*. 2022;132(9).
45. Martínez-Reyes I, Chandel NS. Mitochondrial one-carbon metabolism maintains redox balance during hypoxia. *Cancer discovery*. 2014;4(12):1371-3.
46. Armstrong J, Steinauer K, Hornung B, Irish J, Lecane P, Birrell G, et al. Role of glutathione depletion and reactive oxygen species generation in apoptotic signaling in a human B lymphoma cell line. *Cell Death & Differentiation*. 2002;9(3):252-63.
47. Lúcio M, Nunes C, Gaspar D, Ferreira H, Lima JL, Reis S. Antioxidant activity of vitamin E and Trolox: understanding of the factors that govern lipid peroxidation studies in vitro. *Food Biophysics*. 2009;4:312-20.
48. Diao Q, Zhang J, Zhao T, Xue F, Gao F, Ma S, et al. Vitamin E promotes breast cancer cell proliferation by reducing ROS production and p53 expression. *Eur Rev Med Pharmacol Sci*. 2016;20(12):2710-7.
49. Coca-Pelaz A, Rodrigo JP, Lopez F, Shah JP, Silver CE, Al Ghuzlan A, et al. Evaluating new treatments for anaplastic thyroid cancer. *Expert review of anticancer therapy*. 2022;22(11):1239-47.
50. Chang H-S, Nam K-H, Chung WY, Park CS. Anaplastic thyroid carcinoma: a therapeutic dilemma. *Yonsei medical journal*. 2005;46(6):759-64.
51. Chintakuntlawar AV, Yin J, Foote RL, Kasperbauer JL, Rivera M, Asmus E, et al. A phase 2 study of pembrolizumab combined with chemoradiotherapy as initial treatment for anaplastic thyroid cancer. *Thyroid*. 2019;29(11):1615-22.
52. Shih S-R, Chen K-H, Lin K-Y, Yang P-C, Chen K-Y, Wang C-W, et al. Immunotherapy in anaplastic thyroid cancer: Case series. *Journal of the Formosan Medical Association*. 2022;121(6):1167-73.
53. Maniakas A, Dadu R, Busaidy NL, Wang JR, Ferrarotto R, Lu C, et al. Evaluation of overall survival in patients with anaplastic thyroid carcinoma, 2000-2019. *JAMA oncology*. 2020;6(9):1397-404.
54. Sun WY, Kim HM, Jung W-H, Koo JS. Expression of serine/glycine metabolism-related proteins is different according to the thyroid cancer subtype. *Journal of translational medicine*. 2016;14(1):1-12.
55. Jeon MJ, You M-H, Han JM, Sim S, Yoo HJ, Lee WK, et al. High phosphoglycerate dehydrogenase expression induces stemness and aggressiveness in thyroid cancer. *Thyroid*. 2020;30(11):1625-38.
56. Wen S-S, Zhang T-T, Xue D-X, Wu W-L, Wang Y-L, Wang Y, et al. Metabolic reprogramming and its clinical application in thyroid cancer. *Oncology*

Letters. 2019;18(2):1579-84.

57. Pranzini E, Pardella E, Muccillo L, Leo A, Nesi I, Santi A, et al. SHMT2-mediated mitochondrial serine metabolism drives 5-FU resistance by fueling nucleotide biosynthesis. *Cell Reports*. 2022;40(7).

58. Kashihara T, Mukai R, Oka S-i, Zhai P, Nakada Y, Yang Z, et al. YAP mediates compensatory cardiac hypertrophy through aerobic glycolysis in response to pressure overload. *The Journal of Clinical Investigation*. 2022;132(6).

59. Lukey MJ, Katt WP, Cerione RA. Targeting amino acid metabolism for cancer therapy. *Drug discovery today*. 2017;22(5):796-804.

60. Li AM, Ducker GS, Li Y, Seoane JA, Xiao Y, Melemenidis S, et al. Metabolic profiling reveals a dependency of human metastatic breast cancer on mitochondrial serine and one-carbon unit metabolism. *Molecular Cancer Research*. 2022;18(4):599-611.

61. Zhao Y, Butler EB, Tan M. Targeting cellular metabolism to improve cancer therapeutics. *Cell death & disease*. 2013;4(3):e532-e.

62. Meijer TW, Peeters WJ, Dubois LJ, van Gisbergen MW, Biemans R, Venhuizen J-H, et al. Targeting glucose and glutamine metabolism combined with radiation therapy in non-small cell lung cancer. *Lung Cancer*. 2018;126:32-40.

63. Morrison AJ. Cancer cell metabolism connects epigenetic modifications to transcriptional regulation. *The FEBS Journal*. 2022;289(5):1302-14.

64. Palm W. Metabolic plasticity allows cancer cells to thrive under nutrient starvation. *Proceedings of the National Academy of Sciences*. 2021;118(14):e2102057118.

65. Alfarouk KO, Ahmed SB, Elliott RL, Benoit A, Alqahtani SS, Ibrahim ME, et al. The pentose phosphate pathway dynamics in cancer and its dependency on intracellular pH. *Metabolites*. 2020;10(7):285.

66. Yoo HC, Park SJ, Nam M, Kang J, Kim K, Yeo JH, et al. A variant of SLC1A5 is a mitochondrial glutamine transporter for metabolic reprogramming in cancer cells. *Cell metabolism*. 2020;31(2):267-83. e12.

67. Liu C-L, Hsu Y-C, Lee J-J, Chen M-J, Lin C-H, Huang S-Y, et al. Targeting the pentose phosphate pathway increases reactive oxygen species and induces apoptosis in thyroid cancer cells. *Molecular and cellular endocrinology*. 2020;499:110595.

68. Savvides P, Nagaiah G, Lavertu P, Fu P, Wright JJ, Chapman R, et al. Phase II trial of sorafenib in patients with advanced anaplastic carcinoma of the thyroid. *Thyroid*. 2013;23(5):600-4.

69. Takahashi S, Kiyota N, Yamazaki T, Chayahara N, Nakano K, Inagaki L, et al. A Phase II study of the safety and efficacy of lenvatinib in patients with advanced thyroid cancer. *Future oncology*. 2019;15(7):717-26.

70. Lee YS, Kim S-M, Kim B-W, Chang HJ, Kim SY, Park CS, et al. Anti-cancer effects of HNHA and lenvatinib by the suppression of EMT-mediated drug

- resistance in cancer stem cells. *Neoplasia*. 2018;20(2):197-206.
71. Dierks C, Seufert J, Aumann K, Ruf J, Klein C, Kiefer S, et al. Combination of lenvatinib and pembrolizumab is an effective treatment option for anaplastic and poorly differentiated thyroid carcinoma. *Thyroid*. 2021;31(7):1076-85.
72. Yun HJ, Kim HJ, Kim J, Kim SY, Chang H-S, Park CS, et al. Synergistic anticancer activity of n-hydroxy-7-(2-naphthylthio) heptanamide, sorafenib, and radiation therapy in patient-derived anaplastic thyroid cancer models. *International journal of molecular sciences*. 2021;22(2):536.
73. Davidson CD, Tomczak JA, Amiel E, Carr FE. Inhibition of Glycogen Metabolism Induces Reactive Oxygen Species-Dependent Cytotoxicity in Anaplastic Thyroid Cancer in Female Mice. *Endocrinology*. 2022;163(12):bqac169.
74. Otto AM. Metabolic constants and plasticity of cancer cells in a limiting glucose and glutamine microenvironment—A pyruvate perspective. *Frontiers in Oncology*. 2020;10:596197.
75. Krasteva N, Georgieva M. Promising therapeutic strategies for colorectal cancer treatment based on nanomaterials. *Pharmaceutics*. 2022;14(6):1213.
76. Zheng J, Dou R, Zhang X, Zhong B, Fang C, Xu Q, et al. LINC00543 promotes colorectal cancer metastasis by driving EMT and inducing the M2 polarization of tumor associated macrophages. *Journal of translational medicine*. 2023;21(1):153.
77. Riihimäki M, Hemminki A, Sundquist J, Hemminki K. Patterns of metastasis in colon and rectal cancer. *Scientific reports*. 2016;6(1):29765.
78. Vu T, Datta PK. Regulation of EMT in colorectal cancer: a culprit in metastasis. *Cancers*. 2017;9(12):171.
79. Sistigu A, Di Modugno F, Manic G, Nisticò P. Deciphering the loop of epithelial-mesenchymal transition, inflammatory cytokines and cancer immunoediting. *Cytokine & growth factor reviews*. 2017;36:67-77.
80. van Staalduinen J, Baker D, Ten Dijke P, van Dam H. Epithelial-mesenchymal-transition-inducing transcription factors: new targets for tackling chemoresistance in cancer? *Oncogene*. 2018;37(48):6195-211.
81. Menezes S, Okail MH, Jalil SMA, Kocher HM, Cameron AJ. Cancer-associated fibroblasts in pancreatic cancer: new subtypes, new markers, new targets. *The Journal of Pathology*. 2022;257(4):526-44.
82. Rodrigues J, Heinrich MA, Teixeira LM, Prakash J. 3D in vitro model (R) evolution: unveiling tumor-stroma interactions. *Trends in cancer*. 2021;7(3):249-64.
83. Quail DF, Joyce JA. Microenvironmental regulation of tumor progression and metastasis. *Nature medicine*. 2013;19(11):1423-37.
84. Chen Z, Zhou L, Liu L, Hou Y, Xiong M, Yang Y, et al. Single-cell RNA sequencing highlights the role of inflammatory cancer-associated fibroblasts in bladder urothelial carcinoma. *Nature communications*. 2020;11(1):5077.
85. Malik S, Westcott JM, Brekken RA, Burrows FJ. CXCL12 in pancreatic

- cancer: Its function and potential as a therapeutic drug target. *Cancers*. 2021;14(1):86.
86. Bhattacharjee S, Hamberger F, Ravichandra A, Miller M, Nair A, Affo S, et al. Tumor restriction by type I collagen opposes tumor-promoting effects of cancer-associated fibroblasts. *The Journal of clinical investigation*. 2021;131(11).
87. Wu SZ, Roden DL, Wang C, Holliday H, Harvey K, Cazet AS, et al. Stromal cell diversity associated with immune evasion in human triple-negative breast cancer. *The EMBO journal*. 2020;39(19):e104063.
88. Nicolas AM, Pesic M, Engel E, Ziegler PK, Diefenhardt M, Kennel KB, et al. Inflammatory fibroblasts mediate resistance to neoadjuvant therapy in rectal cancer. *Cancer Cell*. 2022;40(2):168–84. e13.
89. Dings MP, Manoukian P, Waasdorp C, Quik JS, Strijker M, Lodestijn SC, et al. Serum levels of iCAF-derived osteoglycin predict favorable outcome in pancreatic cancer. *International Journal of Cancer*. 2023;152(3):511–23.
90. Zhang X, Zheng S, Hu C, Li G, Lin H, Xia R, et al. Cancer-associated fibroblast-induced lncRNA UPK1A-AS1 confers platinum resistance in pancreatic cancer via efficient double-strand break repair. *Oncogene*. 2022;41(16):2372–89.
91. Somerville TD, Biffi G, Daßler-Plenker J, Hur SK, He X-Y, Vance KE, et al. Squamous trans-differentiation of pancreatic cancer cells promotes stromal inflammation. *Elife*. 2020;9:e53381.
92. Li D, Schaub N, Guerin TM, Bapiro TE, Richards FM, Chen V, et al. T Cell-Mediated Antitumor Immunity Cooperatively Induced By TGF $\beta$ R1 Antagonism and Gemcitabine Counteracts Reformation of the Stromal Barrier in Pancreatic Cancer. *Molecular cancer therapeutics*. 2021;20(10):1926–40.
93. Luo H, Xia X, Huang L-B, An H, Cao M, Kim GD, et al. Pan-cancer single-cell analysis reveals the heterogeneity and plasticity of cancer-associated fibroblasts in the tumor microenvironment. *Nature Communications*. 2022;13(1):6619.
94. Grauel AL, Nguyen B, Ruddy D, Laszewski T, Schwartz S, Chang J, et al. TGF $\beta$ -blockade uncovers stromal plasticity in tumors by revealing the existence of a subset of interferon-licensed fibroblasts. *Nature communications*. 2020;11(1):6315.
95. Murray ER, Menezes S, Henry JC, Williams JL, Alba-Castellon L, Baskaran P, et al. Disruption of pancreatic stellate cell myofibroblast phenotype promotes pancreatic tumor invasion. *Cell Reports*. 2022;38(4).
96. Öhlund D, Handly-Santana A, Biffi G, Elyada E, Almeida AS, Ponz-Sarvisé M, et al. Distinct populations of inflammatory fibroblasts and myofibroblasts in pancreatic cancer. *Journal of Experimental Medicine*. 2017;214(3):579–96.
97. Jia X-q, Zhang S, Zhu H-j, Wang W, Zhu J-h, Wang X-d, et al. Increased expression of PHGDH and prognostic significance in colorectal cancer. *Translational oncology*. 2016;9(3):191–6.

98. Zhang Z, Zhu H, Li Q, Gao W, Zang D, Su W, et al. Gene expression profiling of tricarboxylic acid cycle and one carbon metabolism related genes for prognostic risk signature of colon carcinoma. *Frontiers in Genetics*. 2021;12:647152.
99. Gao X, Sanderson SM, Dai Z, Reid MA, Cooper DE, Lu M, et al. Dietary methionine influences therapy in mouse cancer models and alters human metabolism. *Nature*. 2019;572(7769):397-401.
100. Kalluri R. The biology and function of fibroblasts in cancer. *Nature Reviews Cancer*. 2016;16(9):582-98.
101. Zhong B, Cheng B, Huang X, Xiao Q, Niu Z, Chen Y-f, et al. Colorectal cancer-associated fibroblasts promote metastasis by up-regulating LRG1 through stromal IL-6/STAT3 signaling. *Cell Death & Disease*. 2021;13(1):16.
102. Chen X, Liu Y, Zhang Q, Liu B, Cheng Y, Zhang Y, et al. Exosomal miR-590-3p derived from cancer-associated fibroblasts confers radioresistance in colorectal cancer. *Molecular Therapy-Nucleic Acids*. 2021;24:113-26.
103. Adegboyega PA, Mifflin RC, DiMari JF, Saada JI, Powell DW. Immunohistochemical study of myofibroblasts in normal colonic mucosa, hyperplastic polyps, and adenomatous colorectal polyps. *Archives of pathology & laboratory medicine*. 2002;126(7):829-36.
104. Powell D, Adegboyega P, Di Mari J, Mifflin R. Epithelial cells and their neighbors I. Role of intestinal myofibroblasts in development, repair, and cancer. *American Journal of Physiology-Gastrointestinal and Liver Physiology*. 2005;289(1):G2-G7.
105. Ring SS, Cupovic J, Onder L, Lütge M, Perez-Shibayama C, Gil-Cruz C, et al. Viral vector-mediated reprogramming of the fibroblastic tumor stroma sustains curative melanoma treatment. *Nature communications*. 2021;12(1):4734.
106. Vaish U, Jain T, Are AC, Dudeja V. Cancer-associated fibroblasts in pancreatic ductal adenocarcinoma: an update on heterogeneity and therapeutic targeting. *International journal of molecular sciences*. 2021;22(24):13408.
107. Geng X, Chen H, Zhao L, Hu J, Yang W, Li G, et al. Cancer-associated fibroblast (CAF) heterogeneity and targeting therapy of CAFs in pancreatic cancer. *Frontiers in cell and developmental biology*. 2021;9:655152.
108. Zhou H, Liu Z, Wang Y, Wen X, Amador EH, Yuan L, et al. Colorectal liver metastasis: molecular mechanism and interventional therapy. *Signal transduction and targeted therapy*. 2022;7(1):70.
109. Shinkawa T, Ohuchida K, Nakamura M. Heterogeneity of cancer-associated fibroblasts and the tumor immune microenvironment in pancreatic cancer. *Cancers*. 2022;14(16):3994.
110. Zhang Y, Zhao Y, Li Q, Wang Y. Macrophages, as a promising strategy to targeted treatment for colorectal cancer metastasis in tumor immune microenvironment. *Frontiers in Immunology*. 2021;12:685978.
111. Kather JN, Halama N. Harnessing the innate immune system and local

immunological microenvironment to treat colorectal cancer. *British journal of cancer*. 2019;120(9):871–82.

112. Weng J, Li S, Zhu Z, Liu Q, Zhang R, Yang Y, et al. Exploring immunotherapy in colorectal cancer. *Journal of hematology & oncology*. 2022;15(1):1–28.

113. Qi J, Sun H, Zhang Y, Wang Z, Xun Z, Li Z, et al. Single-cell and spatial analysis reveal interaction of FAP+ fibroblasts and SPP1+ macrophages in colorectal cancer. *Nature communications*. 2022;13(1):1742.

114. McNamee MJ, Michod D, Niklison-Chirou MV. Can small molecular inhibitors that stop de novo serine synthesis be used in cancer treatment? *Cell death discovery*. 2021;7(1):87.

115. Li J, Luo X, Wei M, Li Z, Li Y, Zhao H, et al. YY2/PHGDH axis suppresses tumorigenesis by inhibiting tumor cell de novo serine biosynthesis. *Biomedicine & Pharmacotherapy*. 2023;165:115006.

116. Pelon F, Bourachot B, Kieffer Y, Magagna I, Mermet-Meillon F, Bonnet I, et al. Cancer-associated fibroblast heterogeneity in axillary lymph nodes drives metastases in breast cancer through complementary mechanisms. *Nature communications*. 2020;11(1):404.

117. Jang M, Kim SS, Lee J. Cancer cell metabolism: implications for therapeutic targets. *Experimental & molecular medicine*. 2013;45(10):e45–e.

118. Mello AM, Ngodup T, Lee Y, Donahue KL, Li J, Rao A, et al. Hypoxia promotes an inflammatory phenotype of fibroblasts in pancreatic cancer. *Oncogenesis*. 2022;11(1):56.

119. Tafani M, Sansone L, Limana F, Arcangeli T, De Santis E, Polese M, et al. The interplay of reactive oxygen species, hypoxia, inflammation, and sirtuins in cancer initiation and progression. *Oxidative medicine and cellular longevity*. 2016;2016.

120. Balamurugan K. HIF-1 at the crossroads of hypoxia, inflammation, and cancer. *International journal of cancer*. 2016;138(5):1058–66.

121. Abu el Maaty MA, Terzic J, Keime C, Rovito D, Luttinger R, Yanushko D, et al. Hypoxia-mediated stabilization of HIF1A in prostatic intraepithelial neoplasia promotes cell plasticity and malignant progression. *Science Advances*. 2022;8(29):eabo2295.

122. Shi Y, Riese DJ, Shen J. The role of the CXCL12/CXCR4/CXCR7 chemokine axis in cancer. *Frontiers in pharmacology*. 2020;11:574667.

123. Cheng Y, Song Y, Qu J, Che X, Song N, Fan Y, et al. The chemokine receptor CXCR4 and c-MET cooperatively promote epithelial-mesenchymal transition in gastric cancer cells. *Translational oncology*. 2018;11(2):487–97.

124. Mezzapelle R, Leo M, Caprioglio F, Colley LS, Lamarca A, Sabatino L, et al. CXCR4/CXCL12 activities in the tumor microenvironment and implications for tumor immunotherapy. *Cancers*. 2022;14(9):2314.

125. Chen J, Xu-Monette ZY, Deng L, Shen Q, Manyam GC, Martinez-Lopez A,

- et al. Dysregulated CXCR4 expression promotes lymphoma cell survival and independently predicts disease progression in germinal center B-cell-like diffuse large B-cell lymphoma. *Oncotarget*. 2015;6(8):5597.
126. Montironi C, Muñoz-Pinedo C, Eldering E. Hematopoietic versus solid cancers and T cell dysfunction: Looking for similarities and distinctions. *Cancers*. 2021;13(2):284.
127. Song W, Mazziari R, Yang T, Gobe GC. Translational significance for tumor metastasis of tumor-associated macrophages and epithelial-mesenchymal transition. *Frontiers in immunology*. 2017;8:1106.
128. Dominguez C, Müller S, Keerthivasan S, Koeppen H, Hung J, Gierke S, et al. Single-cell RNA sequencing reveals stromal evolution into LRRC15+ myofibroblasts as a determinant of patient response to cancer immunotherapy. *Cancer Discov* 10: 232–253. CD-19-0644. Crossref| PubMed| ISI; 2020.
129. Kieffer Y, Hocine HR, Gentric G, Pelon F, Bernard C, Bourachot B, et al. Single-cell analysis reveals fibroblast clusters linked to immunotherapy resistance in cancer. *Cancer Discovery*. 2020;10(9):1330–51.

## ABSTRACT(IN KOREAN)

## 암 미세환경에서 항암제의 저항성 획득 및 상피간엽이행 기전 연구

&lt;지도교수 황성순&gt;

연세대학교 대학원 의과학과

황예성

다양한 종류의 암은 종양 형성을 위한 환경을 유지하기 위해 세린 의존적인 일탄소대사를 사용한다. 암세포는 트랜스포터 혹은 해당과정이나 포도당신생합성 유래 3P를 통해서 세린을 직접적으로 섭취한다. 세린은 그 다음으로 ROS 균형, 퓨린 과 DNA 합성을 포함한 다양한 생리화학적 과정에 관여한다. 본 연구에서는 난치성 암인 두 종류의 갑상선 미분화암과 대장암에서 종양형성에 대한 일탄소대사의 역할을 관찰하였다.

갑상선 미분화암은 예후가 매우 좋지 않은 악성 종양 중 하나이다. 갑상선 유두암이 일탄소대사 관련 단백질의 발현이 높고 갑상선 미분화암으로 진행되는 점을 기초로 하여, 우리는 갑상선 미분화암과 갑상선 유두암 사이에 일탄소대사를 비교하였다. 단일 세포 분석을 통해 갑상선 유두암이 갑상선 미분화암으로 진행될 때 일탄소대사가 강화됨을 확인했다. 또한 우리는 갑상선 미분화암이 HER-2 단백질의 과발현과 베타 카데닌 단백질의 핵으로의 빈번한 이동

과 같은, 글루타민 대사의 상향조절의 몇 가지 생물학적 특징과 관련되어 있다는 점에 기초하여 글루타민 분해 경로를 억제시킨다면 갑상선 미분화암세포의 사멸이 발생할 것이라고 생각하였다. 그럼에도 불구하고 글루타민 분해 경로를 억제 시 갑상선 미분화암세포는 ATF4 매개 일탄소대사를 증가시켜 ROS 항상성을 조절하고 세포의 증식 억제를 회피함을 확인했다. 다음으로 글루타민 분해 경로와 일탄소대사를 동시에 억제시켰을 경우, 협력 작용을 통해 갑상선 미분화암 환자에서 사용되고 있는 항암제의 효과를 높이는 것을 확인했다.

대장암은 발병 빈도가 세 번째로, 사망률이 두 번째로 높은 암이다. 흔히 대장암 환자는 상피간엽이행이 동반되어 간 또는 폐로 전이를 겪게 된다. 본 연구에서는 단일세포분석을 통해 섬유모세포 클러스터들이 일탄소대사의 활성화에 따라 크게 두 개로 나뉘고 일탄소대사가 높은 클러스터에 상피간엽이행과 관련이 높은 염증성 암 관련 섬유모세포가 지배적으로 존재하는 것을 보고하였다. 특히 간으로 전이가 발생한 대장암 환자 중 세린 합성이 높은 환자군이 염증성 암 관련 섬유모세포 및 상피간엽이행 유전자의 발현이 높음을 확인하였다. 세린 합성 및 염증성 암 관련 섬유모세포 유전자 발현이 동시에 높은 대장암 3, 4단계 환자의 예후가 더 안 좋은 것을 확인하였다. 이를 통해, 대장암 환자에서 일탄소대사는 염증성 암 관련 섬유모세포와 양의 상관 관계를 가지고 상피간엽이행을 통한 전이를 일으키는 데 관여함을 알 수 있었다. 일탄소대사가 높은 섬유모세포는 *CXCL12*를 T 세포 및 대식세포와 같은 면역세포의 CXCR4 수용체와 결합하여 조절 T 세포 및 종양 연관 대식세포의 침윤 유도 가능성을 관찰했다. 마지막으로 *CXCL12*는 *SNAI2*, *VIM*과 같은 여러 상피간엽이행 유전자와 양의 상관 관계를 보였다. 우리의 결과는 일탄소대사는 대사 스트레스 상황에서 세포의 운명을 조절하거나 종양미세환경 구성성분 중 하나인 염증성 섬유모세포를 통해 상피간엽이행을 촉진시키는 등 종양형성에 대한 잠

재적 역할을 지님을 입증한다. 즉, 일탄소대사는 난치성 암에서 항암 효과를 높여 환자의 생존율을 높일 수 있는 치료적 타겟이 될 수 있다.

---

핵심되는 말 : 일탄소대사, 난치성암, RNA 시퀀싱

## PUBLICATION LIST

Hwang YS, Yun HJ, Jeong JW, Kim MK, Joo SY, Lee HK et al. Co-inhibition of glutaminolysis and one carbon metabolism promotes ROS accumulation leading to enhancement of chemotherapeutic efficacy in anaplastic thyroid cancer. *Cell Death and Disease* 2023;14(8):515.